



Progress, problems and prospects: An overview of the Guadalupian Series of South China and North America

Shu-zhong Shen^{a,*}, Dong-xun Yuan^{b,*}, Charles M. Henderson^c, Qiong Wu^{a,b}, Yi-chun Zhang^b, Hua Zhang^b, Lin Mu^b, Jahandar Ramezani^d, Xiang-dong Wang^a, Lance L. Lambert^e, Douglas H. Erwin^f, Jonena M. Hearst^g, Lei Xiang^b, Bo Chen^b, Jun-xuan Fan^a, Yue Wang^b, Wen-qian Wang^a, Yu-ping Qi^b, Jun Chen^h, Wen-kun Qie^b, Tian-tian Wangⁱ

^a State Key Laboratory for Mineral Deposits Research and School of Earth Sciences and Engineering, Nanjing University, 163 Xianlin Avenue, Nanjing 210023, China

^b State Key Laboratory of Palaeobiology and Stratigraphy, Nanjing Institute of Geology and Palaeontology and Center for Excellence in Life and Paleoenvironment, Chinese Academy of Sciences, Nanjing 210008, China

^c Department of Geoscience, University of Calgary, Calgary, AB T2N 1N4, Canada

^d Department of Earth, Atmospheric and Planetary Sciences, Massachusetts Institute of Technology, Cambridge, MA 02139, USA

^e Department of Geological Sciences, University of Texas at San Antonio, One UTSA Circle, San Antonio, TX 78249, USA

^f Department of Paleobiology, MRC-121, National Museum of Natural History, Washington, D.C. 20013-7012, USA

^g Guadalupe Mountains National Park, Salt Flat, TX 79847, USA

^h State Key Laboratory of Isotope Geochemistry, Guangzhou Institute of Geochemistry, Chinese Academy of Sciences, Guangzhou 510640, China

ⁱ State Key Laboratory of Biogeology and Environmental Geology, China University of Geosciences, Beijing 100083, China

ARTICLE INFO

Keywords:
Guadalupian
Biostratigraphy
Chemostratigraphy
Conodonts
South China
North America

ABSTRACT

The Guadalupian Epoch is marked by the formation of the Pangean supercontinent, global sea-level change, rifting and drifting of the Cimmerian continents, formation of large igneous provinces and dramatic biotic changes. A high-resolution biostratigraphic, chemostratigraphic and high-precision geochronologic framework of this critical transition is fundamental to understanding these events. Extensive studies of the latest Cisuralian and Guadalupian Series in both South China and North America reveal the same conodont lineages, but the conodont interval zones based on *Jinogondolella* within the Guadalupian Series are slightly diachronous. High-precision U-Pb geochronological studies (CA-ID-TIMS method) calibrate the base of the Guadalupian Series (base Roadian) at 273.01 ± 0.14 Ma. A previously reported age from an ash bed overlying the Emeishan flood basalts, 259.51 ± 0.21 Ma, is adopted for the Guadalupian/Lopingian boundary (GLB). Based on recently published geochronology and Bayesian age modeling from the Guadalupian Series, the base of the Capitanian is constrained at 264.28 ± 0.16 Ma and the base of the Wordian is interpolated to be 266.9 ± 0.4 Ma. The Illawarra Reversal is of early-middle Wordian age. Both North America and South China possess a distinct negative $\delta^{13}\text{C}_{\text{carb}}$ excursion of 3-5‰ at the latest Kungurian and early Roadian (LK-ER CIE), which coincides with the early stages of a significant 3rd order sea-level rise. The large end-Guadalupian $\delta^{13}\text{C}_{\text{carb}}$ negative excursion may have been affected by post-depositional diagenesis or a warming event associated with the Emeishan volcanism. The $^{87}\text{Sr}/^{86}\text{Sr}$ ratios in both regions declined from the latest Kungurian to the late Capitanian, but have different ratios and reveal several fluctuations in the middle Guadalupian. Measured $\delta^{18}\text{O}_{\text{apatite}}$ values suggest that the Delaware Basin was 3-4°C cooler than the eastern Yangtze Block. Analysis of a new high-resolution database of marine taxa indicates only a minor pre-Lopingian diversity drop from 261.04 Ma to 259.98 Ma, which coincides with the peak Emeishan volcanism. The widely-perceived “end-Guadalupian mass extinction” in North America is evidently masked by, and possibly an artefact of, a stratigraphic truncation effect due to rapid lithofacies changes from limestone to laminated evaporites with the closure of the west Texas basins.

* Corresponding authors.

E-mail addresses: szshen@nju.edu.cn (S.-z. Shen), dxyuan@nigpas.ac.cn (D.-x. Yuan).

1. Introduction

The Guadalupian Epoch (Middle Permian) is one of the most critical transitions in the Phanerozoic, with major changes in the Earth's geological, geochemical and biological systems. These include:

- 1) A critical transition of the supercontinent Pangea from assembly to dispersal. This transition is marked by normal polarity at the Illawarra Reversal (IR), which records the end of the long Kiaman Reverse Superchron (Late Carboniferous to middle Guadalupian), and the beginning of frequent polarity reversals during the Permian-Triassic Mixed Superchron (middle Guadalupian to Triassic) (Isozaki, 2009). The inception of the Mixed Superchron coincides with massive eruptions of the Emeishan large igneous province (ELIP) basalts. The marine carbonate $^{87}\text{Sr}/^{86}\text{Sr}$ isotopic trend, which is a proxy for ocean floor spreading versus continental weathering, reached its lowest value of the Phanerozoic during the late mid-Capitanian (McArthur et al., 2012; Kani et al., 2013; Liu et al., 2013; Wang et al., 2018a).
- 2) The late Paleozoic Ice Age (LPIA) finally ended during the Guadalupian with the onset of a full greenhouse climate (Isbell et al., 2003; Fielding et al., 2008; Shi and Waterhouse, 2010; Haig et al., 2017; Liu et al., 2017a; Garbelli et al., 2019; Wang et al., 2020). Temperatures in the tropics and southern hemisphere gradually increased from the Cisuralian (Early Permian) to the Guadalupian (Chen et al., 2011, 2013). Superimposed on this trend was a possible cooling event (Kamura Event) before the GLB followed by a warming event near the GLB (Isozaki et al., 2007a, 2011; Zhang et al., 2020; Wang et al., 2020).
- 3) A major sea-level rise is recorded in transgressive facies typical of the lower deposits of this series, including the contact between the Chihsia and Maokou formations of South China and within the lower Cutoff Formation (Shumard and El Centro members) of West Texas. The greatest sea-level lowstand of the Paleozoic concluded the Guadalupian, which resulted in the emergence of vast swaths of the supercontinent Pangea. Seawater withdrew from western North America, the southern Urals, Russia and Gondwana, producing widespread evaporites and continental deposits throughout Pangea (Ross and Ross, 1987; Haq and Schutter, 2008). In South China, a distinct episode of uplift called the Dongwu Movement generated a widespread unconformity between the Guadalupian and Lopingian Series (upper Permian) (Hu, 1994; He et al., 2005; Cao et al., 2018; Hou et al., 2020).
- 4) Associated with these major tectonic and climatic changes are dramatic biotic and environmental changes, including a widely documented pre-Lopingian or end-Guadalupian crisis (Jin, 1993; Jin et al., 1994; Stanley and Yang, 1994; Wang and Sugiyama, 2000; Shen and Shi, 2002; Clapham et al., 2009; Chen and Xu, 2019), as well as the rise and extinction of dinocephalian therapsids on land (Lucas, 2009, 2017a; Rubidge et al., 2013; Liu, 2013; Day et al., 2015).

Understanding the tempo and interrelationships among the geological and biotic events requires a high-resolution chronostratigraphic framework that would allow integration of lithostratigraphic, biostratigraphic, chemostratigraphic, magnetostratigraphic and radio-isotopic age data from geographically disparate successions. Achieving a high-resolution, integrated view of this interval will facilitate analysis of the biological response to an interval of pervasive change in climate, ocean structure, land-sea configurations, and atmospheric chemistry.

Such a high-resolution multidisciplinary temporal framework is in early stages of development, but as an initial step, in this paper we provide an overview of the state-of-the-art knowledge of Guadalupian biostratigraphy, geochronology, and cyclostratigraphy, primarily focused on marine sections from South China and North America. In addition, we present new $\delta^{13}\text{C}$, $\delta^{18}\text{O}$ and $^{87}\text{Sr}/^{86}\text{Sr}$ chemostratigraphy,

and U-Pb geochronology based on Guadalupian sections in the Guadalupe Mountains National Park (GMNP) in West Texas and New Mexico, USA and in South China (Fig. 1), which facilitate the integration of records from these two key sequences.

2. Studied sections and general stratigraphy

The South China block was situated in the eastern part of the Paleotethys during the Guadalupian (Hou et al., 2020). The local chronostratigraphic unit of the Guadalupian is the Maokouan, which comprises the lower Kuhfengian and the upper Lengwuan regional stages. The Kuhfengian is basically correlative with the Roadian and Wordian together and the Lengwuan is correlative with the Capitanian of the international timescale (Jin et al., 1994, 1997), but the precise correlations of stage boundaries from the Maokouan to those of the Guadalupian in North America have not been resolved (Fig. 2). There are two main Guadalupian marine facies in South China. The first is the Kuhfeng Formation, composed of thin-bedded chert containing multiple ash beds and abundant radiolarians (Kametaka et al., 2009; Ito et al., 2013; Zhu et al., 2013; Wu et al., 2017; Zhang et al., 2019a; Wei et al., 2020). This facies is usually no more than 20 m thick in southeast China and the lowest part of the formation contains a 0.5–1 m unit with abundant phosphorus nodules. The second, more widely distributed facies, is a carbonate platform facies, the Maokou Formation (Sha et al., 1990). It is much thicker (~100 m) than the equivalent Kuhfeng Formation (Shen et al., 2019b). Both formations basically represent the Guadalupian Series in South China. The underlying Kungurian Stage is mainly represented by widespread carbonates of the Chihsia Formation with abundant fusulines, conodonts and rugose corals (Sha et al., 1990; Shen et al., 2007). In this paper, we discuss two carbonate sections of the Maokou Formation and one section of the Kuhfeng Formation.

The Penglaitan section ($23^{\circ}41'43''\text{N}$, $109^{\circ}19'16''\text{E}$) in the Laibin area, Guangxi Province has been defined as the GSSP section for the base of the Lopingian Series (Jin et al., 2006). The Chihsia and Maokou formations at Penglaitan are very well exposed along the Hongshui River (Fig. 3A, B), and their lithologic boundary is readily distinguished by a thick, massive limestone at the top of the Chihsia Formation with much less cherty material. The strata studied are continuous from the late Kungurian *Sweetognathus subsymmetricus* Zone to the early Wuchiapingian *Clarkina postbitteri postbitteri* Zone (Jin et al., 2006; Shen et al., 2007; Yuan et al., 2017). The Dukou section ($31^{\circ}41'31.26''\text{N}$, $108^{\circ}17'50.04''\text{E}$) in Xuanhan (Fig. 3C), Sichuan Province contains a carbonate succession of the Maokou Formation yielding abundant conodonts and fusulines, which is ideal for high-resolution biostratigraphy, chemostratigraphy and cyclostratigraphy (Mei et al., 1994a, 1994b; Shen et al., 2013a; Fang et al., 2015, 2017). Biostratigraphy suggests that the section contains a conodont succession from the *Sweetognathus subsymmetricus* Zone to the *Jinogondolella xuanhanensis* Zone (Mei et al., 1994a; this study). The uppermost Capitanian is commonly missing due to the end-Guadalupian lowstand in South China.

We also studied the Kuhfeng Formation in the type section of the index conodont species *Jinogondolella nankingensis* at Zhengpanshan ($32^{\circ}9'43.42''\text{N}$, $119^{\circ}4'50.56''\text{E}$) near Nanjing City, Jiangsu Province for geochronology and ammonoids (Fig. 3D). In some areas of South China, a thin (<10 m) chert unit is often present in the topmost Guadalupian (e.g. the Dukou section studied in this paper), but this unit is underlain by the thick Maokou Limestone Formation. This chert unit represents only a small part of the uppermost Guadalupian immediately below the GLB sequence boundary in southwest China (Fig. 3C).

In North America, the Guadalupian Series is well developed in the Glass and Guadalupe Mountains. Traditionally, the Guadalupian Series was composed of the Word and Altuda formations in the Glass Mountains and the Brushy Canyon, Cherry Canyon and Bell Canyon formations in the GMNP. The Road Canyon Formation in the Glass Mountains and the Cutoff Formation in the Guadalupe Mountains were previously assigned to the underlying Leonardian (King, 1948). The Roadian,

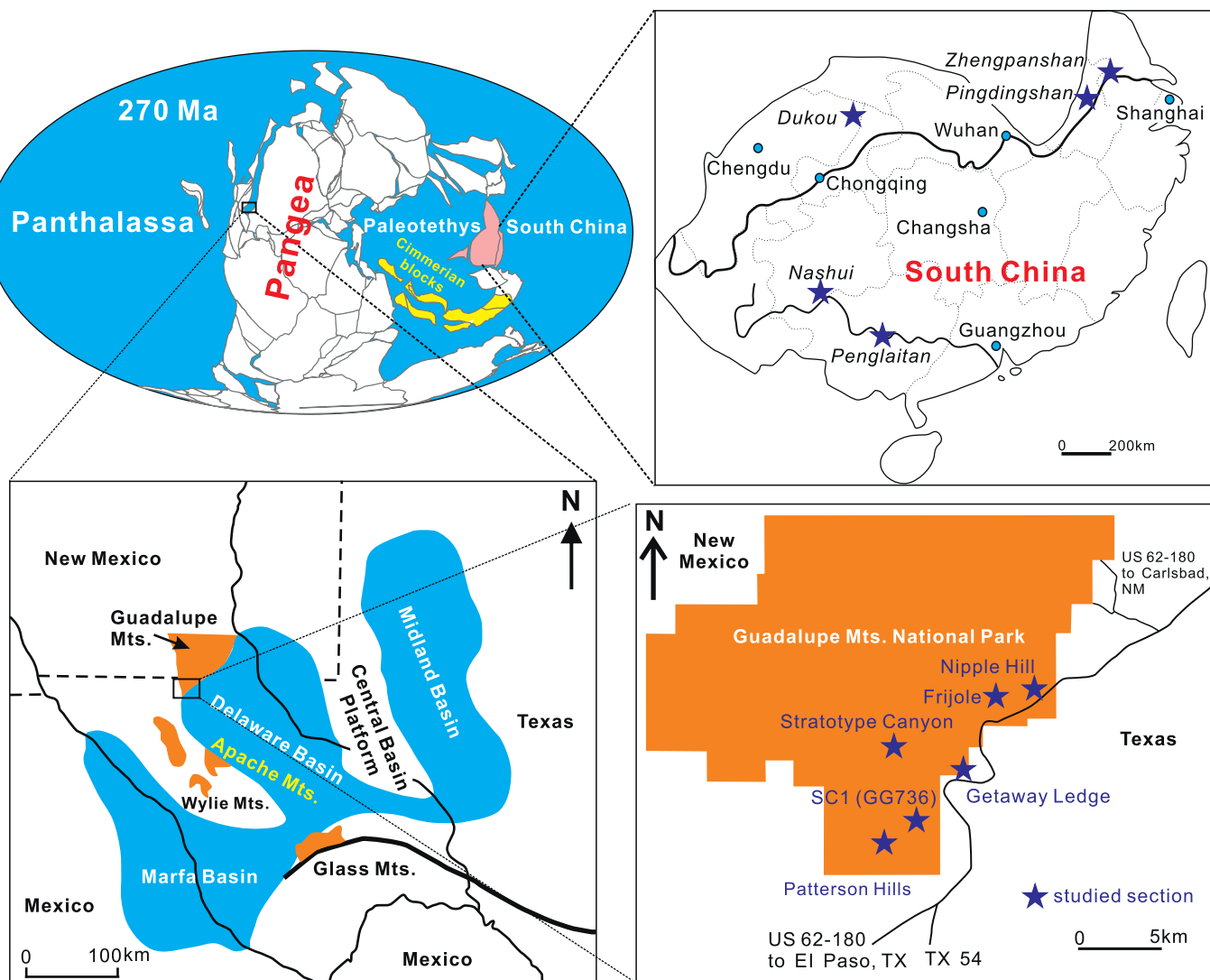


Fig. 1. Locality and reconstruction maps showing the studied regions and sections indicated with blue stars. (For interpretation of the references to colour in this figure legend, the reader is referred to the web version of this article.)

Wordian and Capitanian stages were proposed to constitute the Guadalupian Series by Glenister et al. (1992). This timescale was adopted by the International Subcommission on Permian Stratigraphy (Jin et al., 1997) and the three GSSPs were ratified by IUGS in 1999 (Glenister et al., 1999) (Fig. 2).

The GMNP was selected as the type area where the international Guadalupian Series is defined (Jin et al., 1997; Glenister et al., 1999; Wardlaw, 2000; Lambert, 2000; Lambert et al., 2000) because most of the Glass Mountains lies on private land. Strata in the GMNP are more than 1500 m thick and a single complete section from upper Kungurian throughout the Guadalupian is not available (Williamson, 1980), but the detailed sequence stratigraphic analyses of these units allows well supported correlation between sections (e.g. Lambert, 2000; Wardlaw, 2000; Nestell et al., 2006; Kerans et al., 2014; Hurd et al., 2016; Playton and Kerans, 2018). We sampled stratigraphic intervals from different sections in the GMNP and made a composite section (Fig. 4). Sections sampled were Stratotype Canyon (upper Kungurian through Roadian) ($31^{\circ}52'36.12''N$, $104^{\circ}52'36.48''W$; Fig. 4B, C), Getaway Ledge (lower Wordian) ($31^{\circ}51'57.97''N$, $104^{\circ}49'57.92''W$; Fig. 4D, E), Nipple Hill (upper Wordian to Capitanian) ($31^{\circ}54'32.71''N$, $104^{\circ}47'21.02''W$; Fig. 4F, G), Patterson Hills (upper Wordian through Capitanian) ($31^{\circ}49'34.80''N$, $104^{\circ}52'33.43''W$; Fig. 4A), Frijole ($31^{\circ}54'15.09''N$, $104^{\circ}49'12.93''W$), and Section SC1 (GG736, the principal reference

section for the Reef Trail Member, upper Capitanian) ($31^{\circ}49'53.28''N$, $104^{\circ}52'4.20''W$; Fig. 4H) (Bell et al., 2015). The line of measurement we used for samples from Section SC1 and described here (Fig. 1) deviates ~30 m east from that of Bell et al. (2015).

The main controversy in Guadalupian correlation between South China and North America is the base of the series. The Chinese local timescale previously included a part of the Xiangboan Stage, constrained by the base of the fusuline *Cancellina* Zone, as part of the Guadalupian. The upper part of the Xiangboan Stage contained the fusuline *Neoschawagerina simplex* Zone, which ranges across the Chihsian/Maokouan boundary. Thus, the Xiangboan Stage overlapped with the Roadian as defined by the conodont *Jinogondolella nankingensis* Zone (Jin et al., 1999). This problem has been resolved by redefining the Xiangboan Stage in South China, with the base defined by the fusuline *Cancellina elliptica* and its top is defined by the first occurrence of the conodont *Jinogondolella nankingensis* (Shen et al., 2019b; Henderson and Shen, 2020). Thus, the Xiangboan Stage is assigned to Cisuralian and the Maokouan Subseries is completely assigned to the Guadalupian in South China (Fig. 2).

This is the first study to address the correlations of the internal stages of the Guadalupian Series between South China and North America. The Kuhfengian Stage is generally correlative with the Roadian and Wordian. The Lengwuan Stage is equivalent to the Capitanian, but the

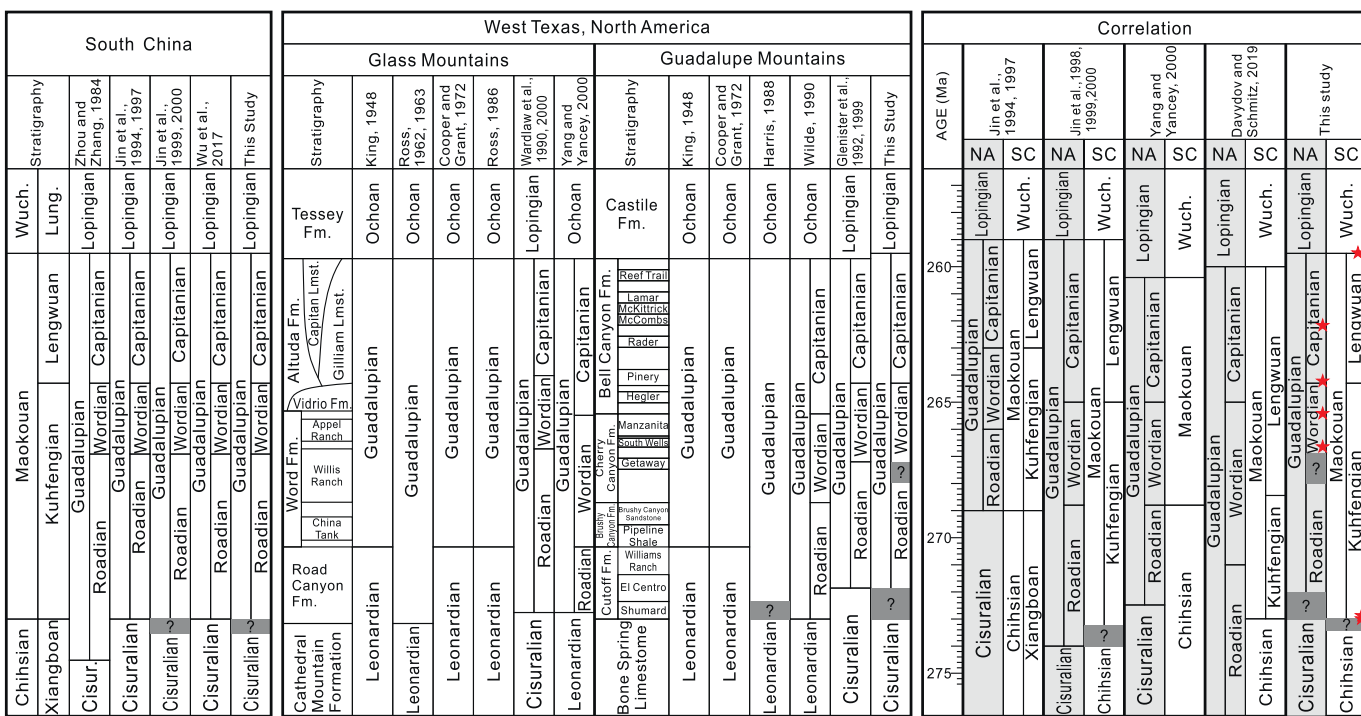


Fig. 2. History of Guadalupian temporal framework in South China and North America and their correlations. The dark gray intervals suggest that the precise boundaries remain not fixed, based on current biostratigraphic data. The red stars represent the high-precision zircon U-Pb dates reported in this paper. Abbreviations: NA-North America; SC-South China. Note: in the correlation column, stage boundaries vary in position because of new age dates for boundaries. Stratigraphic and correlation data between South China and North America are from King (1948), Ross (1962, 1963, 1986), Cooper and Grant (1972), Zhou and Zhang (1984), Harris (1988), Wilde (1990), Glenister et al. (1992, 1999), Jin et al. (1994, 1997, 1998, 1999, 2000), Wardlaw et al. (1990, 2000), Yang and Yancey (2000), Wu et al. (2017) and Davydov and Schmitz (2019). (For interpretation of the references to colour in this figure legend, the reader is referred to the web version of this article.)

Lengwuan Stage at its type locality in Zhejiang Province remains unstudied so far.

3. Biostratigraphy

3.1. Conodonts

The Permian System is divided into the Cisuralian, Guadalupian and Lopingian series, in ascending order. They are respectively defined by strata in the southern Urals, Russia, the Guadalupe Mountains at the GMNP in west Texas, USA, and South China (see a review by Lucas and Shen, 2018). The Guadalupian Series is constrained at the base by the First Appearance Datum (FAD) of the conodont *Jinogondolella nankingensis* at the Stratotype Canyon section (Figs. 1, 4B) in the GMNP, West Texas, USA and at the top by the FAD of the conodont *Clarkina postbitteri postbitteri* at the Penglaitan section (Fig. 3B) in the Laibin area, Guangxi, South China. There are, however, some unresolved issues of conodont taxonomy and biostratigraphy for the Guadalupian Series and underlying uppermost Kungurian Stage (Fig. 5).

The Roadian, Wordian and Capitanian stages are defined by the FADs of *Jinogondolella nankingensis*, *J. aserrata* and *J. postserrata*, respectively, in the GMNP, West Texas (Jin et al., 1997; Glenister et al., 1999). The three GSSPs of the Guadalupian Series were ratified more than two decades ago, and all three index species have been reported from both South China and North America. However, consistent identification of those species is a little difficult due to the index species have not yet been illustrated from the GSSP sections since the GSSPs were ratified (e.g. Wardlaw, 2000; Mei and Henderson, 2002; Lambert, 2006; Shen et al., 2012; Yuan et al., 2017). The index species *J. nankingensis* was based on hand-drawn pictures of relatively advanced specimens with more rounded posterior end and relatively shallow serration on the anterior part of the platform from the basal part of the Kuhfeng Formation (~25

cm above the base of the formation) at the Zhengpanshan section near Nanjing City, southeast China (Fig. 3D); thus the FAD could be lower. Extensive collecting and processing of conodont samples below the Kuhfeng Formation at Zhengpanshan have recently yielded some serrated gondolellids that are not yet well studied. Sohn (1961) first illustrated serrated gondolellids from the Getaway Member of the Cherry Canyon Formation, which were later assigned to *Gondolella serrata* by Clark and Ethington (1962) and Clark and Mosher (1966). It has been widely accepted that *G. serrata* is a synonym of *Jinogondolella nankingensis* (Glenister et al., 1992, 1999; Wang, 1995; Jin et al., 1997; Wardlaw, 2000; Lambert et al., 2007; Henderson et al., 2012; Henderson, 2018; Shen et al., 2019b). Nevertheless, the temporal relationship between North American *Gondolella serrata* and South China *Jinogondolella nankingensis* still needs to be tested by other correlation markers. Previous reports have suggested these three index species range through the whole Guadalupian in South China (Sun et al., 2008), but these would be as form species, not as sample-population species concepts. Thus, the stratigraphic levels of these three similar species may be diachronous inter-regionally. Taking the FAD of *J. nankingensis* with distinct serration on its anterior lateral margin of the platform as the marker of the base of the Guadalupian (e.g. Mei et al., 1994a, 1998), the Guadalupian Series of the chert facies is only about 13 m thick in Nanjing, South China (Fig. 3D), whereas the equivalent strata in the GMNP in West Texas are more than 400 m thick, thus the accumulation of sediment was very different.

Recent studies have identified some correlation problems with the biostratigraphic markers of the three GSSPs of the Guadalupian Series. The first occurrence of serrated gondolellids has been used for recognizing the base of the Guadalupian (Mei et al., 1998). However, rare specimens with serrated platform margins also occur in other gondolellid species (*Jinogondolella* aff. *nankingensis* in this paper) at lower horizons (Lambert, 2000; Lambert et al., 2007). Serrated specimens

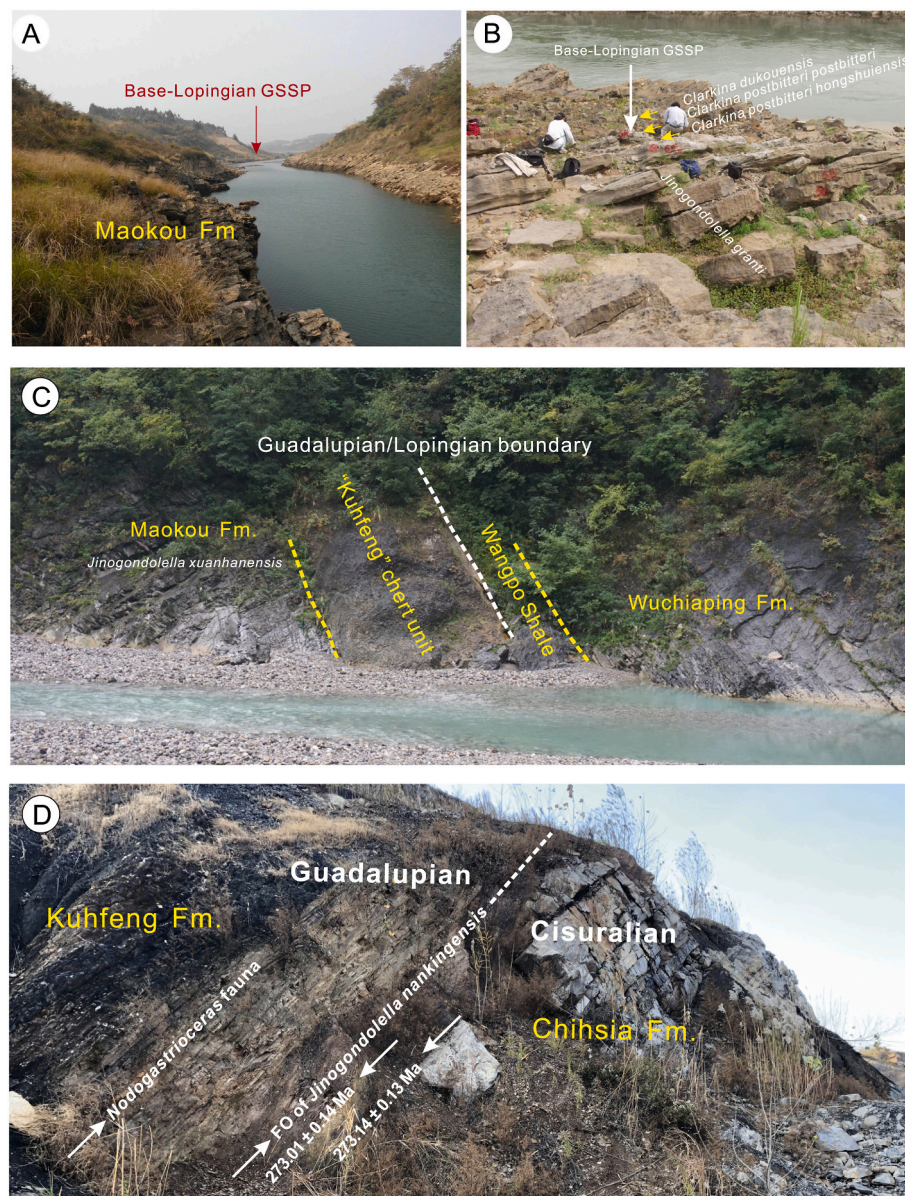


Fig. 3. Outcrops of studied sections in South China. A, the Maokou Formation at the Penglaitan section; B, the GLB interval with the base-Lopingian GSSP; C, the Guadalupian/Lopingian transition at the Dukou section with a chert unit underlain by the thick Maokou Limestone; D, the Zhengpanshan section with the Cisuralian/Guadalupian boundary (CGB) and high-precision dates.

have recently been found ~100 m below the FAD sample at the Stratotype Canyon GSSP section in the GMNP in West Texas, USA. Similar serrated specimens have also been recognized from the upper part of the Chihsia Formation in South China. Thus, the first occurrence of serrated forms among gondolellids should not be considered as a reliable marker to separate the Guadalupian from the Cisuralian. The base of the Guadalupian Series was defined by the FAD of *J. nankingensis* within the lineage *Mesogondolella lamberti*→*Jinogondolella nankingensis* at the Stratotype Canyon section (Fig. 4B). The discovery of serrated specimens in the late Kungurian *Mesogondolella lamberti* Zone may necessitate changes to the current concept of the *Jinogondolella* lineage. Research is continuing on the evolutionary and taxonomic relationships with younger and typical *Jinogondolella nankingensis*.

The base of the Wordian Stage was defined by the FAD (Fig. 4E) of the conodont species *Jinogondolella aserrata* within the lineage *J. nankingensis*→*J. aserrata*. However, a recent study of the GSSP section for the base of the Wordian Stage did not confirm the presence of the index species from the designated FAD level at the Getaway Ledge

section (Yuan et al., 2020a). Instead, specimens of the species *J. aserrata* are common below the GSSP level down to the base of the Getaway carbonate unit (Fig. 4D, E) in the GMNP (Yuan et al., 2020a). Thus, the exact position of the FAD of *J. aserrata* is uncertain, and may occur within the Cherry Canyon Sandstone, from which conodonts have not been recovered. Wardlaw and Nestell (2015) reported a complete conodont succession from questionable *J. nankingensis behnkeni* to *J. aserrata* to *J. postserrata* from the Hegler and Pinery Limestone members in the southern part of the Patterson Hills, at a road cut exposed along US Highway Route 62/180. The stratigraphic interval of the road cut section was studied to address the base-Capitanian GSSP problem, and is obviously younger than the Getaway Member for the base of the Wordian Stage.

The base of the Capitanian Stage was defined by the FAD of *Jinogondolella postserrata* within the lineage *J. aserrata*→*J. postserrata* at the Nipple Hill section (Fig. 4F). However, only about 0.5 m strata above the GSSP (Fig. 4G) are preserved at the top of Nipple Hill. Specimens recognized as *J. postserrata* are rare in the FAD sample as well as the

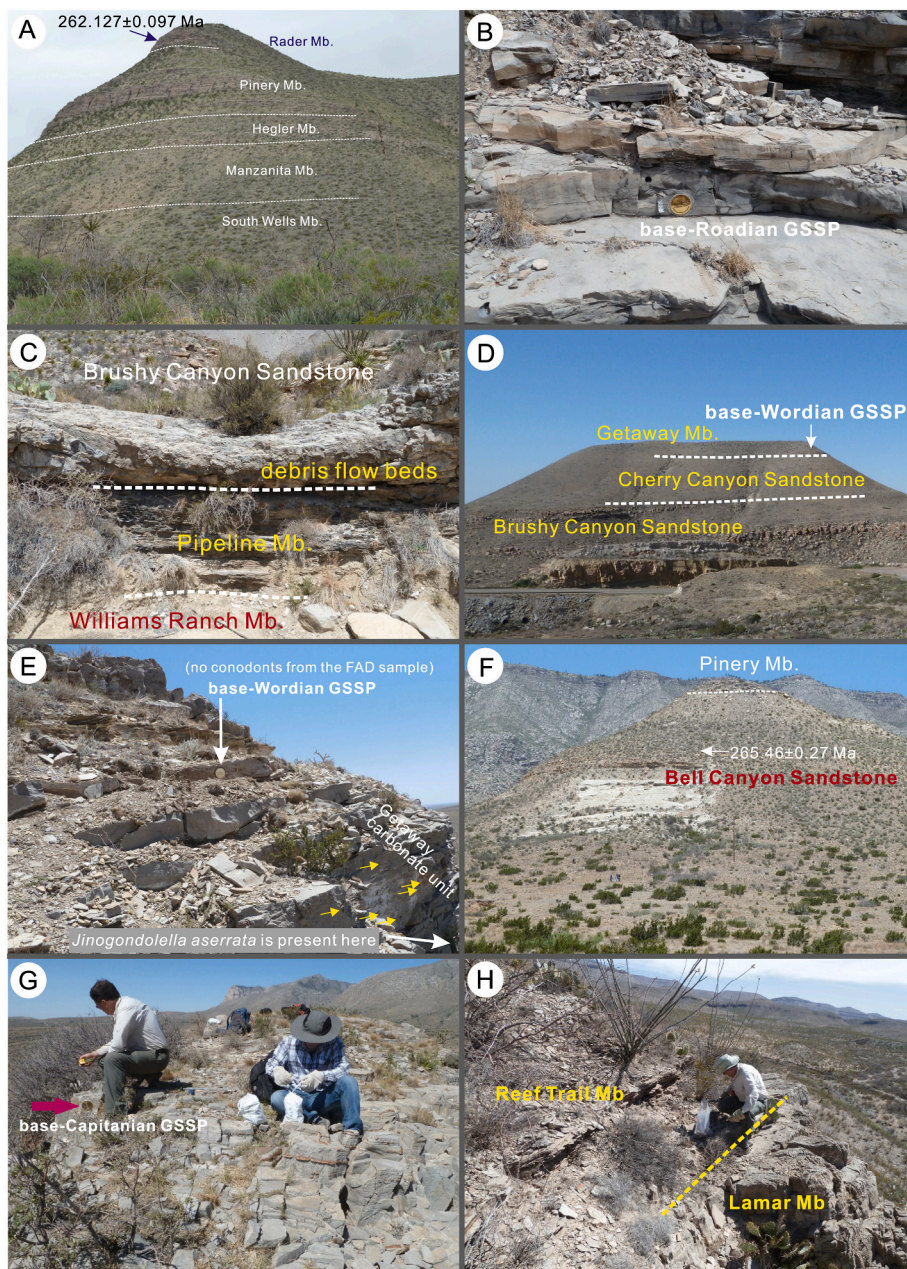


Fig. 4. Outcrops of studied sections in the Guadalupe Mountains National Park (GMNP), West Texas, USA. A, The Patterson Hills section; B, the current base-Roadian GSSP at the Stratotype Canyon section with the golden GSSP marker. So far only rare juvenile specimens possibly belonging to *Jinogondolella nankinensis* are found from the FAD sample; C, the lithologic boundary interval from Williams Ranch, Pipeline Member to the Brushy Canyon Sandstone marked by a debris flow deposit unit; D, the Getaway Ledge section with the current GSSP of base-Wordian. Small yellow arrows indicate numerous salt pseudomorphs. The Cherry Canyon and Brushy Canyon sandstones do not contain conodonts and datable ash beds. E, Current GSSP of the base-Wordian Stage showing the golden GSSP marker. There are no conodonts from the FAD sample here, but many *J. aserrata* below the GSSP. F, The Nipple Hill section with the GSSP of the base-Capitanian Stage showing a thin Pinery Member on the top of the Hill and the level of the ash bed with the date; G, the top of the Nipple Hill with the GSSP marker Charles Henderson sitting beside. Only 0.5 m left above the GSSP at Nipple Hill; H, Section SC1 showing the boundary interval between the Lamar and the Reef Trail members (Charles Henderson for scale). (For interpretation of the references to colour in this figure legend, the reader is referred to the web version of this article.)

sample 0.5 m higher. A more complete nearby section was studied to clarify the conodont populations of the index species and the conodont succession above the GSSP. The Frijoles section (Fig. 1), about 2 km away from the Nipple Hill GSSP section, contains ash beds with high-precision dates and provides insights to resolve this correlation (Wu et al., 2020).

Jinogondolella shannoni begins immediately above the *J. postserata* Interval Zone, at the top of the Lamar Limestone Member, and then evolved to *J. altudaensis*. Thus, two more conodont zones, the *J. shannoni* and *J. altudaensis* zones, have been recognized in the uppermost part of the Guadalupian Series in the GMNP (Lambert et al., 2010). The *Jinogondolella postserata* Interval Zone in South China and GMNP differ greatly in cyclostratigraphy possibly related to sampling and taxonomic discrepancies. In the topmost part of the Reef Trail Member of the Capitanian (Fig. 4H), *Clarkina hongshuiensis*, *Jinogondolella crofti*, and *J. altudaensis* were reported (Lambert et al., 2010; Nestell et al., 2019). However, the specimens assigned to *Clarkina hongshuiensis* could be assigned to *Jinogondolella* sp. and *J. crofti* may be comparable to *J. xuanhanensis* in South China. At this time a drop in relative sea-level

restricted the Delaware Basin from Panthalassa and isolated conodont populations. These species may have become entirely endemic just before dying off with the onset of deposition of the Castile evaporites. The same assumptions could be applied to the Apache Mountains EF section (Lambert et al., 2002; Wardlaw and Nestell, 2010). If this alternate interpretation is correct, the GLB in the GMNP probably lies in the lower part of the Castile Formation where transitional facies are present between the Reef Trail Member and the Castile Formation (Hill, 1996; Lambert et al., 2002, 2010) (Fig. 5). Resolving these taxonomic discrepancies requires further detailed comparison of conodont sample-populations (Mei et al., 2004) from both South China and North America are necessary.

The *Jinogondolella shannoni* and *J. altudaensis* zones in the Guadalupian of South China cannot be distinguished temporally at some sections. They are successively overlain by the *J. prexuanhanensis*, *J. xuanhanensis*, *J. granti* and *Clarkina postbitteri hongshuiensis* zones at the Penglaitan GSSP section of the base-Lopingian Series (Mei et al., 1998; Henderson et al., 2002; Jin et al., 2006; Shen et al., 2007). The two

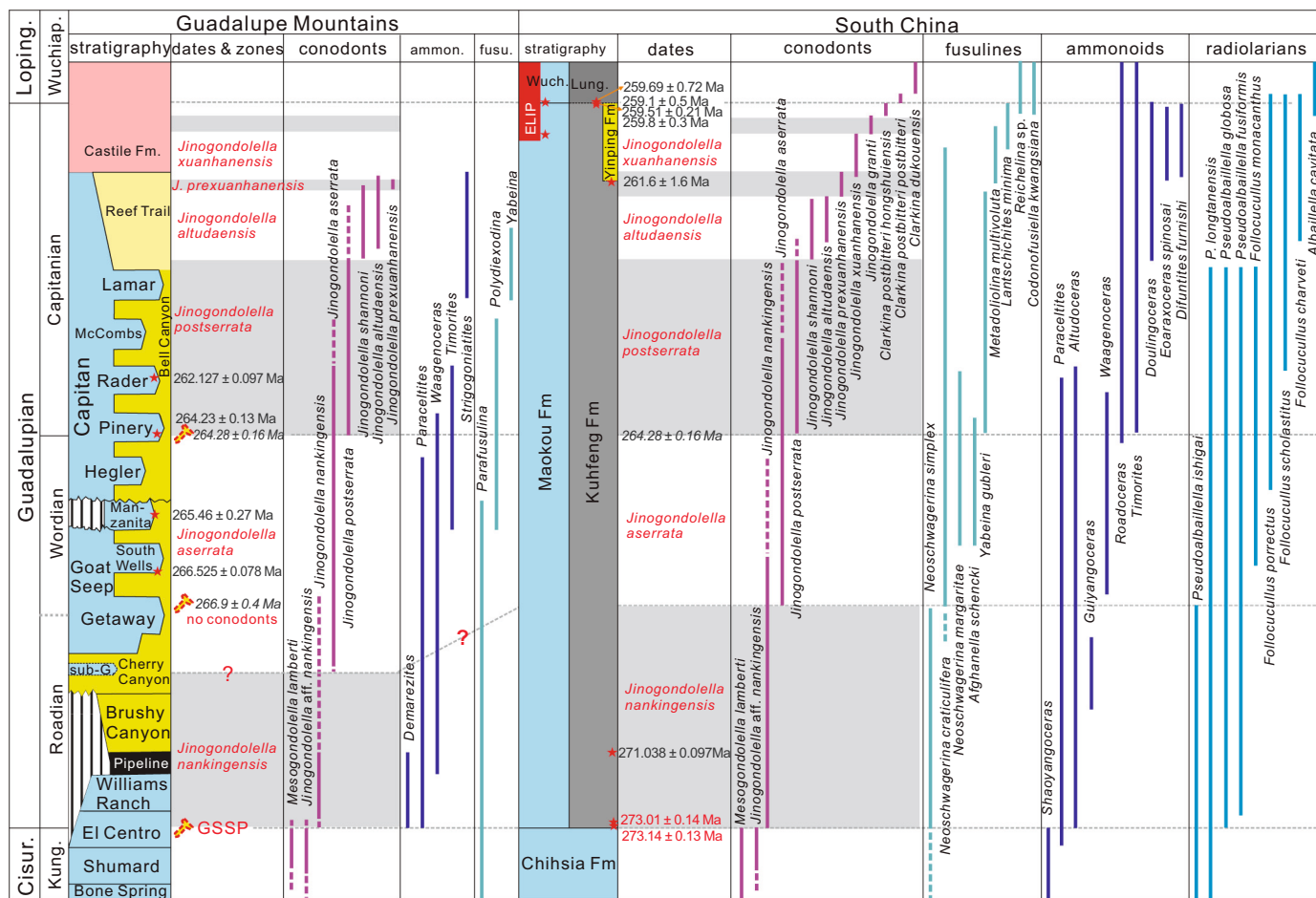


Fig. 5. Guadalupian conodont, fusuline, ammonoid and radiolarian successions and their correlation between South China and North America. Isotopic radiometric dates are from Wu et al. (2020). Ammonoids are from Glenister et al. (1999), Zhou (2017), and Leonova (2018); fusulines are revised from Zhang and Wang (2018); radiolarians are from Zhang et al. (2018). Gray dashed line at Wordian/Roadian boundary suggests that the base-Wordian GSSP is pending future study. Abbreviations: Cisur.-Cisuralian; Kung.-Kungurian; Loping.-Lopingian; Wuchiap.-Wuchiapingian; Wuch.-Wuchiaping Fm; Lung.-Lungtan Fm; ammon.-ammonoids; fusulines; ELIP-Emeishan Large Igneous Province.

highest conodont zones have only been confirmed in the uppermost part of the Douling Formation in southern Hunan (Shen and Zhang, 2008), and the Fengshan section in Liuzhou, Guangxi, South China (Mei et al., 1998; Shen et al., 2020). Although *Clarkina postbitteri hongshuiensis* has been reported from the Maoershan section in Hubei (Zhang et al., 2007), the Dachongling section in Guangxi (Sun and Xia, 2006; Xia et al., 2006), and a Permian pelagic chert sequence in the Gujo-Hachiman section, Gifu, southwest Japan (Nishikane et al., 2011), it is not yet clear whether these reports establish presence of the uppermost Guadalupian in these localities (e.g. Yuan et al., 2017; Zhong et al., 2020). As a result of the greatest Phanerozoic global sea-level lowstand event (King, 1942; Kendall and Harwood, 1989; Haq and Schutter, 2008) and subsequent rapid deepening event (Anderson et al., 1972; Hill, 1996; Bell et al., 2015) the conodont zones above the *Jinogondolella prexuanhanensis* Zone of the Guadalupian Series are mostly absent or represented by only smooth gondolellids-bearing or conodont-barren strata all over the world. It is possible that this lowstand, documented in a continuous succession at Penglaitan, was also responsible for the Delaware Basin becoming increasingly restricted and evaporative.

3.2. Fusulines

The Kungurian to Guadalupian fusuline biostratigraphy from the Tethyan region is based largely on neoschwagerinids (Xiao et al., 1986; Zhang and Wang, 2018). The Roadian and Wordian stages include two

fusuline zones; the *Neoschwagerina craticulifera* Zone in the lower and the *N. margaritae* Zone in the upper (Sheng and Jin, 1994). Both zones include many common neoschwagerinid and verbeekinid genera such as *Neoschwagerina*, *Verbeekina*, *Afghanella* and *Pseudodoliolina*. Other schwagerinid genera include *Parafusulina*, *Chusenella*, *Schwagerina* and *Pseudofusulina*. The overlying fusulines are characterized by the presence of *Yabeina*, with the *Yabeina gubieri* and *Metadolliolina multivoluta* zones recognized (Xiao et al., 1986). Common genera within these two zones include *Yabeina*, *Metadolliolina*, *Lepidololina*, *Sumatrina*, *Kahlerina*, *Lantschichites* and *Chenella*. Both zones were conventionally ascribed to the Capitanian stage (Xiao et al., 1986; Zhang and Wang, 2018; Shen et al., 2019b). However, the recent study of the fusulines from the Tsunemori Formation in Japan suggests that *Lepidololina*, *Sumatrina* and *Kahlerina* range downward to the Wordian Stage (Davydov and Schmitz, 2019). Consequently, the base of the *Yabeina* Zone in South China corresponds to the upper part of the Wordian Stage. In the late Guadalupian, with the extinction of large-sized schwagerinids and neoschwagerinids, the remaining fusulines are dominated by small schubertellids and ozawainellids such as *Lantschichites*, *Dunbarula*, *Codonofusiella* and *Reichelina* in South China and Panthalassa (Ota and Isozaki, 2006; Wignall et al., 2009; Kasuya et al., 2012), which were grouped into the *Lantschichites minima* Zone (Zhang and Wang, 2018; Shen et al., 2019b) (Fig. 5).

By contrast, the Guadalupian fusulines from North America are dominated by diverse schwagerinids and small schubertellids (Wilde,

2000; Yang and Yancey, 2000; Nestell et al., 2006, 2019). The Road Canyon and Word formations in the Glass Mts., Texas contain diverse *Parafusulina* species, which were divided into five zones: the *Parafusulina boesei*, *P. rothi*, *P. trumptyi*, *P. sellardsi* and *P. antimonioensis* zones in ascending order (Yang and Yancey, 2000). The overlying Vidrio Formation or equivalent formations in the Guadalupe Mts. is characterized by diverse *Polydiexodina* species with small fusulines such as *Rauslerella*, *Reichelina* and *Codonofusiella* (Yang and Yancey, 2000; Nestell et al., 2006). Those fusulines were grouped into the *Polydiexodina shumardi* Zone (Yang and Yancey, 2000). The base of this zone was traditionally regarded as the base of the Capitanian Stage. However, according to the latest high-precision U-Pb dates, the base of this zone corresponds to the upper part of the Wordian Stage (Davydov and Schmitz, 2019). After the extinction of the large *Polydiexodina* species, the overlying fusulines are dominated by small taxa such as *Codonofusiella*, *Reichelina* and *Paradoxiella*, which were named as the *Reichelina lamarensis* Zone (Yang and Yancey, 2000). Equivalent fusulines were reported from the upper part of the Yates Formation in the Guadalupe Mts. as well (Nestell et al., 2006, 2019). Interestingly, *Yabeina texana*, the only neoschwagerinid species in North America, occurs in the Lamar Limestone and the overlying Tansill Formation in the GMNP area where it coexists with *Reichelina* and *Codonofusiella* (Nestell et al., 2006). This assemblage is also present in the equivalent strata in the nearby Apache Mountains (Nestell et al., 2019). Its emergence in North America is enigmatic. The smaller fusulines that prevailed after the extinction of *Yabeina texana* were ascribed to the *Lantschichites splendens* Zone (Yang and Yancey, 2000) (Fig. 5).

Strong provincialism makes correlations between the Tethyan region and the North American successions using fusulines difficult (Ross, 1967; Zhang and Wang, 2018). For example, North America is dominated by the *Parafusulina-Polydiexodina* lineage. But, reliable *Polydiexodina* is not present in the Tethyan region. Moreover, *Parafusulina* species played a subordinate role in biostratigraphy in the Tethyan region. Similarly, neoschwagerinids such as *Neoschwagerina*, *Yabeina*, and *Lepidoliolina* dominate the Tethyan region, but they are almost absent in North America except for some exotic terranes in British Columbia, Canada. Although *Yabeina texana* has been reported from North America, this species is substantially different from all other *Yabeina* species in the Tethyan region. With the disappearance of larger schwagerinids and neoschwagerinids in North America and Tethyan region, the smaller fusulines such as *Lantschichites* and *Reichelina* dominated assemblages in both regions. However, whether or not they are synchronous remains even more so than the conodont correlations (Fig. 5).

3.3. Ammonoids

The temporal resolution of Permian and especially Guadalupian ammonoid biostratigraphy is coarser in South China and North America than that of conodonts and fusulinids, and has not been well established globally (Leonova, 2011, 2018; Korn and Klug, 2015). The Guadalupian type region is characterized by a succession of three ammonoid zones of successive cyclobin genera: *Demarezites*, *Waagenoceras*, and *Timorites*. Before GSSPs were established on the basis of conodont zones, the *Demarezites* Zone signified the Roadian, the *Waagenoceras* Zone the Wordian, and the *Timorites* Zone the Capitanian stages (Glenister and Furnish, 1987). Here we discuss five mostly global and China-based zones that have been recognized for Guadalupian strata (Fig. 5):

3.3.1. Altudoceras-paraceltites Zone

This zone has a wide distribution in South China. It is characterized by more primitive *Altudoceras* and *Paraceltites*. In addition to these two well-known genera, other associated ammonoids include *Daubichites*, *Erinoceras* and *Shangraoceras* from Zhejiang, Fujian, Anhui and other localities of South China. In North America, Leonova (2018) proposed the *Daubichites fortieri-Demarezites ovensi* Zone for the Roadian Stage. The former species is known from the Arctic and comparable species are

known from Paleotethys, North America and Australia. All species of *Demarezites* are restricted to the Roadian and are known from both North America and Paleotethys. *Daubichites* is also present in the *Altudoceras-Paraceltites* Zone in southeast China. Therefore, the two zones between North America and South China are at least in part correlative. It is noteworthy that an endemic ammonoid species, *Nodogastrioceras discum*, is extremely abundant in the basal part of the Kuhfeng Formation in southeast China. This species, together with another species within this genus, *N. dongwuliense* from the Dongwuli Member, Dingjiashan Formation, Lijia, Jiangde, west Zhejiang, are both restricted to the Roadian–Wordian (Zhou, 2007) and its horizon is very close to the first occurrence of the conodont *Jinogondolella nankingensis* at the Zhengpanshan section near Nanjing, South China, which also has high-precision geochronologic dates (Fig. 3D).

3.3.2. Guiyangoceras Zone

This zone was found in Guiyang County, Hunan Province, South China and includes *Guiyangoceras* and *Liuzhouceras*. *Guiyangoceras* is so far considered as the most primitive species of the cyclobids. The ammonoids associated with *Liuzhouceras* in Guangxi, South China include *Shengoceras* and *Strigogoniatis*, both are found in the lower part of the Kuhfeng Formation in southeast China. *Mexicoceras*, as the last representative of Kufengoceratinæ, has also been found to be abundant in the Delaware Basin in Texas as an important index genus of the Wordian *Waagenoceras* Zone. The Wordian Stage was named after the Word Formation in the Glass Mountains of West Texas, which generally corresponded to the classical *Waagenoceras* Zone (Böse, 1917; Miller, 1938; Miller and Furnish, 1940; Furnish, 1973), and contains the genera *Neogeoceras*, *Sosioceras*, *Anatsabites*, *Adrianites*, *Mexicoceras* and *Waagenoceras*. *Waagenoceras* was found from the Jushitan Formation of Gansu Province, the Wenbisan Formation of Fujian Province, and the Shaiwa Formation of Guizhou Province, China, but the conodont-based GSSP was chosen within the Getaway Member of the Cherry Canyon Formation, making its correlative boundary horizon within the Word Formation succession. Precise correlation of the *Waagenoceras* Zone still needs more study.

3.3.3. Timorites Zone

Capitanian ammonoids are common in basin and slope deposits of the GMNP region, and the stage was long considered to be represented by the *Timorites* Zone. Advanced species of *Waagenoceras*, with more numerous and more denticulate lobes, also occur through this zone. In China, *Timorites* is rare, although it has been found from exotic limestone blocks within the Neotethyan ophiolite mélange in southern Tibet and the Shaiwa Formation in Guizhou and Yunnan provinces. The correlation between the upper and lower levels of this zone needs additional clarification.

3.3.4. Roadoceras-Doulingoceras Zone

This zone is mainly found in Hunan Province and contains *Altudoceras*, *Paraceltites*, *Roadoceras*, *Doulingoceras*, *Strigogoniatis* and *Cibolites*. Other than *Doulingoceras*, all of these genera are common in what is regarded as the upper *Timorites* Zone in West Texas. Based on the phylogenetic evolution of the ammonoids, the *Roadoceras-Doulingoceras* Zone is considered more primitive than the Capitanian *Eoaraxoceras rughentsevi-Kingoceras kingi* Zone. This zone was previously assigned to the basal Wuchiapingian in South China (Jin et al., 1994, 1997), but ammonoid phylogenetic evolution indicates an older age (Fig. 5).

3.3.5. Eoaraxoceras spinosai-Difuntites furnishi Zone

Zhou (2017) established this zone based on collections from the Shaiwa Formation, Guizhou, South China. Representatives of this zone include *Eoaraxoceras spinosai*, *Difuntites furnishi*, *Stacheoceras shaiwaense*, *Epadianites involutus* and *Xenodiscus* sp. The *Eoaraxoceras rughentsevi-Kingoceras kingi* Zone marks the topmost part of the Capitanian in Coahuila, Mexico, North America (Miller and Furnish, 1940), and these taxa

are known from both North America and Paleotethyan localities. Apparently, the zones in the two regions are correlative. Zhou (2017) proposed that there is an overlap between the lower part of the Lopingian of South China and the upper part of the Guadalupian in North America because he mistakenly used data suggesting that the Guadalupian ammonoids occurred in the “Lopingian” at the Shaiwa section in Guizhou, South China. However, previous studies and subsequent field investigation reveal no evidence that the ammonoid-bearing Shaiwa Formation belongs to the lower part of the Lopingian. On the contrary, the conodonts and fusulinids indicate that the Shaiwa Formation is very likely of latest Guadalupian age (Hao et al., 1999; Wang et al., 2016; Shen et al., 2019b).

4. Geochronology

During the past decade, high-precision U-Pb geochronological studies of ash beds from the Lopingian and the Permian-Triassic boundary interval have provided the basis for previously unattainable insights into the rates of biological and geological processes (Shen et al., 2011, 2019a; Burgess et al., 2014; Burgess and Bowring, 2015; Baresel et al., 2017a, 2017b; Yang et al., 2018; Zhong et al., 2020). Although the development of an equally high-resolution temporal framework for Guadalupian events lagged behind for some time, great progress has been made in recent years. These studies have focused on the U-Pb geochronology of the Guadalupian Series in South China and North America, each of which contain multiple volcanic ash layers (Wu et al., 2017, 2020; Ramezani and Bowring, 2018; Davydov et al., 2018a; Zhang et al., 2019a; Zhong et al., 2020; Yan et al., 2020).

The Global Boundary Stratotype Section and Point (GSSP) for the base of the Roadian Stage at the Stratotype Canyon of the GMNP has not yet yielded any ash beds (Hurd et al., 2016). The Kuhfeng Formation in southeast China, which represents a transgressive unit overlying the late Cisuralian Chihsia Formation (Xu et al., 2004), serves as a suitable correlative. The base of the Kuhfeng Formation at the Pingdingshan section in Chaohu, Anhui Province, contains an ash bed with a weighted mean $^{206}\text{Pb}/^{238}\text{U}$ date of 272.95 ± 0.11 Ma (Wu et al., 2017).

The Kuhfeng Formation is well exposed along a new highway at the type locality of *Jinogondolella nankingensis* in the Zhengpanshan section, Jiangsu Province. Here we present new U-Pb zircon geochronology from two ash beds from this section, one 10 cm below the first occurrence of *J. nankingensis* and another 25 cm lower at the Kuhfeng/Chihsia formational boundary. They produced weighted mean $^{206}\text{Pb}/^{238}\text{U}$ dates of $273.01 \pm 0.14/0.19/0.35$ Ma ($n = 5$, MSWD = 1.6) and $273.14 \pm 0.13/0.19/0.35$ Ma ($n = 6$, MSWD = 0.31), respectively, by the U-Pb CA-ID-TIMS technique, following the same methodology and protocols (e.g. U-Pb tracer) employed by Shen et al. (2019a) and Wu et al. (2020) (Figs. 3D, 5, 6; Table 1). The 273.01 ± 0.14 Ma date from Jiangsu is statistically indistinguishable to the 272.95 ± 0.11 Ma date from Anhui (Wu et al., 2017) mentioned above and provides a direct, high-precision, calibration of the first occurrence of the conodont *J. nankingensis* at its type locality (Jin, 1960) in South China. Although some weakly serrated gondolellids have been found from the uppermost part of the Chihsia Formation in South China, more work is necessary to clarify their taxonomic affinity. Assuming that the first occurrences of *J. nankingensis* in South China and North America were synchronous, the 273.01 ± 0.14 Ma date serves as the best calibration for the base of the Guadalupian Series at present.

Two recently reported, high-precision, U-Pb CA-ID-TIMS dates of 274.00 ± 0.12 Ma and 273.12 ± 0.13 Ma from Permian tuff beds in the periphery of the Okhotsk Massif, NE Russia, by Davydov et al. (2018b) have been used to calibrate the Roadian Stage (lower Guadalupian). The older of the two dates is derived from a tuff horizon immediately above a mudstone unit with the ammonoid *Sverdrupites harkeri* in the lower part of the Khuren Formation. This interval also contains the bivalve *Kolymia cf. plicata* and the brachiopod *Tumarinia* sp., but no conodonts. The ammonoid *Sverdrupites harkeri* and other Roadian ammonoids are

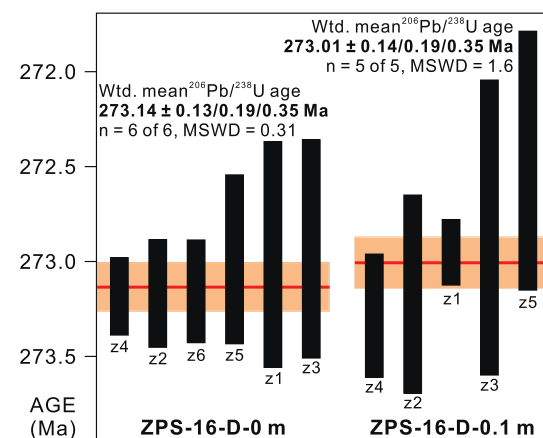


Fig. 6. Date distribution plots for the analyzed zircons from the samples of the two ash beds from the basal part of the Kuhfeng Formation at Zhengpanshan near Nanjing City, southeast China. Black bar heights are proportional to 2σ analytical uncertainty of individual analyses. Horizontal lines signify calculated sample dates and the width of the brownish band represents internal uncertainty in the weighted mean date at 95% confidence level. Data are shown in Table 1.

associated with the Roadian *Jinogondolella nankingensis gracilis* in the lower part of the transgressive Assistance Formation in Arctic Canada (Henderson and Mei, 2007). Therefore, Davydov et al. (2018b) interpreted the base of the Roadian Stage as at least 274 Ma, assuming that the ammonoid *Sverdrupites harkeri* in the Russian Far East and Canada, and the first occurrences of the conodont *Jinogondolella nankingensis gracilis* in Canada and *J. nankingensis* in the GMNP are all synchronous. Since the full range of occurrence of the ammonoid *Sverdrupites harkeri* and the conodont *Jinogondolella nankingensis gracilis* are unknown, such transcontinental interpolation for the base of the Guadalupian is challenging, even though both taxa are found in the lower part of the transgressive facies of the Assistance Formation in the Canadian Arctic. However, the correlation using *Sverdrupites harkeri* and *Jinogondolella nankingensis gracilis* is related to the first serrated forms in the Canadian Arctic. It is possible that a better comparison may be with the older serrated forms recently found in the upper part of the Bone Spring Formation and the Shumard Member of west Texas, and in the upper Chihsia Formation of south China. They would therefore be older than 273 Ma. The geochronologic data suggest that the lower part of the Khuren Formation in the Russian Far East is synchronous with the base of the Kuhfeng Formation or the top of the Chihsia Formation in South China (Davydov et al., 2018b; Wu et al., 2020).

Davydov et al. (2018b) interpolated a 277 Ma age for the base of the Guadalupian, but this age is too old and would shift much of the Chihsia Formation with typical Kungurian conodonts and fusulines into the Guadalupian in South China (Wu et al., 2017) (Fig. 3D). Davydov et al. (2018b) also extrapolated a 271 Ma age for the Roadian-Wordian boundary.

A few other high-precision dates are available from the Guadalupian Series in South China. An ash bed located 1 m above the 272.95 ± 0.11 Ma ash at the base of the Kuhfeng Formation in Anhui was dated as 271.038 ± 0.097 Ma (Wu et al., 2017). This sample is not constrained by conodont biostratigraphy because it is difficult to extract conodonts from chert. However, radiolarians and ammonoids are abundant in the lower phosphorus-bearing member in the nearby sections of the Chaohu area and a Roadian-Wordian *Pseudoolbaillella longtanensis*-*P. fusiformis* Assemblage Zone was recognized in this area (Kametaka et al., 2009; Ito et al., 2013) (Fig. 5).

Bentonite beds from the Guadalupian of west Texas, including GMNP, have been known since the pioneering work of P. B. King and other geologists (Nicklen, 2011; Nicklen et al., 2015; Wu et al., 2020,

Table 1

U-Pb isotopic data for CA-ID-TIMS zircon analyses for the two samples from the basal part of the Kuhfeng Formation at Zhengpanshan near Nanjing, Jiangsu, South China.

Sample Fractions	Composition				Ratios								Ages (Ma)																				
	Pb(c) (pg)	Pb*/Pb(c)	U (pg)	Th/U	$^{206}\text{Pb}/^{204}\text{Pb}$		$^{208}\text{Pb}/^{206}\text{Pb}$		$^{206}\text{Pb}/^{238}\text{U}$		err(2σ%)		$^{207}\text{Pb}/^{235}\text{U}$		err(2σ%)		$^{207}\text{Pb}/^{206}\text{Pb}$		err(2σ%)		$^{206}\text{Pb}/^{238}\text{U}$		err(2σ)		$^{207}\text{Pb}/^{235}\text{U}$		err(2σ)		$^{207}\text{Pb}/^{206}\text{Pb}$		err(2σ)		corr.
	(a)	(b)	(b)	(c)	(d)	(e)	(f)	(f)	(f)	(f)	(f)	(f)	(f)	(f)	(f)	(f)	(f)	(f)	(f)	(f)	(f)	(f)	(f)	(f)	(f)	(f)	(f)	(f)	(f)	(f)			
ZPS-16-D-0 m: $273.14 \pm 0.13/0.19/0.35$ Ma (n = 6, MSWD = 0.31)																																	
z1	0.35	11.4	81	0.90	632.5	0.284	0.043253	(.22)	0.31482	(1.98)	0.05281	(1.92)	272.97	0.60	277.9	4.8	320	44	0.33														
z2	0.29	25.4	159	0.61	1482.2	0.194	0.043286	(.11)	0.31151	(.83)	0.05222	(.81)	273.17	0.28	275.3	2.0	294	18	0.32														
z3	0.51	12.9	140	0.66	751.9	0.208	0.043248	(.22)	0.31395	(1.63)	0.05267	(1.57)	272.94	0.58	277.2	3.9	314	36	0.32														
z4	0.18	48.8	194	0.54	2888.3	0.171	0.043289	(.08)	0.30955	(.45)	0.05189	(.42)	273.19	0.20	273.8	1.1	279.4	9.7	0.39														
z5	0.25	16.3	89	0.61	957.6	0.192	0.043257	(.17)	0.30948	(1.30)	0.05191	(1.26)	272.99	0.45	273.8	3.1	280	29	0.30														
z6	0.29	42.2	268	0.55	2490.3	0.175	0.043285	(.10)	0.30995	(.55)	0.05196	(.53)	273.16	0.27	274.1	1.3	283	12	0.31														
ZPS-16-D-0.1 m: $273.01 \pm 0.14/0.19/0.35$ Ma (n = 5, MSWD = 1.6)																																	
z1	0.33	54.4	418	0.34	3390.1	0.107	0.043251	(.06)	0.30975	(.37)	0.05196	(.35)	272.95	0.17	273.98	0.89	282.8	8.1	0.36														
z2	0.33	11.4	82	0.51	694.0	0.162	0.043287	(.19)	0.31303	(1.78)	0.05247	(1.73)	273.17	0.52	276.5	4.3	305	39	0.34														
z3	0.41	19.7	179	0.51	1183.1	0.162	0.043230	(.29)	0.30814	(1.32)	0.05172	(1.22)	272.82	0.78	272.7	3.2	272	28	0.43														
z4	0.28	19.9	119	0.67	1149.6	0.210	0.043305	(.12)	0.31112	(1.07)	0.05213	(1.04)	273.29	0.32	275.0	2.6	290	24	0.32														
z5	0.26	7.6	43	0.49	468.1	0.155	0.043173	(.26)	0.31235	(2.68)	0.05250	(2.60)	272.47	0.68	276.0	6.5	306	59	0.35														

Notes: Mass fractionation correction of $0.18\%/\text{amu} \pm 0.04\%/\text{amu}$ (atomic mass unit) was applied to single-collector Daly analyses, where single Pb tracer was used.

All common Pb assumed to be laboratory blank. Total procedural blank less than 0.1 pg for U.

Blank isotopic composition: $^{206}\text{Pb}/^{204}\text{Pb} = 18.15 \pm 0.47$, $^{207}\text{Pb}/^{204}\text{Pb} = 15.30 \pm 0.30$, $^{208}\text{Pb}/^{204}\text{Pb} = 37.11 \pm 0.87$.

Corr. coef. = correlation coefficient.

Ages calculated using the decay constants $\lambda_{238} = 1.55125\text{E-}10 \text{ y}^{-1}$ and $\lambda_{235} = 9.8485\text{E-}10 \text{ y}^{-1}$ (Jaffey et al., 1971).

a Thermally annealed and pre-treated single zircon. Data used in calculation are in bold.

b Total common-Pb in analyses. Pb* is radiogenic Pb content.

c Total sample U content.

d Measured ratio corrected for spike and fractionation only.

e Radiogenic Pb ratio.

f Corrected for fractionation, spike and blank. Also corrected for initial Th/U disequilibrium using radiogenic ^{208}Pb and $\text{Th}/\text{Umagma} = 2.8$.

Table 1). However, few have been successfully dated (Wu et al., 2020, Table 1). A dark green bentonite near the base of the South Wells Limestone Member of the Cherry Canyon Formation at Monolith Canyon yielded a weighted mean $^{206}\text{Pb}/^{238}\text{U}$ age of 266.525 ± 0.078 Ma (Wu et al., 2020). This sample occurs stratigraphically above the Getaway Limestone, and therefore above the base of the Wordian at the Getaway Ledge section (Nicklen, 2011; Nicklen et al., 2015). Another ash bed 37.2 m below the GSSP of the Capitanian Stage (Fig. 4F) in the Manzanita Member at Nipple Hill had a legacy U-Pb date of 265.3 ± 0.2 Ma (Bowring et al., 1998) and has been re-dated to 265.46 ± 0.27 Ma using the modern EARTHTIME analytical protocols (Ramezani and Bowring, 2018).

Recently, two additional high-precision U-Pb dates have been added to the dataset. One ash bed from the lower Pinery Member of the Bell Canyon Formation at the Frijole section yielded a weighted mean $^{206}\text{Pb}/^{238}\text{U}$ age of 264.23 ± 0.13 Ma. Another bentonite layer from 20 m above the base of the Rader Limestone of the Bell Canyon Formation at the Patterson Hills (Back Ridge) section, which correlates with the fusuline *Polydiedoxina* Zone and the conodont *Jinogondolella postserratata* Zone, yielded a weighted mean $^{206}\text{Pb}/^{238}\text{U}$ age of 262.127 ± 0.097 Ma (Fig. 4A). Based on these dates and associated conodonts, the age-stratigraphic model of Wu et al. (2020) placed the base of the Capitanian at 264.28 ± 0.16 Ma using a Bayesian age interpolation method and estimated the base of the Wordian at 266.9 ± 0.4 Ma.

Two ash beds at the lithologic boundary between the Kuhfeng Formation and the overlying Yinping Formation in the Chaohu area (Anhui Province) in southeast China were dated by the LA-ICPMS (in situ) U-Pb zircon technique (Zhang et al., 2019a, 2020). Both samples (CH-3 and PDS-5) yielded overlapping weighted mean $^{206}\text{Pb}/^{238}\text{U}$ ages of 261.6 ± 1.6 Ma and 261.5 ± 1.6 Ma, respectively. These two dates have been taken as evidence that at least a part of the Yinping Formation is of latest Capitanian age (Zhang et al., 2019a, 2020; Wei et al., 2020). However, they overlap the GLB age due to their low precision and are incapable of making a robust determination.

The age calibration for the base of the Wuchiapingian Stage (base Lopingian or GLB) has been controversial due to a widespread unconformity between the Maokou Formation and the overlying Lungtan/Wuchiaping/Heshan formations. Thus, either the end of the ELIP basalt or the age of an ash bed in the Wangpo Shale in the basal part of the Lungtan/Wuchiaping formations has been used as a proxy for the GLB. Two CA-ID-TIMS $^{206}\text{Pb}/^{238}\text{U}$ dates from rocks spatially associated with the Emeishan basalts have provided the closest age estimates for the GLB (basalt itself has not produced zircons for dating). A felsic ignimbrite interstratified with basalt from the Binchuan section (Yunnan Province) was dated at 259.09 ± 0.48 Ma (Zhong et al., 2014), whereas a tuff from the uppermost Puan volcanic succession (Guizhou Province) produced an age of 259.51 ± 0.21 Ma (Yang et al., 2018). Although both ages are statistically consistent within uncertainty, for the purpose of our overview (Fig. 5), we prefer the 259.51 ± 0.21 Ma GLB estimate of Yang et al. (2018). This is because the latter age has a better constrained stratigraphy above the Emeishan basalts and below the Lopingian Lungtan Formation and is more consistent with the CA-ID-TIMS geochronology cited and/or reported here in terms of U-Pb analytical (EARTHTIME) protocols (e.g. chemical abrasion details, U-Pb tracer, use of column chemistry, error propagation algorithm, etc.).

Yang et al. (2018) provided another U-Pb zircon date of 259.69 ± 0.72 Ma from a basal claystone in the immediately overlying Lungtan Formation from a drill core section in southwest China. This claystone bed is likely a volcaniclastic rock, which, together with other correlative claystones in the region, contains weathering products derived from the ELIP and marks the topmost part of the Emeishan basalts (He et al., 2010; Chen and Xu, 2019; Yan et al., 2020; Zhong et al., 2020). Thus, the latter age is stratigraphically closer to the GLB than the ELIP basalts below, because the base-Lopingian GSSP at Penglaitan is above the tuffaceous (carbonate) level and at the onset of the Lopingian transgressive tract in South China (Jin et al., 2006). No ELIP basalts are

exposed at the Penglaitan GSSP. Although the claystone with the age of 259.69 ± 0.72 Ma is closer to the GSSP level by correlation, its uncertainty is significantly larger than the 259.51 ± 0.21 Ma age adopted here for the GLB. Nevertheless, all three ages from Zhong et al. (2014) and Yang et al. (2018) overlap within uncertainties and there is no substantial difference among them. Accordingly, the total duration of the Guadalupian Series in China is now estimated as 13.50 ± 0.25 Myr.

5. Chemostratigraphy

Isotopic geochemistry together with improved biostratigraphic data and high-precision geochronology are yielding not only unprecedented resolution for correlation of many stratigraphic intervals and various events, but also important information on environmental changes. South China and Guadalupe Mountains have rocks appropriate for high-resolution carbon isotope analyses based on whole rock samples (Chen et al., 2013; Jost et al., 2014; Wang et al., 2018a; Smith et al., 2020). In addition, the Guadalupian Series in both North America and South China contains abundant conodonts, which provide good material for carrying out a high-resolution analysis of oxygen and potentially Sr isotopes (Chen et al., 2013).

In total, 644 samples for conodonts, 1341 whole rock samples for $\delta^{13}\text{C}_{\text{carb}}$ and $\delta^{18}\text{O}_{\text{carb}}$ isotopes, 99 whole rock samples for $^{87}\text{Sr}/^{86}\text{Sr}$ ratios and 52 samples for conodont $\delta^{18}\text{O}_{\text{apatite}}$ from the Kungurian throughout the Guadalupian in both South China and the GMNP were collected and analyzed. Methodologies for $\delta^{13}\text{C}_{\text{carb}}$ and $\delta^{18}\text{O}_{\text{carb}}$, $\delta^{18}\text{O}_{\text{apatite}}$, $^{87}\text{Sr}/^{86}\text{Sr}$ isotopes are described in Appendix 1 and detailed results are provided in electronic spreadsheet form (Figs. 7, 9, 10; Appendix 2).

5.1. $\delta^{13}\text{C}_{\text{carb}}$ and $\delta^{18}\text{O}_{\text{carb}}$ profiles

5.1.1. Penglaitan section, Guangxi

In total 378 whole rock samples were collected from the uppermost part of the Chihsia Formation (upper Kungurian) to the basal part of the Lopingian Heshan Formation (lower Wuchiapingian) at the Penglaitan section in Guangxi Province, South China (Fig. 7B; Appendix 2). The $\delta^{13}\text{C}_{\text{carb}}$ values of most samples are between $1.3\text{\textperthousand}$ to $5.2\text{\textperthousand}$ with an average $3.7\text{\textperthousand}$ and the $\delta^{18}\text{O}_{\text{carb}}$ values are between $-7.8\text{\textperthousand}$ and $-2.8\text{\textperthousand}$ with an average value $-4.86\text{\textperthousand}$ and show no correlation with the $\delta^{13}\text{C}_{\text{carb}}$ values, which suggests little diagenetic alteration (Fig. 8A).

The profile from the Penglaitan section shows the $\delta^{13}\text{C}_{\text{carb}}$ values in the upper part of the Chihsia Formation are between $3\text{--}5\text{\textperthousand}$. This is followed by a distinct negative shift through the Kungurian-Roadian boundary interval to $1.1\text{--}3.0\text{\textperthousand}$. $\delta^{13}\text{C}_{\text{carb}}$ values recovered to an average $4.6\text{\textperthousand}$ in the lower part of the *Jinogondolella nankingensis* Zone. A relatively minor negative shift of $\sim 1.1\text{\textperthousand}$ occurred around the boundary between the *J. aserrata* Zone and *J. postserratata* Zone, but this is not confirmed at the other sections. The upper Wordian and whole Capitanian Stage shows a steady state with some very minor fluctuations at an average value $\sim 3.5\text{\textperthousand}$ (Fig. 7B) indicating a stable environmental setting through this interval.

5.1.2. Dukou section, Sichuan

A total of 406 whole rock samples were collected through the Chihsia and Maokou formations at the Dukou section. Most $\delta^{13}\text{C}_{\text{carb}}$ values are between $1\text{--}5\text{\textperthousand}$ with an average value $3.36\text{\textperthousand}$ and the $\delta^{18}\text{O}_{\text{carb}}$ values are between $-9.5\text{\textperthousand}$ $\sim -2.9\text{\textperthousand}$ with an average value $-4.92\text{\textperthousand}$ with no correlation with the $\delta^{13}\text{C}_{\text{carb}}$ values (Fig. 8B; Appendix 2).

The $\delta^{13}\text{C}_{\text{carb}}$ values from the Chihsia Formation are mostly around 4\textperthousand with some minor fluctuations less than 1\textperthousand . The $\delta^{13}\text{C}_{\text{carb}}$ values in the uppermost part of the Chihsia Formation show a negative excursion from 4\textperthousand to $1.6\text{\textperthousand}$ in the uppermost part of the Chihsia Formation, then rapidly recovered to $3.6\text{\textperthousand}$ followed by another large negative shift spanning about 50 m around the Chihsia/Maokou lithologic boundary. Although the most negative value is not revealed due to the cover of the outcrop, the negative shift is $>3\text{\textperthousand}$ based on the values in the

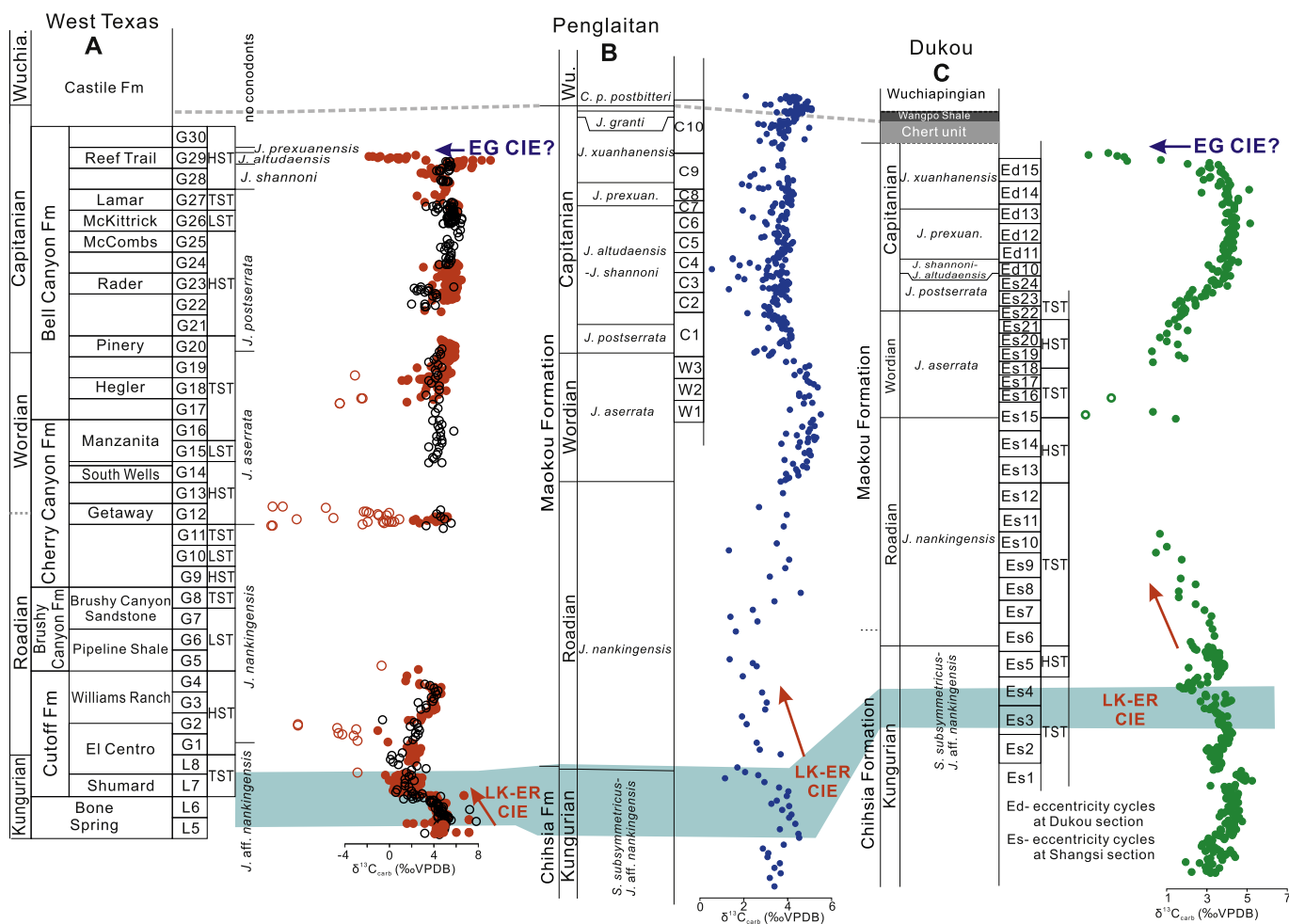


Fig. 7. $\delta^{13}\text{C}_{\text{carb}}$ chemostratigraphy of a composite section in West Texas, USA and two sections of South China and implications for their correlation. Cyclostratigraphy in the GMNP is after Kerans et al. (2014), in South China from Fang et al. (2015, 2017). Red open circles in the West Texas composite section are possibly suffered post-depositional diagenesis; black open circles are from unpublished data of Werner Buggisch. L-Leonardian; G-Gadalupian; W-Wordian; C-Capitanian. (For interpretation of the references to colour in this figure legend, the reader is referred to the web version of this article.)

Jinogondolella aserrata Zone in the uppermost Chihsia and lowest Maokou formations. $\delta^{13}\text{C}_{\text{carb}}$ values recovered to between 4–5‰ in the middle and upper parts of the Maokou Formation followed by a large negative excursion of >6‰ in the upper *J. xuanhanensis* Zone, which is possibly related to diagenesis associated with a sequence boundary (Fig. 7C; Appendix 2).

5.1.3. West Texas, North America

Since the units are thick and no single section from Kungurian throughout Guadalupian is available in the GMNP, we selected a few different well-exposed sections to construct a composite section to study the $\delta^{13}\text{C}_{\text{carb}}$ chemostratigraphy (Figs. 7A, 8C; Appendix 2). With excellent exposures, the lithologic units and formations within the GMNP can be traced over long distances, and stratigraphic correlations are straightforward (Rohr et al., 2000; Wardlaw, 2000; Kerans et al., 2013, 2014; Playton and Kerans, 2018). In total, 557 whole rock samples were collected from the GMNP.

For the upper Kungurian to lower Guadalupian, we selected the Stratotype Canyon section, which has been designated as the base-Guadalupian (also base-Roadian) GSSP section (Glenister et al., 1999). We measured the section from the upper part of the Bone Spring Formation through the Williams Ranch Member of the Cutoff Formation and sampled the “Roadian/Wordian boundary interval” from the Getaway Ledge carbonate section. The Brushy Canyon Formation below the Getaway carbonate unit is composed of an orange sandstone; no

carbonate samples were available (Fig. 4D). The Patterson Hills section and the Nipple Hill section with the base-Capitanian GSSP provide the samples for the Wordian and most of the Capitanian Stage. Finally, the SC1 section contains the Reef Trail Member of the latest Capitanian, which is overlain by the Castile evaporites (Fig. 4H).

$\delta^{13}\text{C}_{\text{carb}}$ values in the upper part of the Bone Spring Formation are basically stable at slightly higher than 4‰ and then decline to 0‰ near the lithologic boundary between the Bone Spring and the Cutoff formations, with an average value of 2.9‰ throughout the entire Shumard Member (Fig. 7A). $\delta^{13}\text{C}_{\text{carb}}$ values start to recover in the El Centro Member before returning to a level slightly above 4‰ in the Williams Ranch Member. Then, the $\delta^{13}\text{C}_{\text{carb}}$ values remain steady at this level until the topmost part of the late Capitanian Reef Trail Member (upper *Jinogondolella altudaensis* conodont Zone). A distinct negative shift from ~5‰ to –2‰ occurs in the *J. prexuanhanensis* Zone (Fig. 7A). This CIE in West Texas may be slightly earlier than the ED CIE in the upper part of the *J. xuanhanensis* Zone in South China. It is very likely the CIE in the top of the Reef Trail Member is due to diagenesis associated with the transition to the evaporites of the Castile Formation (Fig. 7; Hill, 1996). It is noteworthy that some scattered, very negative $\delta^{13}\text{C}_{\text{carb}}$ values (red open circles) that are present in the El Centro Member at the Stratotype Canyon section and the Getaway Member at the Getaway Ledge section, likely reflect meteoric diagenesis because the carbonates above the GSSP contain numerous molds after salt crystals. The upper part of the section is composed of alternating papery shale with carbonate and lack

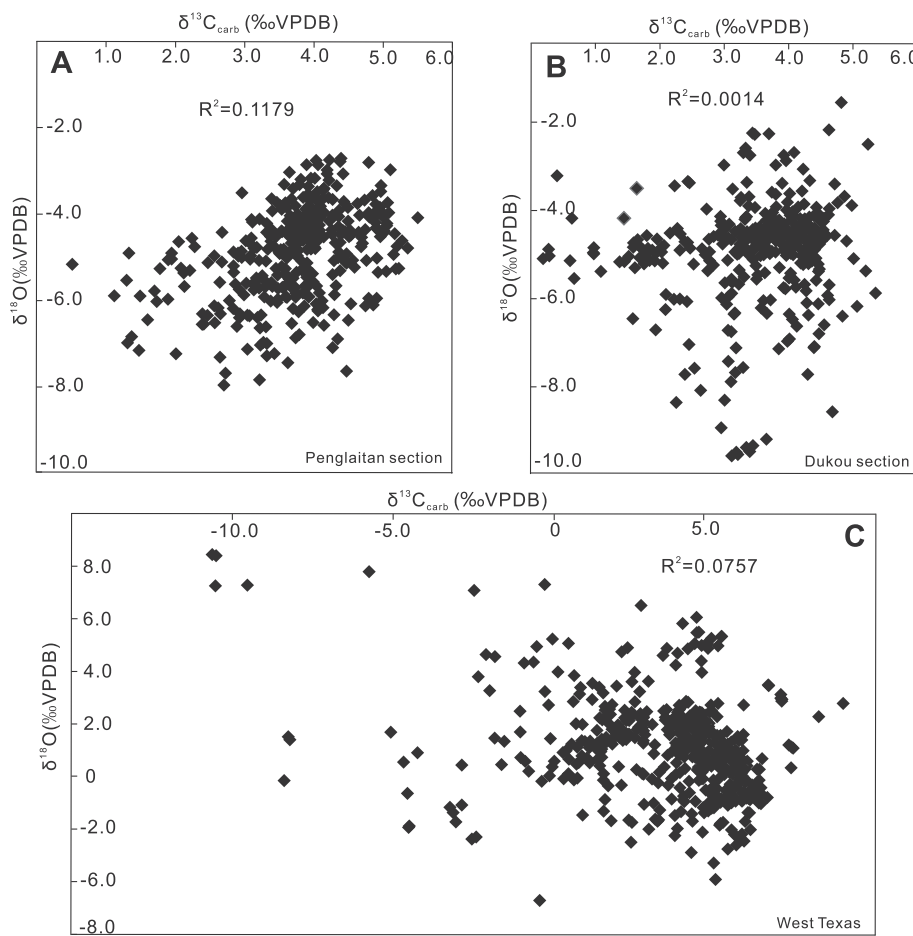


Fig. 8. Cross plots of $\delta^{13}\text{C}_{\text{carb}}$ and $\delta^{18}\text{O}_{\text{carb}}$ of the two sections in South China and all data from North America to show no correlation. A, Penglaitan section; B, Dukou section; C, all other data from North America.

conodonts. These rocks have probably been subjected to diagenetic alteration (Fig. 8C).

$\delta^{13}\text{C}_{\text{carb}}$ analyses based on whole rock samples from the same composite section in West Texas were also carried out by Buggisch et al. (unpublished data), but detailed data were not previously presented. We include these data in the profile (Fig. 7A, black open circles) to demonstrate similarity of results among different labs.

5.2. $^{87}\text{Sr}/^{86}\text{Sr}$ ratios

The Permian $^{87}\text{Sr}/^{86}\text{Sr}$ ratio has been widely used for calibrating ages (Veizer et al., 1999; Korte et al., 2006; Kani et al., 2008; Liu et al., 2013; Wang et al., 2018a; Garbelli et al., 2019) based on the comparison with the LOWESS curve of McArthur et al. (2012). The $^{87}\text{Sr}/^{86}\text{Sr}$ ratios continuously from the Carboniferous/Permian boundary until a low in the mid to late Capitanian (Kani et al., 2008, 2013; Liu et al., 2013; Wang et al., 2018a). This minimum has been constrained to the interval from the *Jinogondolella shannoni*/*J. altudaensis* to *J. xuanhanensis* conodont zones in the late Capitanian based on whole rock samples at the Penglaitan GSSP section (Wang et al., 2018a) (Fig. 9). It is an important marker for chemostratigraphic correlation between South China and North America.

The best materials for measuring $^{87}\text{Sr}/^{86}\text{Sr}$ ratios are brachiopod shells (Korte et al., 2006; Brand et al., 2012; Garbelli et al., 2019) and conodonts. However, most brachiopods from the Guadalupian Series in the GMNP are more or less silicified, and thus not suitable for Sr isotope analysis. In addition, brachiopods are only abundant in a few horizons, and a high-resolution set of samples based on brachiopod shells is not

available (Cooper and Grant, 1972; Olszewski and Erwin, 2009). Thus, we collected whole rock samples from both the Penglaitan section in South China (Wang et al., 2018a) and the Guadalupian Series in the GMNP, West Texas.

The results from the composite section in the GMNP show a generally declining trend from the upper Kungurian until the base of the Getaway Member. A similar trend from late Kungurian to the middle Wordian is also present at Penglaitan, South China (Fig. 9), but the actual values seem to vary at the fourth decimal, which is significant. If this trend were correlative between West Texas and Penglaitan, the interval between the Pipeline Member and the Getaway Member in the GMNP would have been in the early Wordian. However, the values between West Texas and Penglaitan are very different (Fig. 9). The $^{87}\text{Sr}/^{86}\text{Sr}$ ratios rebounded in the Getaway Member at the Getaway Ledge section followed by a valley in the Pinery Member near the Wordian/Capitanian boundary. An increase in salt pseudomorphs in the carbonates suggests this rebound may be due to increased clastic deposits at the Getaway Ledge section derived from more intensive continental weathering. Similarly, the two fluctuations in the $^{87}\text{Sr}/^{86}\text{Sr}$ ratio from the Hegler Member to the McCombs Member may also reflect later diagenetic effects following late Guadalupian restriction of the Delaware Basin (Fig. 9). Above the middle part of the McCombs Member, $^{87}\text{Sr}/^{86}\text{Sr}$ ratios declined steadily until the *Jinogondolella altudaensis* Zone in the upper part of the Reef Trail Member with the lowest value 0.70710; a similar value also occurs in the *J. prexuanhanensis* Zone at Penglaitan. Rock samples suitable for Sr isotopes analysis are not available above the Reef Trail Member because it is overlain by the Castile evaporite. Nevertheless, this lowest value is very likely biostratigraphically close to the late Guadalupian in South

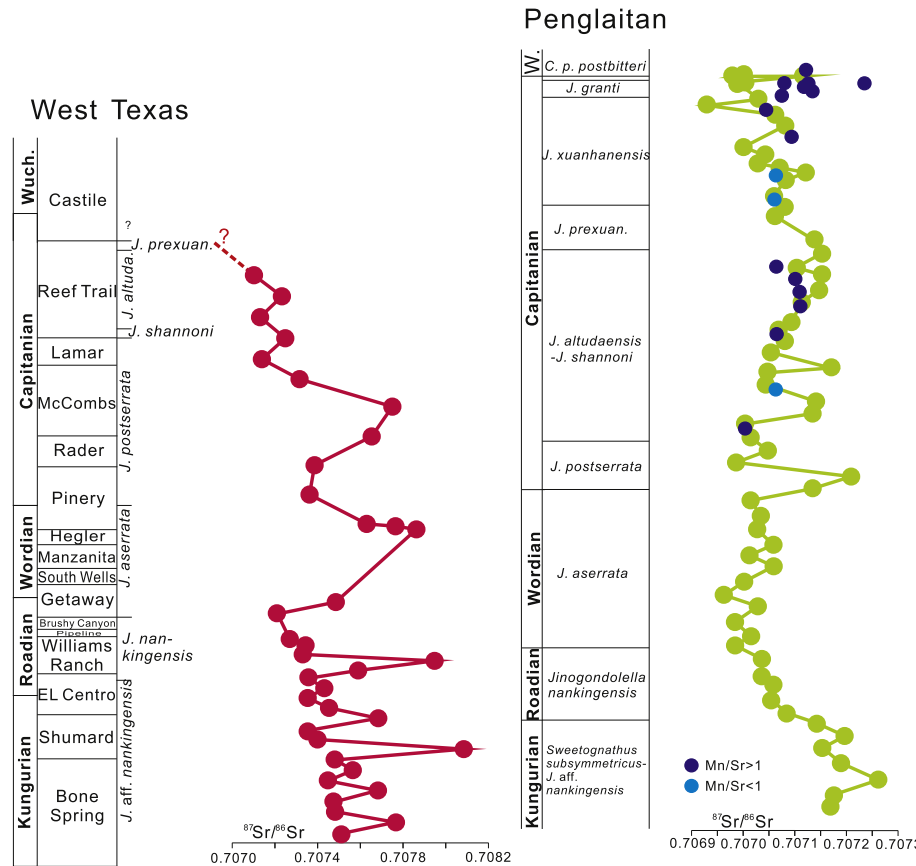


Fig. 9. $^{87}\text{Sr}/^{86}\text{Sr}$ ratios based on whole rock samples and their correlation between North America and South China. Data of blue circles are from Wang et al. (2018a). (For interpretation of the references to colour in this figure legend, the reader is referred to the web version of this article.)

China (Wang et al., 2018a). Generally, all the $^{87}\text{Sr}/^{86}\text{Sr}$ ratios in the GMNP are higher than those of South China, which makes correlation problematic. This may be due to the Delaware Basin in Texas becoming increasingly restricted near the end of the Guadalupian (King, 1942; Kendall and Harwood, 1989; Hill, 1996). The Castile Formation is made up almost entirely of mm thick anhydrite/carbonate couplets.

5.3. $\delta^{18}\text{O}_{\text{apatite}}$

We analyzed $\delta^{18}\text{O}$ in conodont apatite collected from the Guadalupian in South China and GMNP to reconstruct a paleotemperature history. We used the formula of Pucéat et al. (2010) to calculate paleotemperature and assumed the $\delta^{18}\text{O}_{\text{water}}$ was $-1\text{\textperthousand}$. Some $\delta^{18}\text{O}_{\text{apatite}}$ data from the Guadalupian in the GMNP were published by Chen et al. (2013), but have not been discussed. The combined results from Chen et al. (2013) and this study suggest that the $\delta^{18}\text{O}_{\text{apatite}}$ values from the upper Kungurian throughout the Guadalupian are between $20\text{--}21\text{\textperthousand}$ (VSMOW) with an average value $20.5\text{\textperthousand}$ in West Texas, and between $18\text{--}20\text{\textperthousand}$ with an average value $19.2\text{\textperthousand}$ in South China. No obvious excursion through the Guadalupian has been detected based on the samples from West Texas (Fig. 10). However, a vague positive shift ($1\text{--}1.3\text{\textperthousand}$) from the earliest Roadian to early Wordian is present at the Penglaitan section, which may suggest a $3\text{--}4\text{ }^{\circ}\text{C}$ cooling event. A negative excursion ($\sim 1\text{\textperthousand}$) in the top of the Capitanian at the Penglaitan section could indicate a minor ($\sim 4\text{ }^{\circ}\text{C}$) warming event (Fig. 10).

The higher $\delta^{18}\text{O}_{\text{apatite}}$ values from the GMNP samples could have been influenced by higher evaporative rates producing higher seawater $\delta^{18}\text{O}$ values in the semi-enclosed Delaware Basin (Korte et al., 2005). This is consistent with the higher $\delta^{18}\text{O}_{\text{calcite}}$ values of brachiopod shells from the GMNP in comparison to those from other areas (Korte et al., 2005). Alternatively Guadalupian, seawater temperatures in West Texas

could have been $3\text{--}4\text{ }^{\circ}\text{C}$ cooler than those in South China. This interpretation is consistent with the South China block situated in relatively low latitudes open to the Panthalassan Ocean (thus having higher seawater temperatures). In contrast, the Delaware Basin, may have been periodically affected by cold currents flowing south along the western margin of Pangea, as inferred from warm- and cold-water mixed brachiopod faunas during the Guadalupian (Shen and Shi, 2004; Shen et al., 2009).

6. Discussions of the Guadalupian correlation and major events

6.1. Latest Kungurian-early Roadian $\delta^{13}\text{C}_{\text{carb}}$ excursion (LK-ER CIE) and its correlation

The first occurrence of *Jinogondolella nankingensis* in the basal part of the Kuhfeng or Maokou Formation in South China has been widely used to correlate with the FAD of *J. serrata* in the GMNP of North America. However, there are some serrated forms (referred to *J. aff. nankingensis* in this paper) occur lower in both regions. The $\delta^{13}\text{C}_{\text{carb}}$ chemostratigraphy provides a crucial test of this biostratigraphic correlation. We have shown a distinct negative $\delta^{13}\text{C}_{\text{carb}}$ excursion at the Penglaitan and Dukou sections. The LK-ER CIE is $\sim 2\text{\textperthousand}$ at the Penglaitan section, and $\sim 2.5\text{\textperthousand}$ at the Dukou section (Fig. 7). The CIE ranges from the latest Chihidian to the earliest *J. nankingensis* Zone in the Maokouan at the Penglaitan section, and in the latest Chihidian at the Dukou section. These results suggests that the first occurrences of *J. nankingensis* with serrated platform margins may be slightly diachronous in different carbonate sections in South China, as discussed previously (Henderson and Mei, 2003; Shen et al., 2012; Wu et al., 2017; Henderson, 2018).

If the LK-ER CIE reflects a global warming event, the current base-Roadian GSSP within the El Centro Member at the Stratotype Canyon

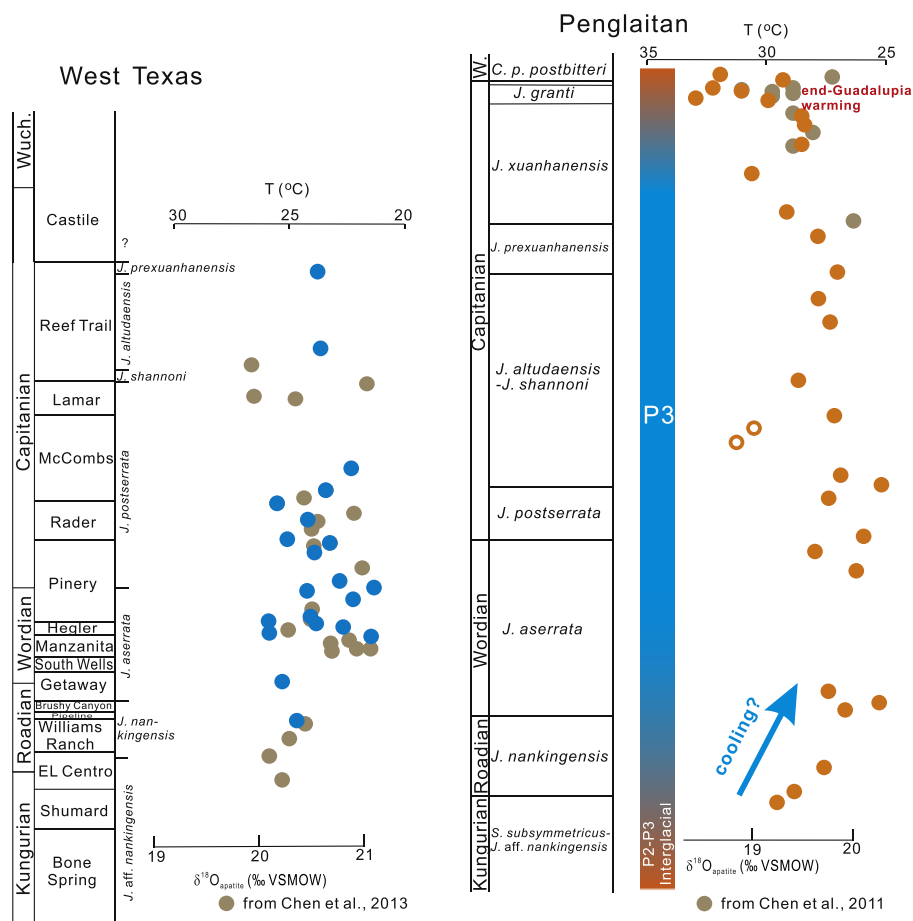


Fig. 10. $\delta^{18}\text{O}_{\text{apatite}}$ changes throughout the Guadalupian between North America and South China and their implications for climate changes. Two outlier values with open circles may be questionable.

section may lie above the base of the Maokou Formation of South China at Penglaitan, with the top of the Shumard Member nearly equivalent to the base of the Maokou Formation at Penglaitan, but slightly below at Dukou based on the onset of the CIE and cyclostratigraphy (Figs. 5, 7, 11). Although slight inconsistency in the correlation between the conodont biostratigraphy and $\delta^{13}\text{C}_{\text{carb}}$ chemostratigraphy is present, both data generally support the correlation between the top of the shumard member and the base of the Maokou Formation at Penglaitan. Above the early Wordian, the $\delta^{13}\text{C}_{\text{carb}}$ record shows no distinct changes in either South China and North America. This is consistent with the recent calibration of P3 glaciation in eastern Australia based on brachiopod shell-based $^{87}\text{Sr}/^{86}\text{Sr}$ calibration (Garbelli et al., 2019).

The LK-ER CIE has also been identified in several previous studies. The $\delta^{13}\text{C}_{\text{carb}}$ profile from the Naqing section in a slope setting in Guizhou, South China shows distinctive CIEs in the Cisuralian and Guadalupian (Buggisch et al., 2011). A relatively smaller CIE (1–2‰) is present in the “latest Kungurian” conodont *Mesogondolella lamberti-Sweetognathus subsymmetricus* Zone. However, the lower part of this conodont zone overlaps with the fusuline *Neoschwagerina craticulifera* Zone, of the Roadian Stage. Thus, whether this CIE is in the latest Kungurian or earliest Roadian remains unresolved (Henderson and Mei, 2003; Shen et al., 2012, 2019b), but appears to be broadly correlative with the LK-ER CIE in this study. Another minor negative CIE is present in the upper part of Roadian at the Naqing section, but occurs with the fusuline *Yabeina invuyei* and thus lies much higher than the LK-ER CIE.

A minor negative CIE of ~2‰ is also present in the uppermost part of the Chihsia Formation at the Tieqiao section in the Laibin area, Guangxi (Tierney, 2010). This excursion is within the conodont *Sweetognathus*

subsymmetricus Zone, and is correlative with the LK-ER CIE. As the sequence at Tieqiao was deposited as a transgressive succession, the lithology changes to pure thin-bedded chert above this negative CIE, so no higher samples are available (Xu et al., 2004; Shen et al., 2007).

A continuous $\delta^{13}\text{C}_{\text{carb}}$ curve was established through the Gongchuan section in the Bama Platform, Guangxi, South China (Liu et al., 2017a, 2017b). This section lacks conodonts and conflicting fusuline biostratigraphic schemes makes chemostratigraphic correlation difficult. According to Liu et al. (2017b), the *Makalaya pamirina* Zone in association with *Misellina claudiae* was assigned to the early Roadian. However, this fusuline zone is assigned to the middle Kungurian by other fusuline workers (e.g. Zhang and Wang, 2018). If the latter scheme is adopted, the broad minor negative excursion from the *Makalaya pamirina* Zone to the *Skinnerella-Parafusulina* Zone at least overlaps with the LK-ER CIE documented in this paper.

The LK-ER CIE is supported by studies of well-preserved brachiopod shells. Korte et al. (2005) documented a minor negative shift of slightly less than 1‰ around the Kungurian-Roadian boundary (=CGB) interval followed by a positive shift from the middle Guadalupian, but the temporal resolution is low because brachiopod shells were sampled in some horizons only. In summary, there is wide evidence from different continents for a negative excursion from latest Kungurian to earliest Roadian (Fig. 7).

The positive $\delta^{13}\text{C}_{\text{carb}}$ excursion corresponds with the decline of $^{87}\text{Sr}/^{86}\text{Sr}$ (Fig. 11), and may indicate a cooling shift into the P3 glaciation and a reduction in chemical weathering. In addition, the Pangean dispersal beginning with the IR may have been associated with mid-oceanic spreading, increased eruption of mantle materials and a

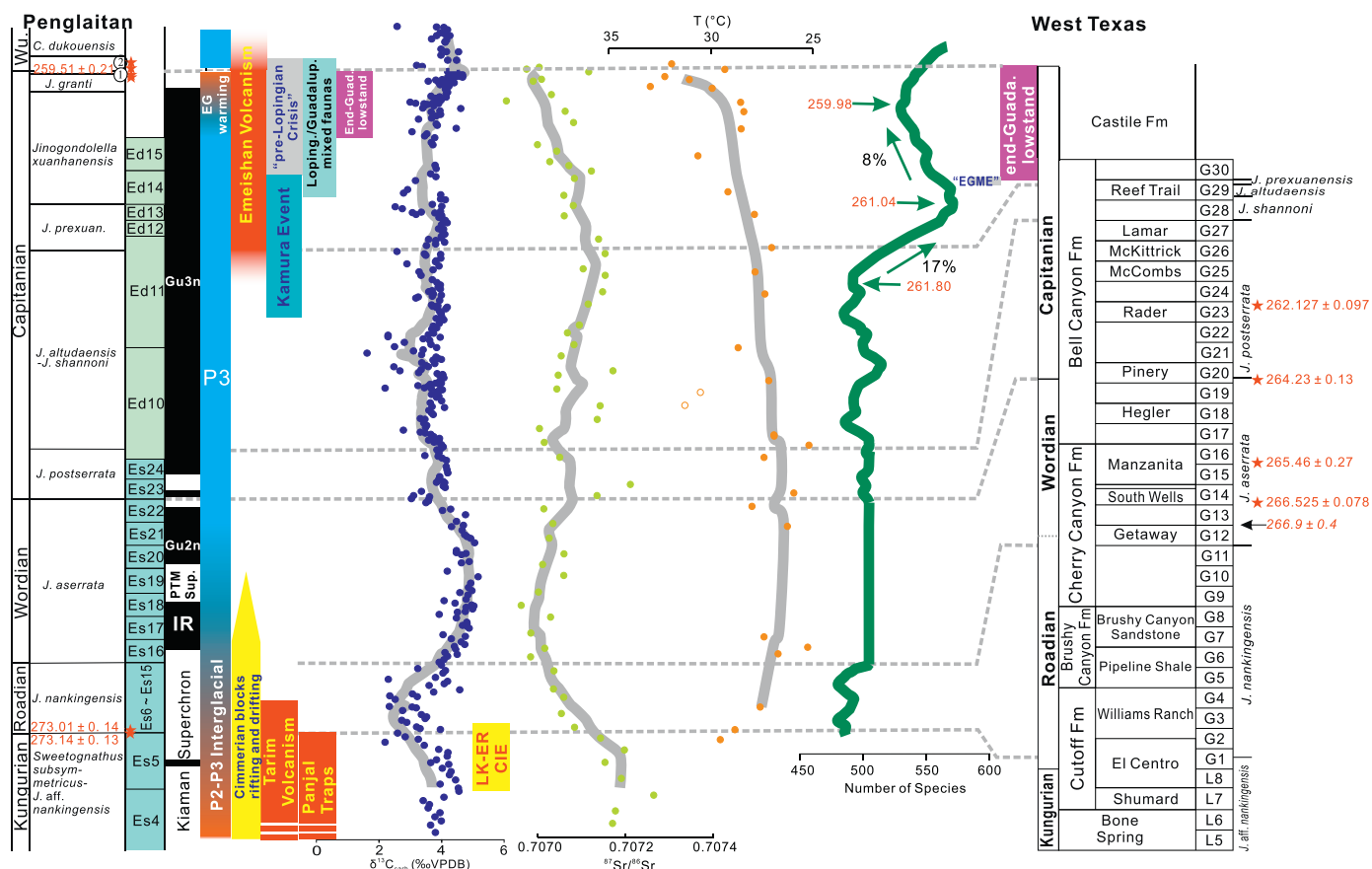


Fig. 11. A summary for the temporal correlation of geologic, paleoclimatic and biological events between South China and North America during the Guadalupian Epoch. Geochronologic dates in North America are from Wu et al. (2020). Cyclostratigraphy in the GMNP is after Kerans et al. (2014), in South China from Fang et al. (2015, 2017). Diversity pattern is calculated from Fan et al. (2020) and adjusted with the new dates in this study (scaled to time). Magenetostratigraphy is from Hounslow and Balabanov (2018).

reduction in the $^{87}\text{Sr}/^{86}\text{Sr}$ ratio. Or both might play roles in the declining $^{87}\text{Sr}/^{86}\text{Sr}$ ratio.

6.2. Climatic transition around the Cisuralian/Guadalupian boundary

The CGB interval has received less attention from the Permian community in the absence of any major biotic crisis or tectonic events. However, recent studies suggest that it is probably one of the most critical climatic transitions during the LPIA (Liu et al., 2017a, 2017b). The negative carbon isotope excursion (LK-ER CIE) around the CGB is temporally consistent with an interglacial warming phase between the P2 (late Artinskian throughout Kungurian) and P3 glaciations (late Wordian-early Capitanian) (Garbelli et al., 2019). However, the $\delta^{18}\text{O}_{\text{apatite}}$ values (Fig. 7) suggest that a positive shift from early Roadian to early Wordian may be related to the transition from this interglacial phase to P3 phase. More data from the upper part of the Chihsia Formation are needed to evaluate these proposals (Figs. 10, 11).

The climate dynamics of this interglacial warming is complicated. Temporally, the late Artinskian-Kungurian interglacial warming is consistent with the end of the Himalayan magmatic province (Panjal Traps volcanism) (Shellnutt et al., 2011; Stojanovic et al., 2016; Shellnutt, 2018) and the Tarim Large Igneous Province (both c. 290–270 Ma) (Zhang et al., 2010; Yang et al., 2013, 2017; Xu et al., 2014). Both the Panjal Traps and the Tarim LIP may have generated increased thermal output (Tang and Li, 2016) and degassing of CO_2 in connection with mantle superplume activity and ended the LPIA (Fig. 11).

The climatic warming during the late Cisuralian and early Guadalupian has been evident from the faunal changes within the Neotethys

Ocean and is consistent with sequence stratigraphy and sea-level changes in North America. Warm faunas, including conodonts (Yuan et al., 2016, 2020b), fusulines (Zhang et al., 2019b) and brachiopods (Shen et al., 2013b; Shen, 2018) and extensive carbonate deposits (Zhang et al., 2013) emerged in the Cimmerian blocks and the Lhasa Block during the latest Kungurian. The emergence of these warm faunas has been interpreted as the result of northward drifting of the Cimmerian blocks and the Lhasa Block. However, a more plausible interpretation is that this warming event reflects interplay of both tectonic movement and global warming (Shen and Shi, 2009; Shen et al., 2013b; Zhang et al., 2013; Yuan et al., 2016) (Fig. 11).

The climatic warming is also consistent with the sea-level changes in both North America and South China. Along the western escarpment of the GMNP, the Cutoff Formation overlies the platform deposits of the Victorio Peak Formation, and the slope and basin deposits of the correlative Bone Spring Formation. The transitional evolution from *Mesogondolella* to *Jinogondolella* took place just above the boundary between the Bone Spring Formation and Cutoff Formation during a pronounced rise of sea level (Kerans and Ruppel, 1994; Lambert, 2000). The Shumard and El Centro members were deposited during a transgression, and the Williams Ranch Member accumulated during a sea level highstand; the sequence boundary is defined by the Cutoff/Brushy Canyon contact. Thus, the Cutoff Formation records a single composite third-order sequence. Similarly, the Guadalupian Kuhfeng Formation in South China was also initiated by a transgression at the base as indicated by the rapid lithologic change from the massive limestone of the Chihsia Formation to a cherty facies of the Kuhfeng Formation with nodules. Above that, a few third-order high-frequency sequences were recognized

(Xu et al., 2004). Thus, the correlation potential with this physical event is also significant.

6.3. Cyclostratigraphy and correlation

Cyclostratigraphic correlation between South China and the GMNP is not straightforward (Figs. 7, 11). A total of 30 high-frequency sequences (HFSs) are recognized in the Guadalupian in GMNP (Kerans et al., 2014; Hurd et al., 2016) where the Roadian, Wordian and Capitanian are composed of ca. 11.75 HFSs, 7.5 HFSs and 10.75 HFSs, respectively. As the GLB is probably located in the lower part of the Castile Formation, the Capitanian could contain additional HFSs.

It is unclear whether the HFSs in the GMNP represent eccentricity cycles (EC). If the HFSs in the northwestern margin of the Delaware Basin during the Guadalupian are controlled by the 405 kyr eccentricity, the base of the Shumard Member is about 21.25 HFSs below the basal Pinery Limestone Member (Kerans et al., 2014; Playton and Kerans, 2018) or 272.8 ± 0.4 Ma, which is consistent with the base-Roadian in South China.

Wu et al. (2020) estimated an average duration of 440 ± 12 kyr for each HFS based on dates from the top of the Rader Limestone Member and the basal South Wells Member. The top of the Reef Trail Member is about 7 HFSs above the date from the Rader Member. Accordingly, the top of the Reef Trail Member can be estimated at 259.05 ± 0.15 Ma, which constrains the GLB in the topmost of the Reef Trail Member, and is in contradiction with the conodont biostratigraphy. Since the GLB may lie in the lower part of the Castile Formation, even if the estimation error is considered, the three conodont zones above the *Jinogondolella prexuanhanensis* Zone would have to have an unusually short duration. Thus, we prefer to view the HFSs as controlled by the 405 kyr EC. The dates from the basal Pinery Limestone Member and the basal South Wells Member (Wu et al., 2020) contain 6 HFSs with an average duration of each HFS of ca. 380 ± 30 kyr, which is consistent with the 405 kyr EC. In this case, correlating the date from the Rader Limestone Member to the top of HFS G24 instead of the top of G23 would make the dates and the ECs fit in with each other. Additional local stratigraphic work is needed to test this suggestion (Figs. 7, 11). Under this revised correlation scheme the top of the Reef Trail Member would be ca. 259.7 Ma, older than the GLB in South China, and consistent with the GMNP conodont biostratigraphy.

Cyclostratigraphic studies at the Dukou and Shangsi sections in Sichuan suggested that the Roadian, Wordian and Capitanian in South China are composed of 9, 7 and at least 8.5 ECs, respectively (Fang et al., 2015, 2017). A similar study at the Tieqiao section in Guangxi identified 9.5 Capitanian ECs (Xue et al., 2015). Cyclostratigraphy was also conducted in the Kuhfeng Formation in Chaohu, Anhui Province, South China (Yao et al., 2015), but it remains difficult to correlate to the carbonate sections in South China due to a lack of high-resolution conodont biostratigraphy.

Although the base of the Roadian Stage is located within a transgressive systems tract in both South China and West Texas, fewer ECs were recorded in South China than the number of HFSs in the GMNP. The cycle numbers of the Wordian Stage in South China and West Texas are roughly comparable. The Wordian started from the basal part of a transgressive systems tract at the Dukou, Tieqiao and Naqing sections in South China (Mei et al., 1999; Fang et al., 2015). If this is a global transgression, the base of the Wordian may be lower than the Getaway Limestone Member, possibly at the base of HFS G11 (Kerans et al., 2014), which is about 9.25 HFSs below the basal Pinery Limestone Member and can be estimated at 268.0 ± 0.4 Ma. The Roadian and Wordian would thus be composed of about 10 and 9.25 HFSs in West Texas, respectively. It appears that the Roadian and Wordian in South China have fewer cycles than in West Texas. However, the duration of the Roadian Stage based on cyclostratigraphy (3.7 ± 0.4 Myr) is shorter than that based on the U-Pb dates (5.0 ± 0.4 Myr) in South China. Therefore, there probably missing ECs in South China. This might also be

responsible for the different lower to middle Capitanian cycle framework between the Tieqiao and Shangsi sections in South China. Specifically, the *Jinogondolella shannoni* - *J. altudaensis* Zone contains 6 ECs at the Tieqiao section, whereas only 1 EC is recognized at the Dukou section. The possibility of conodont species diachronism between South China and West Texas must be considered. The base-Capitanian is located in transgressive system tracts in both regions and the biostratigraphic boundary is considered very close as well. Although the Capitanian HFSs in the GMNP are incomplete, the cycles reveal that durations of the Capitanian conodont zones differ between the two regions. The *J. postserratata* Zone is apparently much longer, while the *J. shannoni* - *J. altudaensis* Zone is much shorter in West Texas than in South China. The dates and chemostratigraphic results presented in this paper should encourage further cyclostratigraphic research to test the biostratigraphy and cycles between the two regions.

6.4. The Illawarra Reversal (IR) and its correlation

The IR has great potential for Guadalupian marine and terrestrial correlation. However, the age for the beginning of the IR is still controversial (Lucas, 2017b). It has been placed in the earliest Wordian (Hounslow and Balabonov, 2018), middle Wordian (Jin et al., 1999; Steiner, 2006; Henderson et al., 2012; Lanci et al., 2013; Shen et al., 2013a, 2019b; Henderson and Shen, 2020) or earliest Capitanian (Menning, 2000; Isozaki, 2009).

Irving and Parry (1963) first classified the Kiama Reverse Superchron from the Gerringong Volcanics located in the southern Sydney Basin of eastern Australia. A normal polarity was reported in the chocolate shales of the Narrabeen Group several hundred meters higher in the section (Irving and Parry, 1963) and the inferred polarity transition was named the Illawarra Reversal. The age of IR in the Sydney Basin was estimated at 263 Ma (Roberts et al., 1996), ~ 267 Ma (Steiner, 2006) or ~ 269 Ma (Lanci et al., 2013). Later studies identified reverse polarity at the base of Saddleback Latite in the Sydney Basin, with reported ages of 263.51 ± 0.05 Ma (U-Pb, TIMS, Metcalfe et al., 2015) and 265.05 ± 0.35 Ma (Ar/Ar, plagioclase; Belica et al., 2017a); an age ~ 265 Ma was estimated for the IR by Belica et al. (2017a).

A Wordian age for the IR has been widely accepted in North America based on the magnetostratigraphic data from the Grayburg Formation of West Texas and the Goose Egg Formation in Wyoming (Steiner, 2006). The Grayburg Formation in the Delaware Basin is correlative to the middle Cherry Canyon Formation above the Cherry Canyon Sandstone Tongue. Since the FAD of the Wordian conodont *Jinogondolella aserrata* may range down into the unfossiliferous Cherry Canyon Sandstone at the Getaway GSSP section (Yuan et al., 2020a), thus the Cherry Canyon Sandstone at the Getaway section could be any time in the Wordian; this also suggests a Wordian age for the IR. Previous magnetostratigraphic studies in the GMNP have not yet been fully published. According to Menning (2000), the Cutoff Formation, Getaway Limestone and Manzanita Limestone of the Cherry Canyon Formation have reverse polarization, with a few normal polarized samples in the Pinery and Lamar Limestone. He places the IR between the Pinery and Manzanita members (late Wordian). An age of 265.4 ± 0.2 Ma for the IR is based on an ash bed at 37.2 m below the base-Capitanian GSSP dated by Bowring et al. (1998) at the Nipple Hill section. This date has been updated as 265.46 ± 0.27 Ma (Ramezani and Bowring, 2018) and another ash bed in the South Wells Member was dated at 266.525 ± 0.078 Ma (Wu et al., 2020). Thus, the age of IR in the GMNP is largely consistent with the latest age of the IR in eastern Australia (Belica et al., 2017a).

The IR was reported to be in the fusuline *Yabeina* Zone in the upper part of the Maokou Formation at Wulong, Sichuan Province (Chen et al., 1992). The *Yabeina* Zone was traditionally assigned to the Lengwan Stage in South China, which is equivalent to the Capitanian Stage (Jin et al., 1999). However, recent dating of ash beds in the *Yabeina* Zone in Japan suggested that this zone can be as early as Wordian (Davydov and Schmitz, 2019).

The Wordian age for the IR is also generally supported by the magnetostratigraphic data from other regions. Kirschvink et al. (2015) identified the IR in the middle Wordian in the upper part of the fusuline *Neoschwagerina craticulifera* Zone based on seamount sections from Panthalassan settings. In the Salt Range, Pakistan, the IR was identified in the lower part of the Wargal Formation of Murgabian age, which may be of early Wordian age.

The IR has also been identified in terrestrial sections. In Russia, the IR has been consistently identified in the lower part of the Tatarian (Urzhumian) (Gialanella et al., 1997; Taylor et al., 2009), which is generally equivalent to part of the Wordian Stage (Lucas, 2017b). However, there are no other precise age dates from the terrestrial Urzhumian deposits. In the Karoo Basin, South Africa, magnetostratigraphy was carried out for the Waterford Formation (the upper part of the Ecca Group) and the overlying Abrahamskraal Formation (lowest part of the Beaufort Group) (Lanci et al., 2013). The N3 in the upper part of the Waterford Formation was correlated to the IR. A series of U-Pb SHRIMP dates from ash beds in the lower Abrahamskraal Formation shows that the N3 is probably as old as 269 Ma (Lanci et al., 2013). However, a younger age for the base of the Beaufort Group is more likely based on the high-precision U-Pb TIMS dates from the lower part for the Beaufort Group (Rubidge et al., 2013). A subsequent magnetostratigraphic study suggested that the Ecca Group is of reverse polarity, indicating it formed during the Kiaman Reverse Superchron. A weighted mean U-Pb SHRIMP age of 269.5 ± 1.2 Ma from a volcanic ash bed located in the uppermost Tierberg Formation (lower part of Ecca Group) (Belica et al., 2017b) yields a ca. 290–265 Ma age range of the Ecca Group, which is younger than that of Lanci et al. (2013). If the age of IR is ~265 Ma, then it is likely that N2 in the lower part of the Abrahamskraal Formation of Lanci et al. (2013) is correlative to the IR.

In Europe, the IR is located in the upper part of the Rotliegend (Menning, 2001). In SW England, the end of the Kiaman Superchron occurs in the uppermost part of the Exeter Group (Hounslow and Balabanov, 2018). In North China, the IR was placed in the lower part of the Upper Shihhotse Formation at Taiyuan, Shanxi Province (Embleton et al., 1996). However, this was questioned by Menning and Jin (1998) and no other data are available to constrain the age of the Upper Shihhetse Formation, beyond plant and palynological assemblages.

Recently, Hounslow and Balabanov (2018) noted a possible short normal chron in the Roadian strata. If this normal chron is confirmed in future, the beginning of IR may become more complicated for stratigraphic correlation (Lucas, 2017b). In general, the IR is around the early-middle Wordian in age (Fig. 11).

6.5. $\delta^{13}\text{C}_{\text{carb}}$ variations around the Guadalupian/Lopingian boundary

Our study shows a large negative CIE at the topmost part of the Maokou Formation at the Dukou section and the topmost part of the Reef Trail Member at Section SC1 in GMNP (Fig. 7). However, the CIE at Dukou is higher in terms of conodont biostratigraphy and is missing from the Penglaitan section (Fig. 7B). Such variability of CIEs around the GLB has been reported from different localities within the Tethyan region (Wang et al., 2004; Wignall et al., 2009; Bond et al., 2010a; Chen et al., 2011; Shen et al., 2013a; Zhang et al., 2015; Shi et al., 2017; Huang et al., 2019).

The most striking $\delta^{13}\text{C}_{\text{carb}}$ excursion around the GLB was from the Xiongjiachang section in Guizhou, South China with a negative shift of ~8‰ from the conodont *Jinogondolella shannoni* Zone to the *J. prexuanhanensis* Zone (Wignall et al., 2009; Bond et al., 2010b). This excursion is roughly correlative with that of the Dukou section (Shen et al., 2013a).

Four negative excursions (N1-N4) have been reported from the middle and upper Capitanian within the *Jinogondolella postserrata-J. shannoni* Zone at the Chaotian section in Sichuan Province (Lai et al., 2008; Saitoh et al., 2013). The N1 excursion of ~7‰ in the topmost limestone unit and the N2-N4 excursions of 3‰ in the overlying siliceous

mudstone unit. The mudstone unit at Chaotian is correlative with the chert unit at Dukou. We think N1 is correlative with that at the Xiongjiachang and Dukou sections based on conodont zones. In contrast to the Chaotian section, the nearby Xiaojiaiba section (about 3 km away) shows a negative CIE of only ~2‰ in the topmost part of the Maokou Formation (Wei et al., 2012). A similar negative CIE was also reported in the topmost part of the Maokou Formation from the Tianfengping section in Enshi, Hubei Province (Wei et al., 2018).

Distinct $\delta^{13}\text{C}_{\text{carb}}$ excursions around the GLB were also reported from a carbonate section in the Kamura area, Kyushu, Japan, which developed on an ancient seamount in mid-Panthalassa. The $\delta^{13}\text{C}_{\text{carb}}$ decreased ~1.5‰ immediately after the abrupt disappearance of all large-shelled fusulines and bivalves. Then, $\delta^{13}\text{C}_{\text{carb}}$ values rapidly increased back to the 5.2‰ level. Another sharp drop of 2.4‰ $\delta^{13}\text{C}_{\text{carb}}$ occurs in the topmost Iwato Formation (Isozaki et al., 2007a). The large fusulines is in the uppermost *Jinogondolella xuanhanensis* Zone at the Penglaitan and Tieqiao sections (Jin et al., 2006). Thus, both negative CIEs are much higher than those at the Xiongjiachang, Chaotian and Dukou sections in South China.

Previously, the GLB at the Abadeh section in central Iran was placed at the lithologic boundary between Unit 5 and Unit 6 (Taraz et al., 1981). However, $\delta^{13}\text{C}_{\text{carb}}$ and $^{87}\text{Sr}/^{86}\text{Sr}$ chemostratigraphy suggested that the GLB is very likely ~46.5 m below this lithologic boundary (Liu et al., 2013).

Based on the $\delta^{13}\text{C}_{\text{carb}}$ data discussed above, it is clear that a variable number of CIEs have been reported during the latest Guadalupian interval, with varying patterns, magnitudes and stratigraphic horizons. There are multiple possible causes of $\delta^{13}\text{C}$ negative shifts, depending on the duration and magnitude of the shift. The most plausible scenario for the $\delta^{13}\text{C}$ negative shift is a response to degassing from basaltic eruptions and release of ^{12}C -enriched CO_2 from organic matter in sedimentary strata, with high-temperature isotope fractionation during the volcanic eruption stage (Ganino and Arndt, 2009; Wignall et al., 2009; Shi et al., 2017; Bagherpour et al., 2018b). An alternative explanation for the end-Guadalupian CIEs is upwelling of oxygen-depleted waters with dissolved inorganic carbon of relatively low carbon isotope values (Saitoh et al., 2013). However, CIEs can also be caused by diagenesis below a sequence boundary. The large negative $\delta^{13}\text{C}$ excursion has been found in all GLB sections with a distinct unconformity, whereas the unique section with a continuous GLB at Penglaitan in Guangxi does not contain such a large CIE. Our view is that the wide-spread end-Guadalupian CIE is related to the oxidation of organic matter in sediments during soil formation associated with the widespread late Guadalupian global regression.

It is worth noting that the EG CIE is preceded by a late Capitanian Kamura event characterized by high $\delta^{13}\text{C}_{\text{carb}}$ values (Isozaki et al., 2007a, 2007b). This event has been widely reported from sections in Japan as well as the upper Velebit Formation in central Croatia (Isozaki et al., 2011). The Kamura event with high $\delta^{13}\text{C}_{\text{carb}}$ values appears to have a great potential as a correlation marker for the late Capitanian interval. However, the Kamura event is not recognized at Penglaitan, Tieqiao and some other sections in South China (Wignall et al., 2009; Tierney et al., 2010; Bond et al., 2010a; Chen et al., 2011). Carbon isotopic values over this interval in South China are highly variable (see discussion above). A late Capitanian interval with high $\delta^{13}\text{C}_{\text{carb}}$ values was reported from the Rencunping section in Hunan, South China. However, this interval was attributed to regional eutrophication along a continental shelf (Cao et al., 2018). The Kamura event is not evident in the section at GMNP. Moreover, there is no evidence for the Kamura cooling event from the conodont apatite oxygen isotope data from South China and North America. Thus, it is still unclear whether the Kamura event reflects a global event and whether it has value in correlation.

6.6. The tempo of the end-Guadalupian extinction (pre-Lopingian crisis)

The marine “end-Guadalupian mass extinction” or “pre-Lopingian crisis” has been discussed by numerous previous studies (Jin, 1993; Jin

et al., 1994; Stanley and Yang, 1994; Shen and Shi, 1996, 2002; Bond and Wignall, 2009; Huang et al., 2019). It was once ranked as the third largest mass extinction, behind only the end-Permian and end-Ordovician mass extinctions (Bambach et al., 2004), or as a major mass extinction (Rampino and Shen, 2020) comparable to the end-Ordovician mass extinction (Isozaki and Servais, 2018). Originally, the end-Guadalupian mass extinction was lumped together with the end-Changhsingian mass extinction, which eliminated about 95% of marine faunas (Raup and Sepkoski, 1982; Sepkoski, 1984). As the temporal resolution of taxonomic data increased, it became apparent that the end-Guadalupian mass extinction was much less severe than the end-Changhsingian mass extinction, at least in low latitude areas (Shen and Shi, 2002; Clapham et al., 2009). A high-resolution analysis with a large database of marine records (Fan et al., 2020) reveals a species diversity increase beginning at 261.80 Ma in the middle Capitanian, reaching a peak at 261.04 Ma with a 17% increase in total species diversity. This increase has been associated with the Kamura cooling event and the onset of the Emeishan volcanism (but see previous discussion of the Kamura event). Biological gigantism (e.g. fusulines, bivalves) occurred during this interval. It is difficult to give a causal-effect explanation for this diversity increase based on available data. After 261.04 Ma, species diversity dropped 8%, until 259.98 Ma, a decline which may represent the proposed end-Guadalupian or pre-Lopingian crisis, and coincides with the peak of Emeishan volcanism (He et al., 2007) (Fig. 11). No major fossil groups disappeared during the latest Guadalupian in South China and other low latitude areas. This is correlative with the U-Pb zircon date (CA-TIMS method) of 260.259 ± 0.081 Ma from a tuff near the top of the *Tapinocephalus* assemblage Zone in the Karoo Basin of South Africa, with a reported 74–80% drop in tetrapod diversity (Day et al., 2015). After 259.98 Ma, species diversity steadily increased until 257.5 Ma, which is the end of the Emeishan volcanism (Bagherpour et al., 2018a; Shellnutt et al., 2020; Zhong et al., 2020).

It is interesting to note that the marine end-Guadalupian event may have been profound in high-latitude areas as recorded in Svalbard and Spitsbergen near Norway and in Arctic Canada (Beauchamp et al., 2009; Bond and Wignall, 2009; Bond et al., 2015), but more robust statistical analyses are needed to compare high- and low-latitude extinction rates (Shi et al., 2019).

Analysis of the end-Guadalupian mass extinction in North America is challenging because of the transition to the evaporites of the Castile Formation. Regardless of shallow-water (King, 1942; Kendall and Harwood, 1989) or deep-water models (Anderson et al., 1972; Bell et al., 2015), this distinct lithofacies change truncates fossil ranges at the top of the Reef Trail Member (Fig. 11).

Several studies have suggested that the end-Guadalupian mass extinction was taxonomically selective (Wang and Sugiyama, 2001; Clapham et al., 2009; Shen and Shi, 2009; Bond et al., 2010a; Fan et al., 2020). Fusulines experienced a distinctive pattern of change across the GLB, with most species disappearing over the course of ~7.5 Myr during the Wordian and Capitanian (Yang et al., 2004; Shi and Yang, 2005; Ota and Isozaki, 2006; Kasuya et al., 2012; Groves and Wang, 2013; Kirschvink et al., 2015). Contrary to earlier views, the “end-Guadalupian event” did not preferentially eliminate large, morphologically complex species in the families Schwagerinidae and Neoschwagerinidae, because most species in those families were already extinct (cf. mid-Capitanian extinction of Bond et al., 2010a). In most areas of South China, the ranges of many late Guadalupian species are also truncated by a distinct unconformity above the *Jinogondolella xuanhanensis* Zone (Hou et al., 2020). In the latest Guadalupian, large Schwagerinidae and Neoschwagerinidae species were replaced by an assemblage of smaller fusulines characterized by *Lantschichites* and *Reichelina* associated with numerous *Codonofusella*. These became the most abundant fusulines during the Wuchiapingian in the Tethyan Realm. The top of *Metadololina* Zone or the *Jinogondolella xuanhanensis* Zone marks the end of many giants such as the Alatoconchidae bivalves and large-sized

Verbeekinidae fusulines (Ota and Isozaki, 2006; Isozaki and Aljinović, 2009; Kasuya et al., 2012; Zhang and Payne, 2012; Kirschvink et al., 2015; Arefifard and Payne, 2020).

Many of the characteristic and abundant Lopingian taxa first appeared during the latest Guadalupian in South China and Iran. The small fusuline *Codonofusella* was already very abundant in the topmost Guadalupian and became the most abundant Lopingian (Zhang and Wang, 2018). The typical Lopingian brachiopods, *Tyloplecta yangtzeensis*, *Spinomarginifera lopingensis* and *Transennatia gratiosa*, occur commonly in the uppermost Guadalupian (Maokouan) Laibin Limestone at the Penglaitan section (Shen and Shi, 2009) and the Capitanian Lengwu Formation in Zhejiang, South China (Liang, 1990; Shen, 2018). The thriving rugose corals of the Lopingian including *Waagenophyllum*, *Ipciphyllum* etc. also began to appear in the latest Guadalupian (Wang et al., 2018b). Huang et al. (2019) showed a metazoan/microbial reef in the Laibin Limestone and discuss extinction of corals, sponges, red algae, microbes as a crisis. Two Hg “spikes” were reported to be related to the crisis. But again this is a turnover in biota and many of the biota did not become extinct. Thus, it is clear that Lopingian/Guadalupian transitional faunas were widely present in the interval above the *Jinogondolella xuanhanensis* Zone in South China, prior to the Lopingian. The end-Guadalupian event largely represents a changeover in species and genera during a major sea-level lowstand rather than a major loss of diversity (Fan et al., 2020) (Fig. 11). Guadalupian/Lopingian mixed faunas are not present in the sections in the Delaware Basin, which suggests that the topmost part of the Guadalupian in North America is not complete or is represented by the evaporite deposits. The absolute time duration for the “end-Guadalupian faunal turnover” is about 1.3 Myr in South China (Fig. 11) (Fan et al., 2020).

7. Perspectives

In future, the priority for Guadalupian correlation is to properly refine the three GSSPs by investigating multiple markers around the three GSSPs and illustrating the index species for the three GSSPs from the GSSP sections. Definitions based on conodonts alone are insufficient for reliable intercontinental correlation. The Subcommission on Permian Stratigraphy may need to seek a new GSSP candidate section for the base of the Wordian Stage because the present FAD sample at Getaway Ledge does not contain conodonts and the defined species *Jinogondolella aserrata* may range downward into the Cherry Canyon Sandstone at the present GSSP section.

The current base of the Roadian Stage in the GMNP is generally consistent with the base of the Maokouan in South China based on carbon isotope chemostratigraphy and conodont biostratigraphy, but more needs to be investigated as well. The key problem for this GSSP is how to deal with the serrated conodonts found from the underlying horizons in both South China and North America. A taxonomic study on those serrated gondolellids is underway to clarify this problem.

The nature, taxonomic selectivity, biogeographic extent and evolutionary impact of the widely-discussed end-Guadalupian biotic event needs to be re-investigated. Evidence presented here suggests that it was not a major biotic crisis in South China, and the record in North America has been obscured by lithologic changes and unconformities. The construction of massive databases of fossil records, integrated with high-resolution geochronologic, geochemical, environmental and other data will be essential for resolving these issues, and particularly whether it is a major event in high latitude areas. In addition, it is important to improve the correlation of the marine GLB with terrestrial sequences. This is critical to understand how the end-Guadalupian event manifested in terrestrial ecosystems. High-precision geochronology will provide the most reliable tool for this problem. Thus, the sections in North China, northwest China (Yang et al., 2010), the Karoo Basin in South Africa (Rubidge et al., 2013, 2016) and the sections in eastern Australia (Shi and Waterhouse, 2010; Metcalfe et al., 2015) have high potential for further investigation. Magnetostratigraphic and reliable

cyclostratigraphic studies will also provide important tools for Guadalupian correlation in these regions.

8. Summary

The Guadalupian Series is marked by the FAD of *Jinogondolella nankingensis* (=*J. serrata*) at the base and terminated by the evaporite deposits of the Castile Formation at the top in West Texas, North America. However, weakly serrated *Jinogondolella* specimens occur below the base-Roadian GSSP in the GMNP and in the upper part of the Kungurian Chihsia Formation in South China. The topmost identified conodont zones of the Guadalupian Series in West Texas may be endemic species equivalent to the range of *J. prexuanhanensis* in South China. The base of the Guadalupian is dated by U-Pb zircon geochronology at 273.01 ± 0.14 Ma at the type locality of *Jinogondolella nankingensis* near Nanjing.

$\delta^{13}\text{C}_{\text{carb}}$ chemostratigraphy suggests both South China and North America sections possess a distinct negative $\delta^{13}\text{C}_{\text{carb}}$ shift from latest Kungurian to early Roadian (LK-ER CIE), which occurs from the *Mesogondolella lamberti* Zone throughout the *Jinogondolella nankingensis* Zone in South China, and its correlative transgressive interval from the basal part of the Shumard Member to the top of the El Centro Member of the Cutoff Formation in the GMNP. The current GSSP for the base-Guadalupian in North America appears to be slightly younger than the base of the Maokouan in South China based on the correlation of the LK-ER CIE and cyclostratigraphy (Figs. 5, 7). A highly variable CIE in different horizons at the end-Guadalupian is present. Although various interpretations (e.g. degassing, warming from Emeishan volcanism, upwelling) are available, it is very likely that the widely-perceived end-Guadalupian CIE is related to the oxidation of organic matter in sediments during the end-Guadalupian global regression.

The base of the Wordian Stage is extrapolated at 266.9 ± 0.4 Ma and the base of the Capitanian Stage is constrained at 264.28 ± 0.17 Ma, with 259.51 ± 0.21 Ma adopted as the age for the top of the Guadalupian. An end-Guadalupian marine bioevent is marked by the disappearances of some giant fusulines at the top of the *Metadolliolina* fusuline zone or *Jinogondolella xuanhanensis* conodont zone, which lasted roughly from ~ 261 Ma to ~ 260 Ma. It is very likely that the pre-Lopingian crisis is a species and genus replacement event, probably resulting from the major sea-level lowstand and effects related to Emeishan volcanism, but without major species diversity loss or even no end-Guadalupian mass extinction.

Declaration of Competing Interest

The authors declared that they have no conflicts of interest to this work.

Acknowledgements

This paper is dedicated to five late distinguished Permian colleagues. Brian F. Glenister worked extensively on Guadalupian ammonoids and visited the Penglaitan section in China on the invitation of Yu-gan Jin in 2003. Jin initiated the idea to study the Guadalupian Series in both South China and North America and he first sent the young research group of Nanjing Institute of Geology and Palaeontology to the USA for field work in 2004. Bruce R. Wardlaw drove and guided the Nanjing group field work at GMNP and Apache Mountains in 2004, and we all benefited from his introduction and numerous discussions of Guadalupian conodonts and biostratigraphic problems. Samuel A. Bowring long had plans to date all the ash beds in the GMNP and he led the team that first dated the Nipple Hill ash bed just below the base-Capitanian GSSP. We also thank Werner Buggisch. He generously provided us his unpublished $\delta^{13}\text{C}_{\text{carb}}$ data from GMNP which enable us to compare our data with his data analyzed in different labs (Fig. 7). Unfortunately, all five colleagues passed away before this work was completed.

The Nanjing Group thanks Spencer Lucas for logistic help in shipping tons of samples from the USA to China. Szs and Dxy thank Shi-long Mei for his kind help in studying the conodonts. We thank Spencer Lucas and two anonymous reviewers for their excellent suggestions for improving the paper. This work is conducted under the support of an international collaborative project funded by the National Natural Science Foundation of China (NSFC) between 2015–2019 (Grant no. 41420104003). It is also supported by the Strategic Priority Research Programs (B) of the Chinese Academy of Sciences (XDB26000000, XDB18000000) and NSFC (41702007, 41830323). CMH acknowledges support from a NSERC Discovery Grant for travel to west Texas and south China and some conodont processing.

Appendix A. Methodology

A.1. $\delta^{13}\text{C}_{\text{carb}}$ and $\delta^{18}\text{O}_{\text{carb}}$ (whole rock)

After a visual inspection to exclude contamination and recrystallization of the samples with calcite veins the rock fragments were powdered to 200 mesh with an agate pestle and mortar, and subsamples of about 100 μg powder was reacted with ultrapure 100% HPO_3 at 72.2°C to release CO_2 in Kiel IV of automated carbonate reaction device, coupled with a Finnigan MAT 253 mass spectrometer to measure $\delta^{13}\text{C}$ and $\delta^{18}\text{O}$. All values are reported in per mil relative to V-PDB (Vienna PeeDee belemnite), and are calibrated to the Chinese National Standard (GBW-04405) with a $\delta^{13}\text{C}$ value of 0.57‰ and $\delta^{18}\text{O}$ value of -8.49‰. The long-term precision and accuracy were better than 0.03‰ (2 sd) for $\delta^{13}\text{C}$ and 0.08‰ (2 sd) for $\delta^{18}\text{O}$. Carbon and oxygen isotope ratios were measured on powdered bulk carbonate samples using a Finnigan MAT 253 mass spectrometer at the Nanjing Institute of Geology and Palaeontology. Analytical error for $\delta^{13}\text{C}_{\text{carb}}$ and $\delta^{18}\text{O}_{\text{carb}}$ was better than 0.03‰ and 0.08‰, respectively.

To evaluate the effects of diagenetic alteration on measured samples, cross plots of carbon and oxygen isotope data are shown in Fig. 7. There is no distinct positive covariation between C and O isotopes. Most of $\delta^{18}\text{O}$ values are between -3 and -8‰, higher than -10‰. We thus interpret the majority of $\delta^{13}\text{C}$ data reported here as not significantly overprinted by subsequent diagenetic alteration. However, some $\delta^{13}\text{C}_{\text{carb}}$ data from the Wordian Stage at the Getaway Ledge section and the El Centro Member at the Stratotype Canyon section show scattered and unusually low values; the primary seawater signal preserved in these samples may have been overprinted by subsequent diagenetic alteration.

A.2. $\delta^{18}\text{O}_{\text{apatite}}$ (conodonts)

Only P_1 elements of *Jinogondolella* were selected, and the conodont colour alteration index (CAI) is 1 to 1.5 in West Texas, but 3 to 4 in the Penglaitan section. Joachimski et al. (2009) showed no alteration of the oxygen isotope ratios of conodonts having a CAI up to 5. Conodont apatite (0.5 to 1.0 mg) was dissolved by 5 ml 2 M HNO_3 , and the phosphate group was re-precipitated as Ag_3PO_4 following the method described in Joachimski et al. (2009). Ag_3PO_4 (~0.3 mg) was performed using a TC-EA (temperature conversion elemental analyzer) coupled online with a Thermo-Finnigan Delta V Plus isotope ratio mass spectrometer. Samples and internal standards were generally measured in triplicate (helium flow rate was 80 ml/s, reactor temperature was set to 1450°C , column temperature was 90°C). At 1450°C , the silver phosphate was reduced and CO formed as the analyte gas (Vennemann et al., 2002). CO was transferred in the helium stream through a gas chromatographic column via a Conflo IV interface to the mass spectrometer. Conodont apatite oxygen isotope values are reported in per mil relative to VSMOW. Reproducibility of triplicate sample measurements was generally better than $\pm 0.2\text{\textperthousand}$ (1 sd). The average oxygen isotope composition of the standard NBS 120c was $21.7 \pm 0.19\text{\textperthousand}$ VSMOW ($n = 19$).

A.3. $^{87}\text{Sr}/^{86}\text{Sr}$ (whole rock)

About 500 mg of the same powder for $\delta^{13}\text{C}_{\text{carb}}$ analysis were used for Sr isotope analysis. The powder samples were washed in deionized water three times and then washed with 1 M ammonium chloride, and dissolved by $\text{NH}_4\text{Ac}/\text{HAc}$ buffer with $\text{pH} = 4.5$ (Birck, 1986; Wang et al., 2007; Cao et al., 2009) in an ultrasonic water bath at 30 °C for 30 min. After centrifugation, the supernatants were decanted to beakers and dried at 120 °C; then were re-dissolved in ultrapure water (Wang et al., 2018a). For the determination of $^{87}\text{Sr}/^{86}\text{Sr}$ ratio, sample aliquots containing ~100 ng of Sr were purified using Eichrom strontium specification ion exchange resin (50–100 mesh) following previously published standard procedure (Ma et al., 2013). Total procedural Sr blanks were consistently <100 pg. Purified Sr was measured using a Thermo-Scientific Neptune Plus Multiple collector inductively coupled plasma mass spectrometer (MC-ICP-MS) at the State Key Laboratory of Isotope Geochemistry, Guangzhou Institute of Geochemistry (GIG), Chinese Academy of Sciences (CAS). During the analysis of $^{87}\text{Sr}/^{86}\text{Sr}$ ratio, the ^{85}Rb ion beam was monitored to ensure that there is no ^{87}Rb isobaric interference of ^{87}Rb on ^{87}Sr . To correct for the instrumental mass bias, a standard bracketing technique in a standard-sample-standard measuring sequence was adopted. Standard sample NBS 987 was measured every five samples, yielding a mean $^{87}\text{Sr}/^{86}\text{Sr}$ ratio of 0.710273 ± 0.000018 (2 sd, $n = 26$). All the results were corrected for the offset between the measured NBS 987 ratio determined in each session and the standard value of 0.710248 (McArthur et al., 2001). The measured a seawater standard (IAPSO; Batch P153) and two basalt rock standards (BCR-2 and JB-3) yield $^{87}\text{Sr}/^{86}\text{Sr}$ ratios of 0.709177 ± 0.000014 , 0.705002 ± 0.000012 , and 0.703541 ± 0.000017 , respectively. All of these values are consistent with published values within uncertainty (Balcaen et al., 2005; Krabbenhoft et al., 2009; Yang et al., 2010), suggesting that inter-laboratory biases for Sr isotopes are negligible.

A.4. U-Pb geochronology

Rock samples were processed by soaking in water for 48 h, followed by complete liquefaction in a blender. Heavy minerals were separated from these clay-rich samples in a sonic dismembrator device designed by Hoke et al. (2014). Heavy-mineral concentrates were achieved through step-wise magnetic as well as high-density liquid separation techniques. The final zircon selection was carried out under a binocular microscope.

Samples contained mixed populations of zircons ranging from sub-rounded to multi-faceted prisms. The prismatic or acicular zircon grains containing elongate glass (melt) inclusions parallel to their long axis are shown to represent the youngest population of zircons in the samples (Ramezani et al., 2011) and were targeted for our analyses. The selected grains were pre-treated by a chemical abrasion (CA) technique modified after Mattinson (2005). Zircon chemical abrasion was achieved by thermal annealing at 900 °C for 60 h, followed by leaching them in 29 M HF inside high-pressure vessels at 210 °C for 11.5 to 12 h. The leached grains were fluxed in several hundred microliters of dilute HNO_3 and 6 M HCl, successively on the hot plate and in an ultrasonic bath for 1 h of each step. The grains were rinsed with several volumes of Millipore water in between to remove the leachates. The thoroughly rinsed grains were spiked with the EARTHTIME ET535 mixed $^{205}\text{Pb}-^{233}\text{U}-^{235}\text{U}$ tracer (Condon et al., 2015; McLean et al., 2015) prior to complete dissolution in 29 M HF at 210 °C for 45 to 48 h. The dissolved U and Pb were chemically purified and separated using 50 µl columns of anion-exchange resin. The purified U and Pb were finally loaded together onto degassed Re filaments mixed with a silica gel emitter solution and their isotopic ratios were measured on an IsotopX X62 multi-collector thermal ionization mass spectrometer equipped with a Daly photomultiplier ion counting system.

Data reduction, error propagation, and U-Pb date calculation were carried out using Tripoli and ET_Redux algorithms (Bowring et al., 2011;

McLean et al., 2011). Complete Pb and U isotopic data are given in Table 1 and illustrated in Fig. 5. Sample dates representing the depositional ages are calculated based on the weighted mean $^{206}\text{Pb}/^{238}\text{U}$ dates from the youngest cluster in each sample. The analyses of each sample define a tight cluster (Fig. 5), and no analyses were excluded from the calculation. The uncertainties of the weighted mean dates are reported at 95% confidence level in the format of $\pm \text{X/Y/Z}$, where X is the 2σ internal (analytical) uncertainty exclusive of all external errors, Y incorporates the U-Pb tracer calibration error, and Z includes Y as well as the U decay constant errors of Jaffey et al. (1971). The two high-precision U-Pb dates are interpreted as the depositional ages of the corresponding bentonite beds.

Appendix B. Supplementary data

Supplementary data to this article can be found online at <https://doi.org/10.1016/j.earscirev.2020.103412>.

References

- Anderson, R.Y., Dean Jr., W.E., Kirkland, D.W., Snider, H.I., 1972. Permian Castile varved evaporite sequence, West Texas and New Mexico. *Geol. Soc. Am. Bull.* 83, 59–86.
- Arefifard, S., Payne, J.L., 2020. End-Guadalupian extinction of larger fusulinids in Central Iran and implications for the global biotic crisis. *Palaeogeogr. Palaeoclimatol. Palaeoecol.* 550, 109743.
- Bagherpour, B., Bucher, H., Yuan, D.X., Leu, M., Zhang, C., Shen, S.Z., 2018a. Early Wuchiapingian (Lopingian, late Permian) drowning event in the South China block suggests a late eruptive phase of Emeishan large Igneous Province. *Glob. Planet. Chang.* 169, 119–132.
- Bagherpour, B., Bucher, H., Schneebeli-Hermann, E., Vennemann, T., Chiaradia, M., Shen, S.Z., 2018b. Early Late Permian coupled carbon and strontium isotope chemostratigraphy from South China: Extended Emeishan volcanism? *Gondwana Res.* 58, 58–70.
- Balcaen, L., Schrijver, I.D., Moens, L., Vanhaecke, F., 2005. Determination of the $^{87}\text{Sr}/^{86}\text{Sr}$ isotope ratio in USGS silicate reference materials by multi-collector ICP-mass spectrometry. *Int. J. Mass Spectrom.* 242, 251–255.
- Bambach, R.K., Knoll, A.H., Wang, S.C., 2004. Origination, extinction, and mass depletions of marine diversity. *Paleobiology* 30, 522–542.
- Baresel, B., Bucher, H., Bagherpour, B., Brosse, M., Guodun, K., Schaltegger, U., 2017a. Timing of global regression and microbial bloom linked with the Permian-Triassic boundary mass extinction: implications for driving mechanisms. *Sci. Rep.* 7, 43630.
- Baresel, B., Bucher, H., Brosse, M., Corday, F., Kuang, G.D., Schaltegger, U., 2017b. Precise age for the Permian-Triassic boundary in South China from high-precision U-Pb geochronology and Bayesian age-depth modeling. *Solid Earth* 8, 361–378.
- Beauchamp, B., Henderson, C.M., Grasby, S.E., Gates, L.T., Beatty, T.W., Utting, J., James, N.P., 2009. Late Permian sedimentation in the Sverdrup Basin, Canadian Arctic: the Lindstrom and Black Stripe Formations. *Bull. Can. Petrol. Geol.* 57, 167–191.
- Belica, M.E., Tohver, E., Pisarevsky, S.A., Jourdan, F., Denysyn, S., George, A.D., 2017a. Middle Permian paleomagnetism of the Sydney Basin, Eastern Gondwana: Testing Pangea models and the timing of the end of the Kiaman reverse Superchron. *Tectonophysics* 699, 178–198.
- Belica, M.E., Tohver, E., Poyatos-Moré, M., Flint, S., Parra-Avila, L.A., Lanci, L., Denysyn, S., Pisarevsky, S.A., 2017b. Refining the chronostratigraphy of the Karoo Basin, South Africa: magnetostratigraphic constraints support an early Permian age for the Eccia Group. *Geophys. J. Int.* 211, 1354–1374.
- Bell, G.L.J., Hearst, J.M., Nestell, M.K., Nestell, G.P., Lambert, L.L., 2015. Stratigraphic framework and biostratigraphic significance of the terminal Guadalupian Reef Trail Member, Bell Canyon Formation in the Patterson Hills, Type Guadalupian Area, Texas. *Stratigraphy* 12 (2), 93–107.
- Birck, J.L., 1986. Precision K-Rb-Sr isotopic analysis: application to Rb-Sr chronology. *Chem. Geol.* 56, 73–83.
- Bond, D.P.G., Wignall, P.B., 2009. Latitudinal selectivity of foraminifer extinctions during the late Guadalupian crisis. *Paleobio.* 35, 465–483.
- Bond, D.P.G., Hilton, J., Wignall, P.B., Ali, J.R., Stevens, L.G., Sun, Y.D., Lai, X.L., 2010a. The Middle Permian (Capitanian) mass extinction on land and in the oceans. *Earth Sci. Rev.* 102, 100–116.
- Bond, D.P.G., Wignall, P.B., Wang, W., Izon, G., Jiang, H.S., Lai, X.L., Sun, Y.D., Newton, R.J., Shao, L.Y., Vedrine, S., Cope, H., 2010b. The mid-Capitanian (Middle Permian) mass extinction and carbon isotope record of South China. *Palaeogeogr. Palaeoclimatol. Palaeoecol.* 292, 282–294.
- Bond, D.P.G., Wignall, P.B., Joachimski, M.M., Sun, Y.D., Savov, I.P., Grasby, S.E., Beauchamp, B., Blomeier, D.P.G., 2015. An abrupt extinction in the Middle Permian (Capitanian) of the Boreal Realm (Spitsbergen) and its link to anoxia and acidification. *Geol. Soc. Am. Bull.* 127, 1411–1421.
- Böse, E., 1917. The Permo-Carboniferous ammonoids of the Glass Mountains, West Texas, and their stratigraphical significance. *Bull. Texas Univ.* 1762, 1–241.

- Bowring, S.A., Erwin, D.H., Jin, Y.G., Martin, M.W., Davidek, K., Wang, W., 1998. U/Pb zircon geochronology and tempo of the end-Permian mass extinction. *Science* 280, 1039–1045.
- Bowring, J.F., McLean, N.M., Bowring, S.A., 2011. Engineering cyber infrastructure for U-Pb geochronology: tripoli and U-Pb Redux. *Geochem. Geophys. Geosyst.* 12, Q0AA19.
- Brand, U., Jiang, G.Q., Azmy, K., Bishop, J., Montañez, I.P., 2012. Diagenetic evaluation of a Pennsylvanian carbonate succession (Bird Spring Formation, Arrow Canyon, Nevada, U.S.A.) -1: Brachiopod and whole rock comparison. *Chem. Geol.* 308–309, 26–39.
- Buggisch, W., Wang, X.D., Alekseev, A.S., Joachimski, M.M., 2011. Carboniferous-Permian carbon isotope stratigraphy of successions from China (Yangtze platform), USA (Kansas) and Russia (Moscow Basin and Urals). *Palaeogeogr. Palaeoclimatol. Palaeoecol.* 301, 18–38.
- Burgess, S.D., Bowring, S.A., 2015. High-precision geochronology confirms voluminous magmatism before, during, and after Earth's most severe extinction. *Sci. Adv.* 1, 1–14.
- Burgess, S.D., Bowring, S.A., Shen, S.Z., 2014. High-precision timeline for Earth's most severe extinction. *Proc. Natl. Acad. Sci.* 111, 3316–3321.
- Cao, C.Q., Love, G.D., Hays, L.E., Wang, W., Shen, S.Z., Summons, R.E., 2009. Biogeochemical evidence for euxinic oceans and ecological disturbance presaging the end-Permian mass extinction event. *Earth Planet. Sci. Lett.* 281, 188–201.
- Cao, C.Q., Cui, C., Chen, J., Summons, R.E., Shen, S.Z., Zhang, H., 2018. A positive C-isotope excursion induced by sea-level fall in the middle Capitanian of South China. *Palaeogeogr. Palaeoclimatol. Palaeoecol.* 505, 305–316.
- Chen, J., Xu, Y.G., 2019. Establishing the link between Permian volcanism and biodiversity changes: insights from geochemical proxies. *Gondwana Res.* 75, 68–96.
- Chen, H.H., Sun, S., Li, J.L., Heller, F., Dobson, J., 1992. Permian-Triassic magnetostratigraphy of Wulong Area, Sichuan. *Sci. China. Ser. B* 12, 1317–1324.
- Chen, B., Joachimski, M.M., Sun, Y.D., Shen, S.Z., Lai, X.L., 2011. Carbon and conodont apatite oxygen isotope records of Guadalupian-Lopingian boundary sections: Climatic or sea-level signal? *Palaeogeogr. Palaeoclimatol. Palaeoecol.* 311, 145–153.
- Chen, B., Joachimski, M.M., Shen, S.Z., Lambert, L.L., Lai, X.L., Wang, X.D., Chen, J., Yuan, D.X., 2013. Permian ice volume and palaeoclimate history: oxygen isotope proxies revisited. *Gondwana Res.* 24, 77–89.
- Clapham, M.E., Shen, S.Z., Bottjer, D.J., 2009. The double mass extinction revisited: reassessing the severity, selectivity, and causes of the end-Guadalupian biotic crisis (Late Permian). *Paleobiol.* 35, 32–50.
- Clark, D.L., Ethington, R.L., 1962. Survey of Permian conodonts in western North America. *Brigham Young University Research Studies. Geol. Ser.* 9, 102–114.
- Clark, D.L., Mosher, L.C., 1966. Stratigraphic, geographic, and evolutionary development of the conodont genus *Gondolella*. *J. Paleontol.* 40, 376–394.
- Condon, D.J., Schoene, B., McLean, N.M., Bowring, S.A., Parrish, R.R., 2015. Metrology and traceability of U-Pb isotope dilution geochronology (EARTHTIME Tracer Calibration Part I). *Geochim. Cosmochim. Acta* 164, 464–480.
- Cooper, G.A., Grant, R.E., 1972. Permian brachiopods of West Texas I. *Smithson. Contrib. Paleobiol.* 1–231.
- Davydov, V.I., Schmitz, M.D., 2019. High-precision radioisotopic ages for the lower Midian (upper Wordian) Stage of the Tethyan time scale, Shigeyasu Quarry, Yamaguchi Prefecture, Japan. *Palaeogeogr. Palaeoclimatol. Palaeoecol.* 527, 133–145.
- Davydov, V.I., Crowley, J.L., Schmitz, M.D., Snyder, W.S., 2018a. New U-Pb constraints identify the end-Guadalupian and possibly end-Lopingian extinction events conceivably preserved in the passive margin of North America: implication for regional tectonics. *Geol. Mag.* 155, 119–131.
- Davydov, V.I., Biakov, A.S., Schmitz, M.D., Silantiev, V.V., 2018b. Radioisotopic calibration of the Guadalupian (middle Permian) series: review and updates. *Earth Sci. Rev.* 176, 222–240.
- Day, M.O., Ramezani, J., Bowring, S.A., Sadler, P.M., Erwin, D.H., Abdala, F., Rubidge, B.S., 2015. When and how did the terrestrial mid-Permian mass extinction occur? Evidence from the tetrapod record of the Karoo Basin, South Africa. *Proc. R. Soc. B Biol. Sci.* 282, 1–8.
- Embleton, B.J.J., McElhinny, M.W., Ma, X.H., Zhang, Z.K., Li, Z.X., 1996. Permo-Triassic magnetostratigraphy in China: the type section near Taiyuan, Shanxi Province, North China. *Geophys. J. Int.* 126, 382–388.
- Fan, J.X., Shen, S.Z., Erwin, D.H., Sadler, P.M., MacLeod, N., Cheng, Q.M., Hou, X.D., Yang, J., Wang, X.D., Wang, Y., Zhang, H., Chen, X., Li, G.X., Zhang, Y.C., Shi, Y.K., Yuan, D.X., Chen, Q., Zhang, L.N., Li, C., Zhao, Y.Y., 2020. A high-resolution summary of Cambrian to Early Triassic marine invertebrate biodiversity. *Science* 367, 272–277.
- Fang, Q., Wu, H.C., Hinnov, L.A., Jing, X.C., Wang, X.L., Jiang, Q.C., 2015. Geologic evidence for chaotic behavior of the planets and its constraints on the third-order eustatic sequences at the end of the Late Paleozoic Ice Age. *Palaeogeogr. Palaeoclimatol. Palaeoecol.* 440, 848–859.
- Fang, Q., Wu, H.C., Hinnov, L.A., Jing, X.C., Wang, X.L., Yang, T.S., Li, H.Y., Zhang, S.H., 2017. Astronomical cycles of Middle Permian Maokou Formation in South China and their implications for sequence stratigraphy and paleoclimate. *Palaeogeogr. Palaeoclimatol. Palaeoecol.* 474, 130–139.
- Fielding, C.R., Frank, T.D., Isbell, J.L., 2008. The Late Paleozoic ice age—a review of current understanding and synthesis of global climate patterns. *Geol. Soc. Am. Spec. Pap.* 441, 343–354.
- Furnish, W.M., 1973. Permian stage names. *Mem. Can. Soc. Petrol. Geol.* 2, 522–548.
- Garino, C., Arndt, N.T., 2009. Climate changes caused by degassing of sediments during the emplacement of large igneous provinces. *Geology* 37, 323–326.
- Garbelli, C., Shen, S.Z., Immenhauser, A., Brand, U., Buhl, D., Wang, W.Q., Zhang, H., Shi, G.R., 2019. Timing of Early and Middle Permian deglaciation of the southern hemisphere: brachiopod-based 87Sr/86Sr calibration. *Earth Planet. Sci. Lett.* 516, 122–135.
- Gianella, P.R., Heller, F., Haag, M., Nurgaliev, D., Borisov, A., Burov, B., Jasonov, P., Khasanov, D., Ibragimov, S., Zharkov, I., 1997. Late Permian magnetostratigraphy on the eastern Russian platform. *Geol. Mijnb.* 76, 145–154.
- Glenister, B.F., Furnish, W., 1987. New Permian representatives of ammonoid superfamilies Marathonitaceae and Cyclobabaceae. *J. Paleontol.* 61, 982–998.
- Glenister, B.F., Boyd, D.W., Furnish, W.M., Grant, R.E., Harris, M.T., Kozur, H., Lambert, L.L., Nassichuk, W.W., Newell, N.D., Pray, L.C., Spinosa, C., Wardlaw, B.R., Wilde, G.L., Yancey, T.E., 1992. The Guadalupian: proposed international standard for a Middle Permian series. *Int. Geol. Rev.* 34, 875–888.
- Glenister, B.F., Wardlaw, B.R., Lambert, L.L., Spinosa, C., Bowring, S.A., Erwin, D.H., Menning, M., Wilde, G.L., 1999. Proposal of Guadalupian and component Roadian, Wordian and Capitanian Stages as international standards for the Middle Permian. *Periophiles* 3–11.
- Groves, J.R., Wang, Y., 2013. Timing and size selectivity of the Guadalupian (Middle Permian) fusulinoidean extinction. *J. Paleontol.* 87, 183–196.
- Haig, D.W., Mory, A.J., McCourtin, E., Backhouse, J., Håkansson, E., Ernst, A., Nicoll, R., Shi, G.R., Bevan, J.C., Davydov, V.I., Hunter, A.W., Keep, M., Martin, S.K., Peyrot, D., Kossavaya, O., Santos, Z.D., 2017. Late Artinskian-Early Kungurian (Early Permian) warming and maximum marine flooding in the East Gondwana interior rift, Timor and Western Australia, and comparisons across East Gondwana. *Palaeogeogr. Palaeoclimatol. Palaeoecol.* 468, 88–121.
- Hao, W.C., Yao, J.X., Liu, J.B., 1999. Permian conodonts from the Shaiwa section in Ziyun, Guizhou. In: Yao, A., Ezaki, Y., Hao, W.C., Wang, X.P. (Eds.), *Biotic and Geological Developments of the Paleo-Tethys in China*. Peking University Press, Beijing, pp. 73–79.
- Haq, B.U., Schutter, S.R., 2008. A chronology of Paleozoic sea-level changes. *Science* 322, 64–68.
- Harris, M.T., 1988. Sedimentology of the Cutoff Formation (Permian), Western Guadalupe Mountains, West Texas. In: Reid, S.T., Bass, R.O., Welch, P. (Eds.), *Guadalupe Mountains Revisited, Texas and New Mexico*, 88–84. West Texas Geological Society, pp. 133–140, 1988 Field Seminar.
- He, B., Xu, Y.G., Wang, Y.M., Xiao, L., 2005. Nature of the Dongwu Movement and its temporal and spatial evolution. *J. China Univ. Geosci.* 30, 89–96.
- He, B., Xu, Y.G., Huang, X.L., Luo, Z.Y., Shi, Y.R., Yang, Q.J., Yu, S.Y., 2007. Age and duration of the Emeishan flood volcanism, SW China: Geochemistry and SHRIMP zircon U-Pb dating of silicic ignimbrites, post-volcanic Xuanwei Formation and clay tuff at the Chaotian section. *Earth Planet. Sci. Lett.* 255, 306–323.
- He, B., Xu, Y.G., Zhong, Y.T., Guan, J.P., 2010. The Guadalupian-Lopingian boundary mudstones at Chaotian (SW China) are clastic rocks rather than acidic tuffs: implication for a temporal coincidence between the end-Guadalupian mass extinction and the Emeishan volcanism. *Lithos* 119, 10–19.
- Henderson, C.M., 2018. Permian conodont biostratigraphy. *Geol. Soc. Lond. Spec. Publ.* 450, 119–142.
- Henderson, C.M., Mei, S.L., 2003. Stratigraphic versus environmental significance of Permian serrated conodonts around the CSB; new evidence from Oman.; *Pangea* special issue; selected papers from the Pangea symposium. *Palaeogeogr. Palaeoclimatol. Palaeoecol.* 191, 301–328.
- Henderson, C.M., Mei, S.L., 2007. Geographical clines in Permian and lower Triassic gondolellids and its role in taxonomy. *Palaeoworld* 16, 190–201.
- Henderson, C.M., Shen, S.Z., 2020. Chapter 24—the Permian period. In: Gradstein, F.M., Ogg, J.G., Schmitz, M.D., Ogg, G.M. (Eds.), *The Geologic Time Scale 2020*. Elsevier, pp. 875–902.
- Henderson, C.M., Mei, S.L., Wardlaw, B.R., 2002. New conodont definitions at the Guadalupian-Lopingian boundary. *Carboniferous and Permian of the world; XIV ICCP proceedings. Mem. Can. Soc. Petrol. Geol.* 19, 725–735.
- Henderson, C.M., Davydov, V.I., Wardlaw, B.R., 2012. The Permian Period. In: Gradstein, F.M., Ogg, J.G., Schmitz, M.D., Ogg, G.M. (Eds.), *The Geological Time Scale 2012*. Elsevier, Amsterdam, pp. 653–680.
- Hill, C., 1996. The geology of the Delaware basin, Guadalupe, Apache and Glass mountains New Mexico and Texas. *Permian Basin SEPM* 96–39, 113–137.
- Hoke, G.D., Schmitz, M.D., Bowring, S.A., 2014. An ultrasonic method for isolating nonclay components from clay-rich material. *Geochem. Geophys. Geosyst.* 15, 492–498.
- Hou, Z.S., Fan, J.X., Henderson, C.M., Dong-xun, Y., Bo-heng, S., Jie, W., Yue, W., Quan-feng, Z., Yi-chun, Z., Qiong, W., Shu-zhong, S., 2020. Dynamic palaeogeographic reconstructions of the Wuchiapingian Stage (Lopingian, Late Permian) for the South China Block. *Palaeogeogr. Palaeoclimatol. Palaeoecol.* 546, 109667.
- Hounslow, M.W., Balabanov, Y.P., 2018. A geomagnetic polarity timescale for the Permian, calibrated to stage boundaries. *Geol. Soc. Lond. Spec. Publ.* 450, 61–103.
- Hu, S.Z., 1994. On the event of Dongwu Movement and its relation with Permian subdivision. *J. Stratigr.* 18, 309–315 (in Chinese with English abstract).
- Huang, Y.G., Chen, Z.Q., Wignall, P.B., Grasby, S.E., Zhao, L.S., Wang, X.D., Kaiho, K., 2019. Biotic responses to volatile volcanism and environmental stresses over the Guadalupian-Lopingian (Permian) transition. *Geology* 47 (2), 175–178.
- Hurd, G.S., Kerans, C., Fullmer, S., Janson, X., 2016. Large-scale inflections in slope angle below the shelf break: a first order control on the stratigraphic architecture of carbonate slopes: Cutoff Formation, Guadalupe Mountains National Park, West Texas, U.S.A. *J. Sediment. Res.* 86, 336–362.
- Irving, E., Parry, L.G., 1963. The magnetism of some Permian rocks from New South Wales. *Geophys. J. Lond.* 7, 395–411.
- Isbell, J.L., Lenaker, P.A., Askin, R.A., Miller, M.F., Babcock, L.E., 2003. Reevaluation of the timing and extent of Late Paleozoic glaciation in Gondwana: Role of the Transantarctic Mountains. *Geology* 31, 977–980.

- Isozaki, Y., 2009. Illawarra Reversal: the fingerprint of a superplume that triggered Pangean breakup and the end-Guadalupian (Permian) mass extinction. *Gondwana Res.* 15, 421–432.
- Isozaki, Y., Aljinović, D., 2009. End-Guadalupian extinction of the Permian gigantic bivalve Alatoconchidae: end of gigantism in tropical seas by cooling. *Palaeogeogr. Palaeoclimatol. Palaeoecol.* 284, 11–21.
- Isozaki, Y., Servais, T., 2018. The Hirnantian (Late Ordovician) and end-Guadalupian (Middle Permian) mass-extinction events compared. *Lethaia* 51, 173–186.
- Isozaki, Y., Kawahata, H., Minoshima, K., 2007a. The Capitanian (Permian) Kamura cooling event: the beginning of the Paleozoic-Mesozoic transition. *Palaeoworld* 16, 16–30.
- Isozaki, Y., Kawahata, H., Ota, A., 2007b. A unique carbon isotope record across the Guadalupian-Lopingian (Middle-Upper Permian) boundary in mid-oceanic paleo-atoll carbonates: the high-productivity “Kamura event” and its collapse in Panthalassa. *Glob. Planet. Chang.* 55, 21–38.
- Isozaki, Y., Aljinovic, D., Kawahata, H., 2011. The Guadalupian (Permian) Kamura event in European Tethys. *Palaeogeogr. Palaeoclimatol. Palaeoecol.* 308, 12–21.
- Ito, T., Feng, Q.L., Matsuoka, A., 2013. Radiolarian faunal change in the Middle Permian Gufeng Formation in the Liuhuang section, Chaohu, South China. *Sci. Rep. Niigata Univ.* 28, 39–49.
- Jaffey, A.H., Flynn, K.F., Glendenin, L.E., Bentley, W.C., Essling, A.M., 1971. Precision measurement of half-lives and specific activities of U^{235} and U^{238} . *Phys. Rev. C* 4, 1889–1906.
- Jin, Y.G., 1960. Conodonts from the Kufeng Suit(Formation) of Lungtan, Nanking. *Acta Palaeontol. Sin.* 8, 242–248 (in Chinese with English abstract).
- Jin, Y.G., 1993. Pre-Lopingian Benthos Crisis. *Comptes Rendus XII ICC-P*, Buenos Aires, pp. 269–278.
- Jin, Y.G., Zhang, J., Shang, Q.H., 1994. Two phases of the end-Permian mass extinction. In: Embry, A.F., Beauchamp, B., Glass, D.J. (Eds.), Canadian Society of Petroleum Geologists, Memoir 17. Can. Soc. Petrol. Geol., Calgary, pp. 813–822.
- Jin, Y.G., Wardlaw, B.R., Glenister, B.F., Kotlyar, C.V., 1997. Permian chronostratigraphic subdivisions. *Episodes* 20, 6–10.
- Jin, Y.G., Wang, W., Wang, Y., Cao, C.Q., 1998. Prospects for global correlation of Permian sequences. In: Shi, G.R., Archbold, N.W., Grover, M. (Eds.), Strzelecki International Symposium on Permian of Eastern Tethys: Biostratigraphy, Palaeogeography and Resources, Proc. Roy. Soc. Victoria, 10, pp. 73–83.
- Jin, Y.G., Shang, Q.H., Wang, X.D., Wang, Y., Sheng, J.Z., 1999. Chronostratigraphic subdivision and correlation of the Permian in China. *Acta Geol. Sin.* 73, 127–138 (English edition).
- Jin, Y.G., Shang, Q.H., Cao, C.Q., 2000. A review of Permian stratigraphy in China: *J. Strat.* 24, 99–108.
- Jin, Y.G., Shen, S.Z., Henderson, C.M., Wang, X.D., Wang, W., Wang, Y., Cao, C.Q., Shang, Q.H., 2006. The Global Stratotype Section and Point (GSSP) for the boundary between the Capitanian and Wuchiapingian stage (Permian). *Episodes* 29, 253–262.
- Joachimski, M.M., Breisig, S., Buggisch, W., Talent, J.A., Mawson, R., Gereke, M., Morrow, J.R., Day, J., Weddige, K., 2009. Devonian climate and reef evolution: insights from oxygen isotopes in apatite. *Earth Planet. Sci. Lett.* 284, 599–609.
- Jost, A.B., Mundil, R., He, B., Brown, S.T., Altiner, D., Sun, Y.D., DePaolo, D.J., Payne, J. L., 2014. Constraining the cause of the end-Guadalupian extinction with coupled records of carbon and calcium isotopes. *Earth Planet. Sci. Lett.* 396, 201–212.
- Kametaka, M., Nagai, H., Zhu, S.Z., Takebe, M., 2009. Middle Permian radiolarians from Anmenkou, Chaohu, Northeastern Yangtze platform, China. *Island Arc* 18, 108–125.
- Kani, T., Fukui, M., Isozaki, Y., Nohda, S., 2008. The Paleozoic minimum of $^{87}\text{Sr}/^{86}\text{Sr}$ ratio in the Capitanian (Permian) mid-oceanic carbonates: a critical turning point in the Late Paleozoic. *J. Asian Earth Sci.* 32, 22–33.
- Kani, T., Hisanabe, C., Isozaki, Y., 2013. The Capitanian (Permian) minimum of $^{87}\text{Sr}/^{86}\text{Sr}$ ratio in the mid-Panthalassan paleo-atoll carbonates and its demise by the deglaciation and continental doming. *Gondwana Res.* 24, 212–221.
- Kasuya, A., Isozaki, Y., Igo, H., 2012. Constraining paleo-latitude of a biogeographic boundary in mid-Panthalassa: Fuseline province shift on the Late Guadalupian (Permian) migrating seamount. *Gondwana Res.* 21, 611–623.
- Kendall, A.C., Harwood, G.M., 1989. Shallow-Water gypsum in the Castile Formation—significance and implications. In: Harris, P.M., Grover, G.A. (Eds.), Subsurface and Outcrop Examination of the Capitan Shelf Margin, Northern Delaware Basin. SEPM Core Workshop no. 13. San Antonio, pp. 451–457.
- Kerans, C., Ruppel, S.C., 1994. San Andres sequence framework, Guadalupe Mountains: implications for San Andres type section and subsurface reservoirs. In: Garber, R.A., Keller, D.R. (Eds.), Field Guide to the Paleozoic Section of the San Andres Mountains, 94–35. PBSSEPM Publication, pp. 105–115.
- Kerans, C., Playton, T.E., Phelps, R., Scott, S.Z., 2013. Ramp to rimmed shelf transition in the Guadalupian (Permian) of the Guadalupe Mountains, West Texas and New Mexico. *SEPM Spec. Publ.* 105, 26–49.
- Kerans, C., Playton, T., Phelps, R., Scott, S.Z., 2014. Ramp to rimmed shelf transition in the Guadalupian (Permian) of the Guadalupe Mountains, West Texas and New Mexico. In: Verwer, K. (Ed.), Deposits, Architecture, and Controls of Carbonate Margin, Slope and Basinal Settings. SEPM Society for Sedimentary Geology, pp. 26–49. Special Publication Volume 105. Tulsa, SEPM Society for Sedimentary Geology.
- King, P.B., 1942. Permian of West Texas and Southeastern New Mexico. *Am. Assoc. Pet. Geol. Bull.* 26, 533–763.
- King, P.B., 1948. Geology of the Southern Guadalupe Mountains, Texas. U. S. Geol. Surv. Prof. Pap. 215, 1–183.
- Kirschvink, J.L., Isozaki, Y., Shibuya, H., Otofuji, Y., Raub, T.D., Hilburn, I.A., Kasuya, T., Yokoyama, M., Bonifacie, M., 2015. Challenging the sensitivity limits of Paleomagnetism: magnetostratigraphy of weakly magnetized Guadalupian–Lopingian (Permian) Limestone from Kyushu, Japan. *Palaeogeogr. Palaeoclimatol. Palaeoecol.* 418, 75–89.
- Korn, D., Klug, C., 2015. Paleozoic ammonoid biostratigraphy. In: Klug, C., Korn, D., De Baets, K., Kruta, I., Mapes, R.H. (Eds.), Ammonoid Paleobiology: From Macroevolution to Paleogeography. Springer Netherlands, pp. 299–328.
- Korte, C., Jasper, T., Kozur, H.W., Veizer, J., 2005. $\delta^{18}\text{O}$ and $\delta^{13}\text{C}$ of Permian brachiopods: a record of seawater evolution and continental glaciation. *Palaeogeogr. Palaeoclimatol. Palaeoecol.* 224, 333–351.
- Korte, C., Jasper, T., Kozur, H.W., Veizer, J., 2006. $^{87}\text{Sr}/^{86}\text{Sr}$ record of Permian seawater. *Palaeogeogr. Palaeoclimatol. Palaeoecol.* 240, 89–107.
- Krabbenhoft, A., Fietzke, J., Eisenhauer, A., Liebetrau, V., Böhm, F., Vollstaedt, H., 2009. Determination of radiogenic and stable strontium isotope ratios ($^{87}\text{Sr}/^{86}\text{Sr}$, $^{88}\text{Sr}/^{86}\text{Sr}$) by thermal ionization mass spectrometry applying an $^{87}\text{Sr}/^{84}\text{Sr}$ double spike. *J. Anal. Atom. Spec.* 24, 1267–1271.
- Lai, X.L., Wang, W., Wignall, P.B., Bond, D.P.G., Jiang, H.S., Ali, J.R., John, E.H., Sun, Y. D., 2008. Palaeoenvironmental change during the end-Guadalupian (Permian) mass extinction in Sichuan, China. *Palaeogeogr. Palaeoclimatol. Palaeoecol.* 269, 78–93.
- Lambert, L.L., 2000. The Guadalupian GSSP-The world standard Middle Permian series—Guadalupe Mountains National Park. In: Crow, C.J., Bell, G.L.J. (Eds.), AAPG-EAGE Field Trip Guidebook: Guadalupian Deposition in Sabkha, Shelf, Reef, and Basin Environments. Guadalupe Mountains, Texas and New Mexico, pp. 57–70.
- Lambert, L.L., 2006. Taxonomic update for Reef Trail conodonts illustrated. In: Hinterlong, G. (Ed.), Basinal Facies of the Uppermost Guadalupian: Applicability to Exploration and Development Projects, Permian Basin Section-SEPM Society for Sedimentary Geology, Publication, 2006–46, pp. 78–85.
- Lambert, L.L., Lehrmann, D.J., Harris, M.T., 2000. Correlation of the Road Canyon and Cuttoff Formations, west Texas, and its relevance to establishing an international Middle Permian (Guadalupian) Series. In: Wardlaw, B.R., Grant, R.E., Rohr, D.M. (Eds.), The Guadalupian Symposium, Smithsonian contributions to the Earth Sciences, 32. Smithsonian Institution, Washington D.C., pp. 153–183.
- Lambert, L.L., Wardlaw, B.R., Nestell, M.K., Nestell, G.P., 2002. Latest Guadalupian (Middle Permian) conodonts and foraminifers from West Texas. *Micropaleontology* 48, 343–364.
- Lambert, L.L., Wardlaw, B.R., Henderson, C.M., 2007. *Mesogondolella* and *Jinogondolella* (Conodonta): Multielement definition of the taxa that bracket the basal Guadalupian (Middle Permian Series) GSSP. *Palaeoworld* 16, 208–221.
- Lambert, L.L., Bell, G.L., Fronimos, J.A., Wardlaw, B.R., Yisa, M.O., 2010. Conodont biostratigraphy of a more complete Reef Trail Member section near the type section, latest Guadalupian Series type region. *Micropaleontology* 56, 233–253.
- Lanci, L., Tohver, E., Wilson, A., Flint, S., 2013. Upper Permian magnetic stratigraphy of the lower Beaufort Group, Karoo Basin. *Earth Planet. Sci. Lett.* 375, 123–134.
- Leonova, T.B., 2011. Permian ammonoids: Biostratigraphic, biogeographical, and ecological analysis. *Paleontol. J.* 45, 1206–1312.
- Leonova, T.B., 2018. Permian ammonoid biostratigraphy. *Geol. Soc. Lond. Spec. Publ.* 450, 185–203.
- Liang, W.P., 1990. Lengwu Formation of Permian and its Brachiopod Fauna in Zhejiang Province. Geological Publishing House, Beijing (in Chinese with English abstract).
- Liu, J., 2013. Osteology, ontogeny, and phylogenetic position of *Sinophoneus Yumenensis* (Therapsida, Dinocephalia) from the middle Permian Dashankou fauna of China. *J. Vertebr. Paleontol.* 33, 1394–1407.
- Liu, X.C., Wang, W., Shen, S.Z., Gorgij, M.N., Ye, F.C., Zhang, Y.C., Furuyama, S., Kano, A., Chen, X.Z., 2013. Late Guadalupian to Lopingian (Permian) carbon and strontium isotopic chemostratigraphy in the Abadeh section, central Iran. *Gondwana Res.* 24, 222–232.
- Liu, C., Jarochowska, E., Du, Y.S., Munnecke, A., Dai, X.D., 2017a. Prevailing anoxia in the Kungurian (Permian) of South China: possible response to divergent climate trends between the tropics and Gondwana. *Gondwana Res.* 49, 81–93.
- Liu, C., Jarochowska, E., Du, Y.S., Vachard, D., Munnecke, A., 2017b. Stratigraphical and $\delta^{13}\text{C}$ records of Permo-Carboniferous platform carbonates, South China: responses to late Paleozoic icehouse climate and icehouse-greenhouse transition. *Palaeogeogr. Palaeoclimatol. Palaeoecol.* 474, 113–129.
- Lucas, S.G., 2009. Timing and magnitude of tetrapod extinctions across the Permo-Triassic boundary. *J. Asian Earth Sci.* 36, 491–502.
- Lucas, S.G., 2017a. Permian tetrapod extinction events. *Earth Sci. Rev.* 170, 31–60.
- Lucas, S.G., 2017b. Identification and age of the beginning of the Permian-Triassic Illawarra Superchron. *Permophiles* 65, 11–14.
- Lucas, S.G., Shen, S.Z., 2018. The Permian chronostratigraphic scale: history, status and prospectus. *Geol. Soc. Lond. Spec. Publ.* 450, 21–50.
- Ma, J.L., Wei, G.J., Liu, Y., Ren, Z.Y., Xu, Y.G., Yang, Y.H., 2013. Precise measurement of stable ($^{88}/^{86}\text{Sr}$) and radiogenic ($^{87}\text{Sr}/^{86}\text{Sr}$) strontium isotope ratios in geological standard reference materials using MC-ICP-MS. *Chin. Sci. Bull.* 58, 3111–3118.
- Mattinson, J.M., 2005. Zircon U-Pb chemical abrasion (“CA-TIMS”) method: combined annealing and multi-step partial dissolution analysis for improved precision and accuracy of zircon ages. *Chem. Geol.* 220, 47–66.
- McArthur, J.M., Howarth, R.J., Bailey, T.R., 2001. Strontium isotope stratigraphy: LOWESS Version 3: best fit to the marine Sr-isotope curve for 0–509 Ma and accompanying look-up table for deriving numerical age. *J. Geol.* 109, 155–170.
- McArthur, J.M., Howarth, R.J., Shields, G.A., 2012. Strontium isotope stratigraphy. In: Gradstein, F.M., Ogg, J.G., Schmitz, M.D., Ogg, G.M. (Eds.), The Geological time scale 2012. Elsevier, Amsterdam, pp. 127–144.
- McLean, N.M., Bowring, J.F., Bowring, S.A., 2011. An algorithm for U-Pb isotope dilution data reduction and uncertainty propagation. *Geochem. Geophys. Geosyst.* 12, Q0AA18.
- McLean, N.M., Condon, D.J., Schoene, B., Bowring, S.A., 2015. Evaluating uncertainties in the calibration of isotopic reference materials and multi-element isotopic tracers (EARTHTIME Tracer Calibration Part II). *Geochim. Cosmochim. Acta* 164, 481–501.

- Mei, S.L., Henderson, C.M., 2002. Conodont definition of the Kungurian (Cisuralian) and Roadian (Guadalupian) boundary, Carboniferous and Permian of the world. XIV ICP proceedings. Mem. Can. Soc. Petrol. Geol. 19, 529–551.
- Mei, S.L., Jin, Y.G., Wardlaw, B.R., 1994a. Succession of conodont zones from the Permian “Kuhfeng” Formation, Xuanhan, Sichuan and its implications in global correlation. *Acta Palaeontol. Sin.* 33, 1–23 (in Chinese with English abstract).
- Mei, S.L., Jin, Y.G., Wardlaw, B.R., 1994b. Succession of Wuchiapingian conodonts from northeastern Sichuan and its worldwide correlation. *Acta Micropalaeontol. Sin.* 11, 121–139.
- Mei, S.L., Jin, Y.G., Wardlaw, B.R., 1998. Conodont succession of the Guadalupian–Lopingian boundary strata in Laibin of Guangxi, China and West Texas, USA. In: Jin, Y.G., Wardlaw, B.R., Wang, Y. (Eds.), *Permian Stratigraphy, Environments and Resources*, Palaeoworld, 9. Nanjing University Press, Nanjing, pp. 53–76.
- Mei, S.L., Shi, X.Y., Chen, X.F., Sun, K.Q., Yan, J.X., 1999. Permian Cisuralian and Guadalupian sequence stratigraphy in south Guizhou and central Guangxi and its relation to conodont evolution. *J. China Univ. Geosci.* 24, 21–31.
- Mei, S.L., Henderson, C.M., Cao, C.Q., 2004. Conodont sample-population approach to defining the base of the Changhsingian Stage, Lopingian Series, Upper Permian. The palynology and micropalaeontology of boundaries. *Geol. Soc. Spec. Publ.* 230, 105–121.
- Menning, M., 2000. Magnetostratigraphic results from the Middle Permian type section, Guadalupe Mountains, West Texas. *Permophiles* 37, 16.
- Menning, M., 2001. A Permian time scale 2000 and correlation of marine and continental sequences using the Illawarra Reversal (265 Ma). *Natura Bresciana* 25, 355–362.
- Menning, M., Jin, Y.G., 1998. Permo-Triassic magnetostratigraphy in China: the type section near Taiyuan, Shanxi Province, North China – Comment. *Geophys. J. Int.* 133, 213–216.
- Metcalf, I., Crowley, J.L., Nicoll, R.S., Schmitz, M., 2015. High-precision U-Pb CA-TIMS calibration of Middle Permian to Lower Triassic sequences, mass extinction and extreme climate-change in eastern Australian Gondwana. *Gondwana Res.* 28, 61–81.
- Miller, A.K., 1938. Comparison of Permian ammonoid zones of Soviet Russia with those of North America. *AAPG Bull.* 22, 1014–1019.
- Miller, A.K., Furnish, W.M., 1940. Permian ammonoids of the Guadalupe Mountain region and adjacent areas. *Geol. Soc. Am. Spec. Pap.* 26, 1–238.
- Nestell, M.K., Nestell, G.P., Wardlaw, B.R., Sweatt, M.J., 2006. Integrated biostratigraphy of foraminifers, radiolarians and conodonts in shallow and deep water Middle Permian (Capitanian) deposits of the “Rader Slide”, Guadalupe Mountains, West Texas. *Stratigraphy* 3, 161–194.
- Nestell, M.K., Nestell, G.P., Wardlaw, B.R., 2019. Integrated fusulinid, conodont, and radiolarian biostratigraphy of the Guadalupian (Middle Permian) in the Permian Basin region, USA. In: Ruppel, S.C. (Ed.), *Anatomy of a Paleozoic Basin: The Permian Basin, USA. Volume 1, Chapter 9*: The University of Texas at Austin, Bureau of Economic Geology Report of Investigations 285; AAPG Memoir, 118, pp. 251–291.
- Nicklen, B.L., 2011. Establishing a Tephrochronologic Framework for the Middle Permian (Guadalupian) Type Area and Adjacent Portions of the Delaware Basin and Northwestern Shelf, West Texas and Southeastern New Mexico, USA. Department of Geology, University of Cincinnati.
- Nicklen, B.L., Bell, G.L.J., Lambert, L.L., Huff, W.D., 2015. Tephrochronology of the Manzano Limestone in the Middle Permian (Guadalupian) Type Area, West Texas and southeastern New Mexico, USA. *Stratigraphy* 12 (2), 123–147.
- Nishikane, Y., Kaiho, K., Takahashi, S., Henderson, C.M., Suzuki, N., Kanno, M., 2011. The Guadalupian-Lopingian boundary (Permian) in a pelagic sequence from Panthalassa recognized by integrated conodont and radiolarian biostratigraphy. *Mar. Micropaleontol.* 78, 84–95.
- Olszewski, T.D., Erwin, D.H., 2009. Change and stability in Permian brachiopod communities from western Texas. *Palaios* 24, 27–40.
- Ota, A., Isozaki, Y., 2006. Fusuline biotic turnover across the Guadalupian-Lopingian (Middle-Upper Permian) boundary in mid-oceanic carbonate buildups: Biostratigraphy of accreted limestone in Japan. *J. Asian Earth Sci.* 26, 353–368.
- Playton, T.E., Kerans, C., 2018. Architecture and genesis of prograding deep boundstone margins and debris-dominated carbonate slopes: examples from the Permian Capitan Formation, Southern Guadalupe Mountains, West Texas. *Sediment. Geol.* 370, 15–41.
- Pucéat, E., Joachimski, M.M., Bouilloux, A., Monna, F., Bonin, A., Motreuil, S., Morinière, P., Hénard, S., Mourin, J., Dera, G., Quesne, D., 2010. Revised phosphate-water fractionation equation reassessing paleotemperatures derived from biogenic apatite. *Earth Planet. Sci. Lett.* 298, 135–142.
- Ramezani, J., Bowring, S.A., 2018. Advances in numerical calibration of the Permian timescale based on radioisotopic geochronology. *Geol. Soc. Lond. Spec. Publ.* 450, 51–60.
- Ramezani, J., Hoke, G.D., Fastovsky, D.E., Bowring, S.A., Therrien, F., Dworkin, S.I., Atchley, S.C., Nordt, L.C., 2011. High-precision U-Pb zircon geochronology of the Late Triassic Chinle Formation, Petrified Forest National Park (Arizona, USA): temporal constraints on the early evolution of dinosaurs. *Geol. Soc. Am. Bull.* 123, 2142–2159.
- Rampino, M.R., Shen, S.Z., 2020. The end-Guadalupian (259.8 Ma) biodiversity crisis: the sixth major mass extinction? *Hist. Biol.* 1–7.
- Raup, D., Sepkoski, J.J.J., 1982. Mass extinctions in the marine fossil record. *Science* 215, 1501–1503.
- Roberts, J., Clauqué-Long, J., Foster, C., 1996. SHRIMP zircon dating of the Permian system of eastern Australia. *Austral. J. Earth Sci.* 43, 401–421.
- Rohr, D.M., Wardlaw, B.R., Rudine, S.E., Haneef, M., Hall, A.J., Grant, R.E., 2000. Guidebook to the Guadalupian Symposium. Smithsonian Contrib. Earth Sci. 32, 5–36.
- Ross, C.A., 1962. Fusulinids from the Leonard Formation (Permian), West Glass Mountains, Texas. *Contrib. Cushman Found. Foram. Res.* 13 (1), 1–21.
- Ross, C.A., 1963. Fusulinids from the Word Formation (Permian), Glass Mountains, Texas. *Contrib. Cushman Found. Foram. Res.* 14 (1), 17–31.
- Ross, C.A., 1967. Development of fusulinid (Foraminifera) faunal realms. *J. Paleontol.* 41, 1341–1354.
- Ross, C.A., 1986. Paleozoic evolution of Southern margin of Permian basin. *Geol. Soc. Am. Bull.* 97 (5), 536–554.
- Ross, C.A., Ross, J.R.P., 1987. Late Paleozoic sea levels and depositional sequences. In: Ross, C.A., Haman, D. (Eds.), *Timing and Depositional History of Eustatic Sequences: Constraints on Seismic Stratigraphy*, Cushman Foundation for Foraminiferal Research: Special Publication, 24, pp. 137–149.
- Rubidge, B.S., Erwin, D.H., Ramezani, J., Bowring, S.A., de Clerk, W.J., 2013. High-precision temporal calibration of Late Permian vertebrate biostratigraphy: U-Pb zircon constraints from the Karoo Supergroup, South Africa. *Geology* 41, 363–366.
- Rubidge, B.S., Day, M.O., Barbolini, N., Hancox, P.J., Choiniere, J.N., Bamford, M.K., Viglietti, P.A., McPhee, B.W., Jirah, S., 2016. Advances in Nonmarine Karoo Biostratigraphy: significance for understanding basin DEVELOPMENT. In: Linol, B., de Wit, M. (Eds.), *Origin and Evolution of the Cape Mountains and Karoo Basin. Regional Geology Reviews*. Springer, Cham, pp. 141–149.
- Saitoh, M., Isozaki, Y., Ueno, Y., Yoshida, N., Yao, J.X., Ji, Z.S., 2013. Middle-Upper Permian carbon isotope stratigraphy at Chaotian, South China: Pre-extinction multiple upwelling of oxygen-depleted water onto continental shelf. *J. Asian Earth Sci.* 67–68, 51–62.
- Sepkoski, J.J.J., 1984. A kinetic model of Phanerozoic taxonomic diversity III. Post-Paleozoic families and mass extinctions. *Paleobiology* 10, 246–267.
- Sha, Q.A., Wu, W.S., Fu, J.M., 1990. Comprehensive Research of Permian in Guizhou-Guangxi Area and Its Petroleum Potential. Science Press, Beijing (in Chinese with English abstract).
- Shellnutt, J.G., 2018. The Panjal traps. *Geol. Soc. Lond. Spec. Publ.* 463, 59–86.
- Shellnutt, J.G., Bhat, G.M., Brookfield, M.E., Jahn, B.M., 2011. No link between the Panjal Traps (Kashmir) and the Late Permian mass extinctions. *Geophys. Res. Lett.* 38, L19308.
- Shellnutt, J.G., Pham, T.T., Denyszyn, S.W., Yeh, M.W., Tran, T.A., 2020. Magmatic duration of the Emeshan large igneous province: insight from northern Vietnam. *Geology* 48, 457–461.
- Shen, S.Z., 2018. Global Permian brachiopod biostratigraphy: an overview. *Geol. Soc. Lond. Spec. Publ.* 450, 289–320.
- Shen, S.Z., Shi, G.R., 1996. Diversity and extinction patterns of Permian Brachiopoda of South China. *Hist. Biol.* 12, 93–110.
- Shen, S.Z., Shi, G.R., 2002. Paleobiogeographical extinction patterns of Permian brachiopods in the Asian-western Pacific region. *Paleobiology* 28, 449–463.
- Shen, S.Z., Shi, G.R., 2004. Capitanian (Late Guadalupian, Permian) global brachiopod palaeobiogeography and latitudinal diversity pattern. *Palaeogeogr. Palaeoclimatol. Palaeoecol.* 208, 235–262.
- Shen, S.Z., Shi, G.R., 2009. Latest Guadalupian brachiopods from the Guadalupian/Lopingian boundary GSSP section at Penglaitan in Laibin, Guangxi, South China and implications for the timing of the pre-Lopingian crisis. *Palaeoworld* 18, 152–161.
- Shen, S.Z., Zhang, Y.C., 2008. Earliest Wuchiapingian (Lopingian, late Permian) brachiopods in southern Hunan, South China: implications for the pre-Lopingian crisis and onset of Lopingian recovery/radiation. *J. Paleontol.* 82, 924–937.
- Shen, S.Z., Wang, Y., Henderson, C.M., Cao, C.Q., Wang, W., 2007. Biostratigraphy and lithofacies of the Permian System in the Laibin-Heshan area of Guangxi, South China. *Palaeoworld* 16, 120–139.
- Shen, S.Z., Xie, J.F., Zhang, H., Shi, G.R., 2009. Roadian-Wordian (Guadalupian, Middle Permian) global palaeobiogeography of brachiopods. *Glob. Planet. Chang.* 65, 166–181.
- Shen, S.Z., Crowley, J.L., Wang, Y., Bowring, S.A., Erwin, D.H., Sadler, P.M., Cao, C.Q., Rothman, D.H., Henderson, C.M., Ramezani, J., Zhang, H., Shen, Y., Wang, X.D., Wang, W., Mu, L., Li, W.Z., Tang, Y.G., Liu, X.L., Liu, L.J., Zeng, Y., Jiang, Y.F., Jin, Y.G., 2011. Calibrating the end-Permian mass extinction. *Science* 334, 1367–1372.
- Shen, S.Z., Yuan, D.X., Henderson, C.M., Tazawa, J., Zhang, Y.C., 2012. Implications of Kungurian (Early Permian) conodonts from Hatahoko, Japan, for correlation between the Tethyan and international timescales. *Micropaleontology* 58, 505–522.
- Shen, S.Z., Cao, C.Q., Zhang, H., Bowring, S.A., Henderson, C.M., Payne, J.L., Davydov, V.I., Chen, B., Yuan, D.X., Zhang, Y.C., Wang, W., Zheng, Q.F., 2013a. High-resolution $\delta^{13}\text{C}_{\text{carb}}$ chemostratigraphy from latest Guadalupian through earliest Triassic in South China and Iran. *Earth Planet. Sci. Lett.* 375, 156–165.
- Shen, S.Z., Zhang, H., Shi, G.R., Li, W.Z., Xie, J.F., Mu, L., Fan, J.X., 2013b. Early Permian (Cisuralian) global brachiopod palaeobiogeography. *Gondwana Res.* 24, 104–124.
- Shen, S.Z., Ramezani, J., Chen, J., Cao, C.Q., Erwin, D.H., Zhang, H., Xiang, L., Schoepfer, S.D., Henderson, C.M., Zheng, Q.F., Bowring, S.A., Wang, Y., Li, X.H., Wang, X.D., Yuan, D.X., Zhang, Y.C., Mu, L., Wang, J., Wu, Y.S., 2019a. A sudden end-Permian mass extinction in South China. *Geol. Soc. Am. Bull.* 131, 205–223.
- Shen, S.Z., Zhang, H., Zhang, Y.C., Yuan, D.X., Chen, B., He, W.H., Mu, L., Lin, W., Wang, W.Q., Chen, J., Wu, Q., Cao, C.Q., Wang, Y., Wang, X.D., 2019b. Permian integrative stratigraphy and timescale of China. *Sci. China Earth Sci.* 62, 154–188.
- Shen, S.Z., Zhang, Y.C., Yuan, D.X., Zheng, Q.F., Zhang, H., Mu, L., Hou, Z.S., Wang, W., Q., Shen, B.H., Cai, Y.F., 2020. Progress report: Location of the replacement section for the base-Lopingian GSSP. *Permophiles* 68, 24–28.
- Sheng, J.Z., Jin, Y.G., 1994. Correlation of Permian deposits in China. In: Jin, Y.G., Utting, J., Wardlaw, B.R. (Eds.), *Permian Stratigraphy, Environments and Resources*, Palaeoworld, 4. Nanjing University Press, Nanjing, pp. 14–113.
- Shi, G.R., Waterhouse, J.B., 2010. Late Palaeozoic global changes affecting high-latitude environments and biotas: An introduction. *Palaeogeogr. Palaeoclimatol. Palaeoecol.* 298, 1–16.

- Shi, Y.K., Yang, X.N., 2005. A statistical test on diversity changes of Early and Middle Permian fusulinacean fauna in South China. *Sci. China Ser. D Earth Sci.* 48, 978–984.
- Shi, Z.J., Yin, G., Li, W.J., Yang, H.X., Zhang, J., Lu, L.X., Tian, Y.M., Wang, Y., 2017. Major geological events in the late Guadalupian and carbon-strontium isotope responses in the Yangtze platform, South China. *Can. J. Earth Sci.* 54, 1025–1032.
- Shi, G.R., Yang, B., Lee, S., Luo, M., 2019. Living in a sea of mud and erratics: exploring the ecological association and interactions between marine benthos and glacial dropstones, Middle Permian, southeast Australia. In: Hartenfels, S., Herbig, H.G., Amler, M.R.W., Aretz, M. (Eds.), Abstracts, 19th International Congress on the Carboniferous and Permian, Cologne, pp. 288–289.
- Smith, B.P., Larson, T., Martindale, R.C., Kerans, C., 2020. Impacts of basin restriction on geochemistry and extinction patterns: a case from the Guadalupian Delaware Basin, USA. *Earth Planet. Sci. Lett.* 530, 115876.
- Sohn, I.G., 1961. Ostracodes and conodonts from the Getaway limestone member of the Cherry Canyon Formation (Permian), Texas, Article 379. U. pp. D244–D245.
- Stanley, S.M., Yang, X.N., 1994. A double mass extinction at the end of the Paleozoic Era. *Science* 266, 1340–1344.
- Steiner, M.B., 2006. The magnetic polarity time scale across the Permian-Triassic boundary. In: Lucas, S.G., Cassinis, G., Schneider, J.W. (Eds.), Non-marine Permian Biostratigraphy and Biochronology, 265. The Geological Society, London, pp. 15–38.
- Stojanovic, D., Aitchison, J.C., Ali, J.R., Ahmad, T., Dar, R.A., 2016. Paleomagnetic investigation of the Early Permian Panjal Traps of NW India; regional tectonic implications. *J. Asian Earth Sci.* 115, 114–123.
- Sun, D.Y., Xia, W.C., 2006. Identification of the Guadalupian-Lopingian boundary in the Permian in a bedded chert sequence, south China. *Palaeogeogr. Palaeoclimatol. Palaeoecol.* 236, 272–289.
- Sun, Y.D., Lai, X.L., Jiang, H.S., Luo, G.M., Sun, S., Yan, C.B., Wignall, P.B., 2008. Guadalupian (Middle Permian) conodont faunas at Shangsi Section, northeast Sichuan Province. *J. China Univ. Geosci.* 19, 451–460.
- Tang, C.A., Li, S.Z., 2016. The Earth evolution as a thermal system. *Geol. J.* 51, 652–668.
- Taraz, H., Golshani, F., Nakazawa, K., Shimizu, D., Bando, Y., Ishii, K., Murata, M., Okimura, Y., Sakagami, S., Nakamura, K., Tokuoka, T., 1981. The Permian and the Lower Triassic Systems in Abadeh Region, Central Iran. Kyoto University, Faculty of Science (Geology and Mineralogy). *Memoirs 47*, 61–133.
- Taylor, G.K., Tucker, C., Twitchett, R.J., Kearsey, T., Benton, M.J., Newell, A.J., Surkov, M.V., Tverdokhlebov, V.P., 2009. Magnetostratigraphy of Permian/Triassic boundary sequences in the Cis-Urals, Russia: No evidence for a major temporal hiatus. *Earth Planet. Sci. Lett.* 281, 36–47.
- Tierney, K.E., 2010. Carbon and Strontium Isotope Stratigraphy of the Permian From Nevada and China: Implications From an Icehouse to Greenhouse Transition, School of Earth Sciences. The Ohio State University, Columbus.
- Veizer, J., Ala, D., Azmy, K., Bruckschen, P., Buhl, D., Bruhn, F., Carden, G.A.F., Diener, A., Ebnet, S., Godderis, Y., Jasper, T., Korte, C., Pawellek, F., Podlaha, O.G., Strauss, H., 1999. $^{87}\text{Sr}/^{86}\text{Sr}$, $\delta^{13}\text{C}$ and $\delta^{18}\text{O}$ evolution of Phanerozoic seawater. *Chem. Geol.* 161, 59–88.
- Vennemann, T.W., Fricke, H.C., Blake, R.E., O'Neil, J.R., Colman, A., 2002. Oxygen isotope analysis of phosphates: a comparison of techniques for analysis of Ag_3PO_4 . *Chem. Geol.* 185, 321–336.
- Wang, C.Y., 1995. A conodont fauna from the lowest Kefeng Formation (Permian). *Acta Palaeontol. Sin.* 12, 293–297.
- Wang, X.D., Sugiyama, T., 2000. Diversity and extinction patterns of Permian coral faunas of China. *Lethaia* 33, 285–294.
- Wang, X.D., Sugiyama, T., 2001. Middle Permian rugose corals from Laibin, Guangxi, South China. *J. Paleontol.* 75, 758–782.
- Wang, W., Cao, C.Q., Wang, Y., 2004. The carbon isotope excursion on GSSP candidate section of Lopingian-Guadalupian boundary. *Earth Planet. Sci. Lett.* 220, 57–67.
- Wang, W., Kano, A., Okumura, T., Ma, Y.S., Matsumoto, R., Matsuda, N., Ueno, K., Chen, X.Z., Kakuwa, Y., Gharai, M.H.M., Ilkhchi, M.R., 2007. Isotopic chronostratigraphy of the microbialite-bearing Permian-Triassic boundary section in the Zagros Mountains, Iran. *Chem. Geol.* 244, 708–714.
- Wang, D.C., Jiang, H.S., Gu, S.Z., Yan, J.X., 2016. Cisuralian-Guadalupian conodont sequence from the Shahei section, Ziyun, Guizhou, South China. *Palaeogeogr. Palaeoclimatol. Palaeoecol.* 457, 1–22.
- Wang, W.Q., Garbelli, C., Zheng, Q.F., Chen, J., Liu, X.C., Wang, W., Shen, S.Z., 2018a. Permian $^{87}\text{Sr}/^{86}\text{Sr}$ chronostratigraphy from carbonate sequences in South China. *Palaeogeogr. Palaeoclimatol. Palaeoecol.* 500, 84–94.
- Wang, X.D., Yao, L., Lin, W., 2018b. Permian rugose corals of the world. *Geol. Soc. Lond. Spec. Publ.* 450, 165–184.
- Wang, W.Q., Garbelli, C., Zhang, F.F., Zheng, Q.F., Zhang, Y.C., Yuan, D.X., Shi, Y.K., Chen, B., Shen, S.Z., 2020. A high-resolution Middle to Late Permian paleotemperature curve reconstructed using oxygen isotopes of well-preserved brachiopod shells. *Earth Planet. Sci. Lett.* 540, 116245.
- Wardlaw, B.R., 2000. Guadalupian conodont biostratigraphy of the Glass and Del Norte Mountains. In: Wardlaw, B.R., Grant, R.E., Rohr, D.M. (Eds.), The Guadalupian Symposium, Smithsonian contributions to the Earth Sciences, 32. Smithsonian Institution, Washington D.C., pp. 37–81.
- Wardlaw, B.R., Nestell, M.K., 2010. Latest Middle Permian conodonts from the Apache Mountains, West Texas. *Micropaleontology* 56, 149–183.
- Wardlaw, B.R., Nestell, M.K., 2015. Conodont faunas from a complete basinal succession of the upper part of the Wordian (Middle Permian, Guadalupian, West Texas). *Micropaleontology* 61, 257–292.
- Wei, H.Y., Chen, D.Z., Yu, H., Wang, J.G., 2012. End-Guadalupian mass extinction and negative carbon isotope excursion at Xiaojiaba, Guangyuan, Sichuan. *Sci. China Earth Sci.* 55, 1480–1488.
- Wei, H.Y., Baima, Q.Z., Qiu, Z., Dai, C.C., 2018. Carbon isotope perturbations and faunal changeovers during the Guadalupian mass extinction in the middle Yangtze Platform, South China. *Geol. Mag.* 155, 1667–1683.
- Wei, H.Y., Geng, Z., Zhang, X., 2020. Guadalupian (Middle Permian) $\delta^{13}\text{C}_{\text{org}}$ changes in the Lower Yangtze, South China. *Acta Geochim.* <https://doi.org/10.1007/s11631-020-00417-3>.
- Wignall, P.B., Sun, Y.D., Bond, D.P.G., Izon, G., Newton, R.J., Vedrine, S., Widdowson, M., Ali, J.R., Lai, X.L., Jiang, H.S., Cope, H., Bottrell, S.H., 2009. Volcanism, mass extinction, and carbon isotope fluctuations in the Middle Permian of China. *Science* 324, 1179–1182.
- Wilde, G.L., 1990. Practical Fusulinid Zonation: the Species Concept; with Permian Basin Emphasis. *W. Tex. Geol. Soc. Bull.* 29 (7), 5–34.
- Wilde, G.L., 2000. Formal Middle Permian (Guadalupian) series; a fusulinacean perspective.; the Guadalupian symposium. *Smithson. Contrib. Earth Sci.* 32, 89–100.
- Williamson, C.R., 1980. Sedimentology of Guadalupian deep-water clastic facies, Delaware Basin, New Mexico and West Texas. In: New Mexico Geological Society Guidebook, Trans-Pecos Region, Field Conference, 31, pp. 195–204.
- Wu, Q., Ramezani, J., Zhang, H., Wang, T.T., Yuan, D.X., Mu, L., Zhang, Y.C., Li, X.H., Shen, S.Z., 2017. Calibrating the Guadalupian Series (Middle Permian) of South China. *Palaeogeogr. Palaeoclimatol. Palaeoecol.* 466, 361–372.
- Wu, Q., Ramezani, J., Zhang, H., Yuan, D.X., Erwin, D.H., Henderson, C.M., Lambert, L.L., Zhang, Y.C., Shen, S.Z., 2020. High-precision U-Pb zircon age constraints on the Guadalupian in West Texas, USA. *Palaeogeogr. Palaeoclimatol. Palaeoecol.* 548, 109668.
- Xia, W.C., Zhang, N., Kakuwa, Y., Zhang, L.L., 2006. Radiolarian and conodont biozonation in the pelagic Guadalupian-Lopingian boundary interval at Dachongling, Guangxi, South China, and mid-upper Permian global correlation. *Stratigr.* 2, 217–238.
- Xiao, W.M., Wang, H.D., Zhang, L.X., Dong, W.L., 1986. Early Permian Stratigraphy and Faunas in Southern Guizhou. The People's Publishing House of Guizhou, Guiyang (in Chinese with English abstract).
- Xu, W., Yue, S.C., Du, J.G., Du, S.G., Sun, C.Y., 2004. Characteristics of outcrop sequence stratigraphy of the Permian Gufeng Formation in the Guichi area. *Anhui. J. Stratigr.* 28 (2), 137–147 (in Chinese with English abstract).
- Xu, Y.G., Wei, X., Luo, Z.Y., Liu, H.Q., Cao, J., 2014. The Early Permian Tarim Large Igneous Province: main characteristics and a plume incubation model. *Lithos* 204, 20–35.
- Xue, W.Q., Li, B., Yan, J.X., Ellwood, B.B., Tomkin, J.H., Wang, Y., Zhu, Z.M., 2015. High-resolution floating point time scale (FPTS) of the Permian Capitanian stage in South China. *Chin. J. Geophys.* 58, 611–627.
- Yan, H., Pi, D.H., Jiang, S.Y., Hao, W.D., Mänd, K., Robbins, L.J., Li, L., Konhauser, K.O., 2020. New constraints on the onset age of the Emeishan LIP volcanism and implications for the Guadalupian mass extinction. *Lithos* 360–361, 105441.
- Yang, Z.D., Yancey, T.E., 2000. Fusulinid biostratigraphy and paleontology of the Middle Permian (Guadalupian) strata of the Glass Mountains and Del Norte Mountains, West Texas; the Guadalupian symposium. *Smithson. Contrib. Earth Sci.* 32, 185–259.
- Yang, X.N., Liu, J.R., Shi, G.J., 2004. Extinction process and patterns of Middle Permian Fusulinaceans in southwest China. *Lethaia* 37, 139–147.
- Yang, Y.H., Zhang, H.F., Chu, Z.Y., Xie, L.W., Wu, F.Y., 2010. Combined chemical separation of Lu, Hf, Rb, Sr, Sm and Nd from a single rock digest and precise and accurate isotope determinations of Lu-Hf, Rb-Sr and Sm-Nd isotope systems using Multi-Collector ICP-MS and TIMS. *Int. J. Mass Spectrom.* 290, 120–126.
- Yang, S.F., Chen, H.L., Li, Z.L., Li, Y.Q., Yu, X., Li, D.X., Meng, L.F., 2013. Early Permian Tarim large igneous province in northwest China. *Sci. China Earth Sci.* 56, 2015–2026.
- Yang, S.F., Chen, H.L., Li, Z.L., Li, Y.Q., Yu, X., 2017. Early Permian Tarim Large Igneous Province in Northwest China. Zhejiang University Press, Elsevier, Hangzhou (in Chinese with English abstract).
- Yang, J.H., Cawood, P.A., Du, Y.S., Condon, D.J., Yan, J.X., Liu, J.Z., Huang, Y., Yuan, D.X., 2018. Early Wuchiapingian cooling linked to Emeishan basaltic weathering? *Earth Planet. Sci. Lett.* 492, 102–111.
- Yao, X., Zhou, Y.Q., Hinnoy, L.A., 2015. Astronomical forcing of a Middle Permian chert sequence in Chaohu, South China. *Earth Planet. Sci. Lett.* 422, 206–221.
- Yuan, D.X., Zhang, Y.C., Shen, S.Z., Henderson, C.M., Zhang, Y.J., Zhu, T.X., An, X.Y., Feng, H.Z., 2016. Early Permian conodonts from the Xainza area, central Lhasa Block, Tibet, and their palaeobiogeographical and palaeoclimatic implications. *J. Syst. Palaeontol.* 14, 365–383.
- Yuan, D.X., Shen, S.Z., Henderson, C.M., 2017. Revised Wuchiapingian conodont taxonomy and succession of South China. *J. Paleontol.* 91, 1199–1219.
- Yuan, D.X., Shen, S.Z., Henderson, C.M., Lambert, L.L., Hearst, J.M., Zhang, Y.C., Chen, J., Qie, W.K., Zhang, H., Wang, X.D., Qi, Y.P., Wu, Q., 2020a. Reinvestigation of the Wordian-base GSSP section, West Texas, USA. In: Newsletters on Stratigr. (in press).
- Yuan, D.X., Aung, K.P., Henderson, C.M., Zhang, Y.C., Zaw, T., Cai, F.L., Ding, L., Shen, S.Z., 2020b. First records of Early Permian conodonts from eastern Myanmar and implications of paleobiogeographic links to the Lhasa Block and northwestern Australia. *Palaeogeogr. Palaeoclimatol. Palaeoecol.* 549, 109363.
- Zhang, Y.C., Payne, J.L., 2012. Size-frequency distributions along a latitudinal gradient in Middle Permian fusulinoideans. *PLoS One* 7, e38603.
- Zhang, Y.C., Wang, Y., 2018. Permian fusuline biostratigraphy. *Geol. Soc. Lond. Spec. Publ.* 450, 253–288.
- Zhang, L.L., Zhang, N., Xia, W.C., 2007. Conodont succession in the Guadalupian-Lopingian boundary interval (Upper Permian) of the Maoershan section, Hubei Province, China. *Micropaleontology* 53, 433–446.

- Zhang, C.L., Li, Z.X., Li, X.H., Xu, Y.G., Zhou, G., Ye, H.M., 2010. A Permian large igneous province in Tarim and Central Asian orogenic belt, NW China: results of a ca. 275 Ma mantle plume? *Geol. Soc. Am. Bull.* 122, 2020–2040.
- Zhang, Y.C., Shi, G.R., Shen, S.Z., 2013. A review of Permian stratigraphy, palaeobiogeography and palaeogeography of the Qinghai-Tibet Plateau. *Gondwana Res.* 24, 55–76.
- Zhang, G.J., Zhang, X.L., Li, D.D., Farquhar, J., Shen, S.Z., Chen, X.Y., Shen, Y., 2015. Widespread shoaling of sulfidic waters linked to the end-Guadalupian (Permian) mass extinction. *Geology* 43, 1091–1094.
- Zhang, L., Feng, Q.L., He, W.H., 2018. Permian radiolarian biostratigraphy. *Geol. Soc. Lond. Spec. Publ.* 450, 143–163.
- Zhang, B.L., Yao, S.P., Wignall, P.B., Hu, W.X., Liu, B., Ren, Y.L., 2019a. New timing and geochemical constraints on the Capitanian (Middle Permian) extinction and environmental changes in deep-water settings: evidence from the Lower Yangtze region of South China. *J. Geol. Soc.* 176, 588–608.
- Zhang, Y.C., Shen, S.Z., Zhang, Y.J., Zhu, T.X., An, X.Y., Huang, B.X., Ye, C.L., Qiao, F., Xu, H.P., 2019b. Middle Permian foraminifers from the Zhabuye and Xiadong areas in the central Lhasa Block and their paleobiogeographic implications. *J. Asian Earth Sci.* 175, 109–120.
- Zhang, B.L., Yao, S.P., Mills, B.J.W., Wignall, P.B., Hu, W.X., Liu, B., Ren, Y.L., Li, L.L., Shi, G., 2020. Middle Permian organic carbon isotope stratigraphy and the origin of the Kamura Event. *Gondwana Res.* 79, 217–232.
- Zhong, Y.T., He, B., Mundil, R., Xu, Y.G., 2014. CA-TIMS zircon U–Pb dating of felsic ignimbrite from the Binchuan section: Implications for the termination age of Emeishan large igneous province. *Lithos* 204, 14–19.
- Zhong, Y.T., Mundil, R., Chen, J., Yuan, D.X., Denysyn, S.W., Jost, A.B., Payne, J.L., He, B., Shen, S.Z., Xu, Y.G., 2020. Geochemical, biostratigraphic, and high-resolution geochronological constraints on the waning stage of Emeishan Large Igneous Province. *Geol. Soc. Am. Bull.* <https://doi.org/10.1130/B35464.1>.
- Zhou, Z.R., 2007. Bizarre Permian ammonoid subfamily Aulacogastrioceratinæ from southeast China. *J. Paleontol.* 81, 797–799.
- Zhou, Z.R., 2017. Permian basinal ammonoid sequence in Nanpanjiang area of South China—possible overlap between basinal Guadalupian and platform-based Lopingian. *J. Paleontol. Mem.* 91 (S74), 1–95.
- Zhou, J.P., Zhang, L.X., 1984. Fusulinids from the Chihsia Formation of MT. Qixiashan, Nanjing. *Acta Palaeontol. Sin.* 23 (6), 716–724 (in Chinese with English abstract).
- Zhu, Z.Y., Jiang, S.Y., Liu, G.X., Zhao, K.D., 2013. Precise dating of the Middle Permian: Zircon U–Pb geochronology from volcanic ash beds in the basal Gufeng Formation, Yangtze region, South China. *Gondwana Res.* 23, 1599–1606.